Regulation of the Na,K-ATPase by FXYD1

Dissertation

Zur Erlangung des akademischen Grades
eines Doktors der Naturwissenschaften
(Dr. rer. nat)

an der

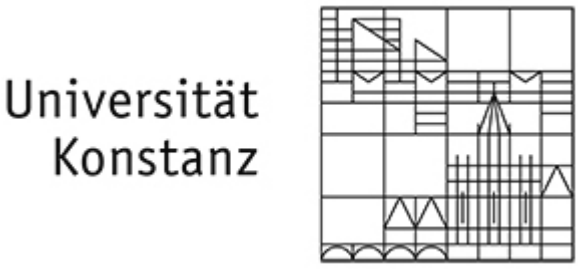

Mathematisch-Naturwissenschaftliche Sektion
Fachbereich Biologie

Vorgelegt von

Erica Cirri

1. Referent: Prof. Dr. H.-J. Apell
2. Referent: Prof. Dr. H. Möller

Tag der mündlichen Prüfung: 22.06.2012

Konstanzer Online-Publikations-System (KOPS)
URL: http://nbn-resolving.de/urn:nbn:de:bsz:352-196365

Table of Contents

CHAPTER 3: *RESULTS*

CHAPTER 4: *DISCUSSION*

Summary (English)

The Na,K-ATPase is an integral membrane protein present in virtually all animal cells, where it actively transports Na^+ and K^+ ions across the plasma membrane using ATP as energy source. For every ATP molecule hydrolyzed, the enzyme pumps three Na^+ ions out of and two K^+ ions into the cell. Because of its fundamental role in many physiological processes, the Na,K-ATPase is the target of specific regulatory mechanisms. Among them, the enzyme is modulated by the interaction with the so-called FXYD proteins, a group of short transmembrane polypeptides named after the invariant extracellular motif FXYD. All mammalian members of the FXYD family are known to associate with the Na,K-ATPase and modulate its properties in a tissue- and isozyme-specific way. FXYD1, also known as phospholemman, has been first identified as the major substrate for protein kinases A and C in the heart. Subsequently, it has been discovered to associate with specific isozymes of the Na,K-ATPase and modulate the enzyme activity in heart and skeletal muscle as well as kidneys and brain.

So far, the effects of FXYD1 on the Na,K-ATPase have been investigated mainly in intact cells, both heterologous systems and native cells. These systems allow a better characterization of the physiological effects of FXYD1, but are of limited use for the investigation of the functional and structural interactions between FXYD1 and the enzyme. A purification procedure of the human α_1/His_{10}-β_1 and α_2/His_{10}-β_1 isozymes of the Na,K-ATPase expressed in yeast *P. pastoris* has been recently developed by the group of Steven Karlish at the Weizmann Institute of Science. The purified, detergent-solubilized α_1/His_{10}-β_1 can be *in vitro* reconstituted with purified, detergent-solubilized human FXYD1 expressed in *E. coli* to obtain the α_1/His_{10}-β_1/FXYD1 complex. The purified recombinant preparations provide a system that enables us to work under well defined conditions and without interference by other cellular components. Unlike in native cells, the effects of FXYD1 on the different isozymes of the Na,K-ATPase can be investigated separately. Moreover, since the phosphorylation state of FXYD1 in the purified preparations is easily controllable, the functional role of the protein kinases-mediated phosphorylation of FXYD1 can be investigated. Therefore, these systems allow the performance of a detailed functional analysis of the effects of FXYD1 on the Na,K-ATPase.

The biophysical techniques based on the fluorescence of external dyes available in our lab allow a thorough characterization of the transport cycle of the Na,K-ATPase. Among them, the electrochromic styryl dye RH421 enables us to monitor the ion movements inside the membrane domain of the enzyme, allowing the detection of ion binding and ion release during the transport cycle. Moreover, the time course of the signals provides information about the kinetics of the processes involved. In contrast, the voltage-sensitive dye Oxonol VI can be successfully applied to detect the ion transport of the Na,K-ATPase reconstituted in lipid vesicles.

In a first step of the current study, the dye RH421 has been applied to the purified α_1/His_{10}-β_1 and α_2/His_{10}-β_1 preparations to ensure that it is suitable to investigate the ion-binding kinetics of detergent-solubilized ion pumps and that the functional properties of the purified recombinant enzymes do not differ significantly from those of the membrane-bound native Na,K-ATPase. Afterwards, the dye RH421 has been applied in steady-state and time-resolved kinetic measurements to characterize the effects of FXYD1 on the different partial reactions of the transport cycle of the α_1/β_1 isozyme of the Na,K-ATPase. These experiments have shown a single kinetic property affected by the presence of FXYD1: in both the enzyme conformations, E_1 and P-E_2, the Na^+-binding affinity is increased of ~ 20-30%. In the final part of the study, the influence of the membrane and its lipid composition on the effect of FXYD1 on the Na^+-binding affinity of the enzyme has been investigated with the

voltage-sensitive dye Oxonol VI in proteoliposomes containing either α_1/His_{10}-β_1 or α_1/His_{10}-β_1/FXYD1. These experiments have revealed an unexpected role of the lipid environment surrounding the complex in the interaction of FXYD1 with the enzyme, probably related to the cytoplasmic segment of the regulatory protein.

Part of the results presented in this thesis have been published already in

- Habeck, M., Cirri, E., Katz, A., Karlish, S. J., and Apell, H. J. (2009) *Biochemistry* 48: 9147-9155
- Mishra, N. K., Peleg, Y., Cirri, E., Belogus, T., Lifshitz, Y., Voelker, D. R., Apell, H. J., Garty, H., and Karlish, S. J. (2011) *J. Biol. Chem.* 286: 9699-9712
- Cirri, E., Katz, A., Mishra, N. K., Belogus, T., Lifshitz, Y., Garty, H., Karlish, S. J., and Apell, H. J. (2011) *Biochemistry* 50: 3736-3748

Summary (German)

Die Na,K-ATPase ist ein integrales Membranprotein in allen tierischen Zellen, in denen sie Na^+- und K^+-Ionen durch die Plasmamembran befördert und dabei ATP als Energiequelle benutzt. Für jedes hydrolysierte ATP-Molekül befördert das Enzym drei Na^+-Ionen aus und zwei K^+-Ionen in die Zelle. Wegen ihrer grundlegende Rolle bei vielen physiologischen Prozessen ist die Na,K-ATPase das Target von spezifischen regulatorischen Mechanismen. Unter diesen gibt es eine Enzymmodulation durch die Wechselwirkung mit den sogenannten FXYD Proteinen, eine Gruppe von kurzen Transmembran-Polypeptiden, die nach einem invarianten extrazellulären Motiv 'FXYD' benannt sind. Von allen Mitgliedern der FXYD-Familie in Säugetieren ist bekannt, dass sie mit der Na,K-ATPase assoziieren und deren Eigenschaften in einer Gewebe- und Isozym-spezifischen Weise modulieren. FXYD1, auch als Phospholemman bekannt, ist zuerst als das wichtigste Substrat für die Proteinkinasen A und C im Herz identifiziert worden. Erst anschließend wurde es entdeckt, dass es mit Isozymen der Na,K-ATPase assoziiert und die Enzymaktivität in Herz- und Skelettmuskeln sowie in der Niere und im Gehirn moduliert.

Bis jetzt ist die Effekte von FXYD1 an der Na,K-ATPase hauptsächlich in intakten Zellen, sowohl an heterologen Systemen und nativen Zellen untersucht worden. Diese Systeme ermöglichen eine gute Charakterisierung der physiologischen Effekte von FXYD1, aber sie sind nur von begrenztem Nutzen für die Untersuchung der funktionellen und strukturellen Wechselwirkungen zwischen dem Enzym und FXYD1. Eine Reinigungsprozedur für die menschlichen α_1/His_{10}-β_1 und α_2/His_{10}-β_1 Isozyme der Na, K-ATPase, exprimiert in der Hefe *P. pastoris*, ist kürzlich von der Gruppe von Steven Karlish am Weizmann Institute of Science entwickelt worden. Das gereinigte, solubilisierte α_1/His_{10}-β_1 Enzym kann *in vitro* mit gereinigtem, solubilisierten menschlichem FXYD1, das in *E. coli* exprimiert worden ist, rekonstituiert werden, um den α1/His10-β1/FXYD1-Komplex zu erhalten. Die gereinigten, rekombinanten Präparationen stellen ein System dar, das erlaubt, unter genau definierten Bedingungen und ohne Störung durch andere zelluläre Komponenten zu arbeiten. Im Gegensatz zu nativen Zellen können an den rekombinanten Präparationen die Effekte von FXYD1 auf die verschiedenen Isozyme der Na,K-ATPase separat untersucht werden. Weil die Phosphorylierung von FXYD1 in den gereinigten Präparationen gut steuerbar ist, kann auch die funktionale Rolle der Proteinkinasen-vermittelte Phosphorylierung von FXYD1 untersucht werden. Daher ermöglichen diese Systeme eine detaillierte Analyse der funktionalen Effekte von FXYD1 auf die Na,K-ATPase.

Die in unserem Labor etablierten biophysikalischen Techniken mit extrinsischen Fluoreszenzfarbstoffen ermöglichen eine gründliche Charakterisierung des Transport-Zyklus der Na,K-ATPase. Der elektrochrome Styrylfarbstoff RH421 erlaubt, die Ionenbewegungen in der Membrandomäne des Enzyms zu verfolgen, um Ionenbindung und -freisetzung während des Transportzyklus zu ermitteln. Darüber hinaus liefert der zeitliche Verlauf der Signale Information über die Kinetik der Prozesse. Im Gegensatz dazu wurde der potenzial-sensitive Farbstoff Oxonol VI erfolgreich eingesetzt, um den Ionentransport der Na,K-ATPase, die in Lipidvesikeln rekonstituiert wurde, erfolgreich zu ermitteln.

In einem ersten Schritt wurde in der vorliegenden Studie der Farbstoff RH421 eingesetzt, um an den gereinigten α_1/His_{10}-β_1 und α_2/His_{10}-β_1 Isozymen nachzuweisen, dass es möglich ist, an solubilisierten Ionenpumpen die Ionen-Bindungskinetik zu untersuchen, und dass die funktionellen Eigenschaften der gereinigten, rekombinanten Enzyme nicht wesentlich von denen der Membran-gebundenen, nativen Na, K-ATPase verschieden sind. Danach wurde der Farbstoff RH421 in stationären und zeitaufgelösten, kinetischen Messungen eingesetzt, um die Effekte von FXYD1 auf die verschiedenen Teilreaktionen des Transportzyklus des α_1/β_1-Isozyms der Na, K-ATPase zu charakterisieren. Diese Versuche haben gezeigt, dass

nur eine einzige kinetische Eigenschaft der Na,K-ATPase in der Anwesenheit von FXYD1 beeinflusst ist, die Na^+-Bindungsaffinität. Diese ist sowohl in der E_1- als auch P-E_2-Konformation um ~ 20-30% verstärkt. Im letzten Teil der Studie wurde der Einfluss der Membran- und ihre Lipidzusammensetzung auf den Effekt von FXYD1 auf die Na^+-Bindungsaffinität des Enzyms in Proteoliposomen mit dem potenzialsensitiven Oxonol VI untersucht. Dabei wurden α_1/His_{10}-β_1 oder α_1/His_{10}-β_1/FXYD1 Komplexe verglichen. Diese Versuche haben eine unerwartete Rolle des umgebenden Lipids auf die Wechselwirkung zwischen FXYD1 und dem Enzym erkennen lassen, die wahrscheinlich auf das zytoplasmatische Segment des regulatorischen Proteins zurückzuführen ist.

Ein Teil der in dieser Arbeit vorgestellten Ergebnisse sind bereit publiziert worden in

- Habeck, M., Cirri, E., Katz, A., Karlish, S. J., and Apell, H. J. (2009) *Biochemistry* 48: 9147-9155
- Mishra, N. K., Peleg, Y., Cirri, E., Belogus, T., Lifshitz, Y., Voelker, D. R., Apell, H. J., Garty, H., and Karlish, S. J. (2011) *J. Biol. Chem.* 286: 9699-9712
- Cirri, E., Katz, A., Mishra, N. K., Belogus, T., Lifshitz, Y., Garty, H., Karlish, S. J., and Apell, H. J. (2011) *Biochemistry* 50: 3736-3748

CHAPTER 1

INTRODUCTION

1.1 Membrane Transport

All living cells are surrounded by a biological membrane that separates the intracellular content from the outside environment. Moreover, eukaryotic cells have additional internal membranes that form different intracellular compartments like the nucleus, the endoplasmic reticulum, and the Golgi apparatus, as well as mitochondria, chloroplasts, and lysosomes. The basic structure of all biological membranes is a lipid bilayer with a thickness of ~ 75 Å (1) (Fig.1). In the physiological aqueous environment, lipid molecules assemble spontaneously with their hydrophilic polar head oriented toward the aqueous medium and their hydrophobic apolar portion inside the bilayer. Due to its hydrophobic interior, the lipid bilayer allows passive diffusion of lipophilic compounds, small apolar molecules like O_2 and CO_2, and small neutral, polar molecules like H_2O (2). In contrast, it acts as a barrier against hydrophilic compounds, and it is almost completely impermeable to ions and large polar molecules.

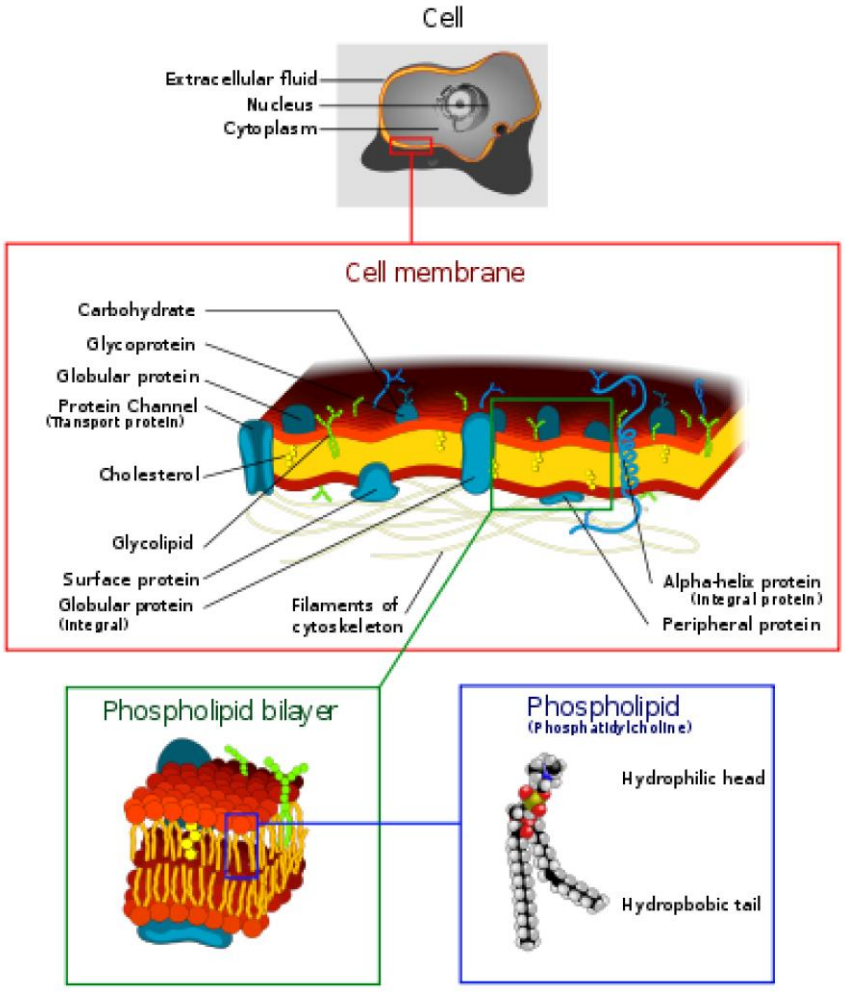

Figure 1. Illustration of an eukaryotic cell membrane with focus on its lipid component (3).

Besides the lipid bilayer, biological membranes also contain a protein fraction (Fig. 2). Membrane proteins represent on average ~ 50% of the membrane mass (2) and carry out almost all its biological functions: they can have a structural role, act as receptors or enzymes, or be involved in the transport of solutes across the membrane. Each membrane is characterized by a different amount and set of proteins depending on cell type and subcellular location. Membrane proteins are classified according to their association with the lipid bilayer. *Integral membrane proteins* are bound firmly to the lipid bilayer by hydrophobic interactions with its apolar interior. They can span the membrane partly or completely. Because of their strong association, these proteins can be removed only by treatment with detergent or organic solvents, able to impair the hydrophobic interactions inside the lipid bilayer. In contrast, *peripheral membrane proteins* do not penetrate the lipid bilayer hydrophobic core. They are weakly associated to the membrane surface by electrostatic interactions or hydrogen bonds with the lipid polar head groups or with integral membrane proteins. They can be removed by treatments with electrolytic solutions without altering the membrane integrity.

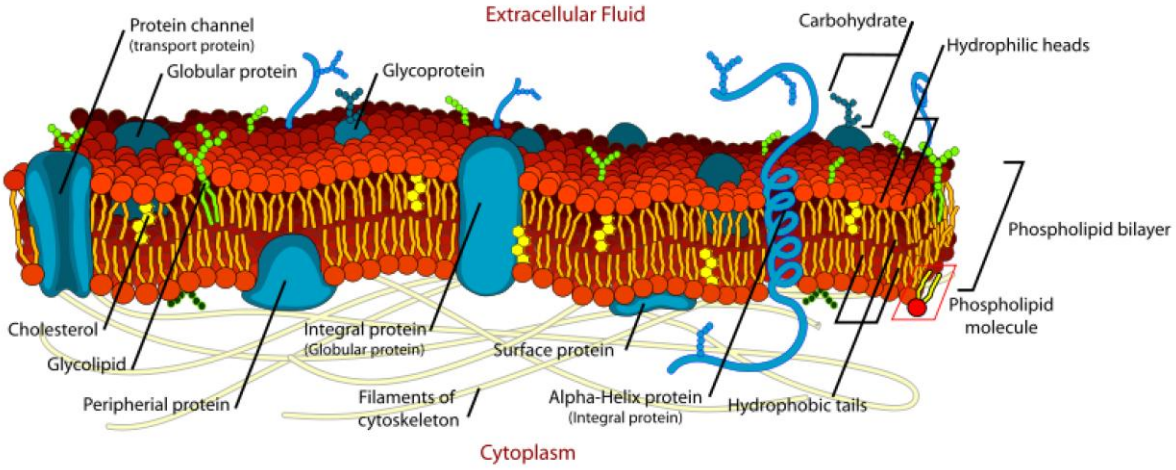

Figure 2. Illustration of an eukaryotic cell membrane with focus on its protein component (4).

To survive and grow, cells need to exchange many substances with the extracellular environment. For example, they require the uptake of nutrients like carbohydrates and amino acids, the expulsion of waste products of their metabolism, and the regulation of the intracellular concentration of inorganic ions. All membrane proteins involved in the transport of solutes across the lipid bilayer are integral membrane proteins. They can mediate *passive* or *active transport*, depending on whether the movement occurs down or up the electrochemical gradient of the transported species (Fig. 3). Active transport requires energy to occur. When the energy derives from an external source such as sun light, a redox reaction, or the hydrolysis of ATP, it is defined as *primary active transport*. In contrast, *secondary active transport* exploits the energy made available from passive co-transport of a second species. In case of transport of two species, it is possible to distinguish between *symport* and *antiport* when the species are moved in the same or in the opposite direction, respectively. Finally, if the transport determines the movement of a net electric charge across the membrane it is defined as *electrogenic*, otherwise as *electro-neutral*.

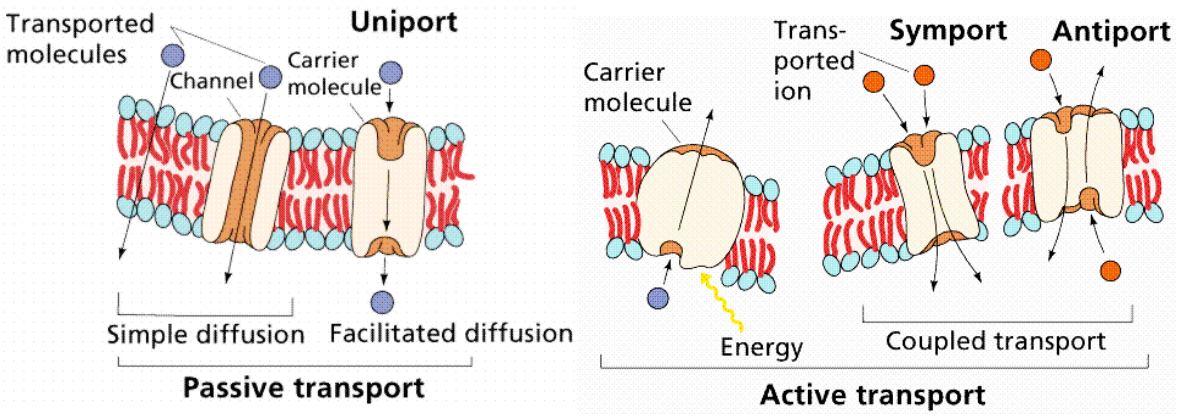

Figure 3. Different types of membrane transport (5).

The cytoplasmic ion composition of a cell is very different from that of the extracellular solution. Sodium and chloride are the most abundant ions in the extracellular matrix, while potassium is the main cation in the cytosol. This difference is fundamental for cell survival. For example, it is necessary for the regulation of form and cell volume as well as pH, for the uptake of nutrients and neurotransmitters, and for cell excitability. The ion transport systems of the membrane are ion channels, ion pumps, and ion exchangers. *Ion channels* function as selective pores that open in response to a chemical or electrophysiological stimulus, allowing the movement of specific ion species in the direction of their electrochemical gradient. Their selectivity depends on the pore diameter and on the amino acid distribution along the channel walls. *Ion pumps* are able to transport ions against their electrochemical gradient using a primary source of energy. Finally, *ion exchangers* are active secondary transporters that use the movement of ions down their electrochemical gradient to co-transport other ions against their gradient. Moreover, lipid-soluble molecules called *ionophores* are able to form membrane channels or complexes with specific ion species and transport them across the lipid bilayer following the ion electrochemical gradient. Many antibiotics and toxins belong to this last group.

1.2 Ion Pumps

Ion pumps are distinguished based on the energy source exploited to sustain the active transport. The energy can derive from the absorption of light or from a chemical reaction like a redox reaction, a decarboxylation reaction, the hydrolysis of pyrophosphate, or the hydrolysis of ATP. A few examples are reported below (6).

Bacteriorhodopsin and Halorhodopsin are light-activated transporters of H^+ and Cl^- ions, respectively. They are found in the cell membrane of halophilic archaebacteria and represent probably the most ancient and structurally simple class of ion pumps. In these proteins, the absorbance of a photon by a chromophore covalently bound to the polypeptide chain induces the conformational changes required to carry on the transport cycle.

Cytochrome c oxidase exploits the energy released by a redox reaction. It is found in the inner mitochondrial membrane of eukaryotic cells where it reduces O_2 to H_2O in the respiratory chain. The energy released in the reaction is used to pump two protons in the intermembrane space of the mitochondria, contributing to the generation of a proton gradient exploited by the ATP synthase to produce ATP.

A particular type of bacterial ion pumps exploits the energy released by decarboxylation reactions to move Na^+ ions across the cell membrane. Among them, oxaloacetate decarboxylase couples the transport to the decomposition of oxaloacetate in pyruvate and carbonic anhydride.

A unique ion pump is the H^+-pyrophosphatase in the vacuolar membrane of higher plants: it transports protons from the cytoplasm into the lumen of the vacuole using the hydrolysis of pyrophosphate as energy source.

The energy source mainly exploited by ion pumps is hydrolysis of ATP in ADP and inorganic phosphate (Fig. 4). These protein systems are called ATPases and represent the largest and most diverse class of ion pumps.

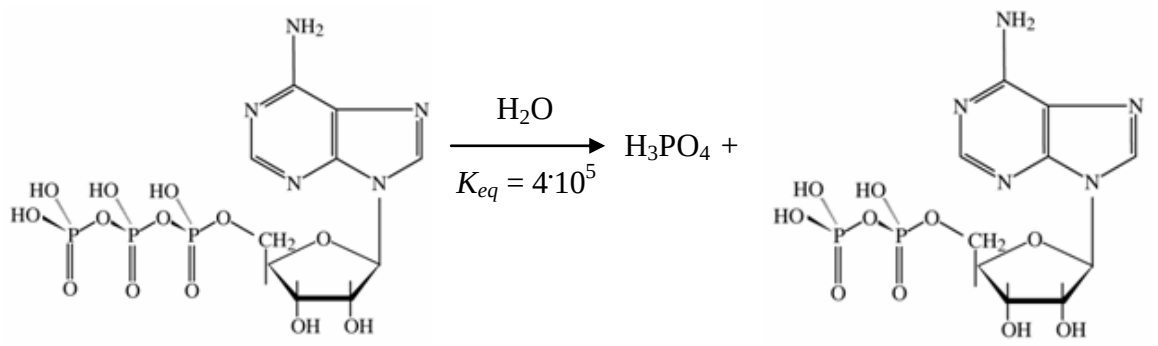

$$\Delta G = RT \ln \frac{[ADP]\cdot[P_i]}{[ATP]} - RT \ln K_{eq} \cong -55\text{kJ/mol}$$

Figure 4. Hydrolysis of ATP in ADP and inorganic phosphate (P_i). The Gibbs free energy, ΔG, released in this reaction is calculated on the basis of the physiological concentrations [*ATP*] ~ 8 mM, [*ADP*] ~ 40 μM and [P_i] ~ 8 mM. It is exploited by ion-transporting ATPases for the active transport of ions (7).

1.2.1 ATPases

Ion-transporting ATPases can be subdivided in three main groups according to their structural and functional features, and to their localization (Fig. 5):

- *F-type ATPases* mediate proton transport across bacterial membranes as well as in the inner mitochondrial membrane and in the thylakoid membrane of chloroplasts (8,9). In contrast to the other ATPases, in physiological conditions F-type ATPases work in the reverse mode, exploiting the energy of a passive proton flow to synthesize ATP from ADP and inorganic phosphate. Therefore, these enzymes are more properly called ATP synthases. F-type ATPases are constituted of a soluble portion, F_1, and a membrane-bound portion, F_o. They have a complex quaternary structure, with F_1 and F_o formed by assemblies of five ($\alpha_3\beta_3\gamma\delta\varepsilon$) and three ($ab_2c_{10\text{-}14}$) subunits, respectively. The peripheral hexamer $\alpha_3\beta_3$ forms the catalytic domain, responsible for ATP synthesis, and is connected to the transmembrane domain, involved in proton translocation, by the $\gamma\varepsilon ab_2$ complex, the so-called stalk. The proposed catalytic model is known as "rotary binding-change mechanism": the proton flow across the membrane via the F_o domain induces the rotation of the transmembrane ring of c subunits and, as a consequence, the γ subunit of the stalk rotates, causing sequential conformational changes in the catalytic $\alpha_3\beta_3$ hexamer that lead to ATP synthesis. Under appropriate conditions, the enzyme reaction can be carried out also in the opposite mode, with ATP hydrolysis driving proton pumping across the membrane.

- *V-type ATPases* are proton ATPases that regulate the acidification of intracellular compartments like clathrin-coated vesicles, endosomes, lysosomes, Golgi-derived vesicles, secretory vesicles, and vacuoles of fungi and plants (10,11). In certain cases, they also transport protons across the plasma membrane of eukaryotic and prokaryotic cells. The structure of V-type ATPases is similar to that of F-type ATPases. They are composed of a peripheral V_1 portion, where ATP hydrolysis occurs, and an integral V_0 domain, responsible for proton translocation. V_1 is a complex of eight different subunits ($A_3B_3CDEFG_2H_{1\text{-}2}$), while V_0 contains five different subunits ($adc_{4\text{-}5}c'c''$). The catalytic mechanism is also supposed to be similar, but works in the opposite direction under physiological conditions: ATP hydrolysis at the catalytic hexamer A_3B_3 induces the rotation of the central stalk, composed of the D and F subunits; the movement drives the rotation of the transmembrane ring of c, c' and c'' subunits that pumps protons against their electrochemical gradient. This mechanism is reversible under non-physiological conditions.

- *P-type ATPases* can transport both small cations like H^+, Na^+, K^+, Ca^{2+}, and Mg^{2+}, and transition metals like Cu^+, Ag^+, Cu^{2+}, Zn^{2+}, Co^{2+}, Cd^{2+}, and Pb^{2+} across eukaryotic and prokaryotic membranes. They have very different structure and catalytic mechanism compared to F-type and V-type ATPases. Since the Na,K-ATPase belongs to this class, P-type ATPases are discussed in detail in paragraph *1.2.2*.

Besides the classes of ion-transporting ATPases described above, a group of *ATP-binding cassette (ABC) transporters* are able to carry out the active transport of ions across the membranes of both eukaryotic and prokaryotic cells (10,11) (Fig. 5). ABC transporters form the largest class of ATP-consuming transporters (12) and can couple the hydrolysis of ATP to the transport of a variety of substrates, including ions: prokaryotes present both importers for nutrients uptake (amino acids, sugars, metal ions, peptides) and exporters (drugs, toxins, polysaccharides, lipids), while eukaryotes have only exporters. They consist of one, two, or

four polypeptide chains organized in two transmembrane and two ATP-binding domains. During transport, the transmembrane portion assumes two different conformations characterized by a different affinity for the substrate and with the substrate-binding site facing outward or inward. Despite a number of potential models, the molecular mechanism that couples ATP hydrolysis and membrane transport is still unclear.

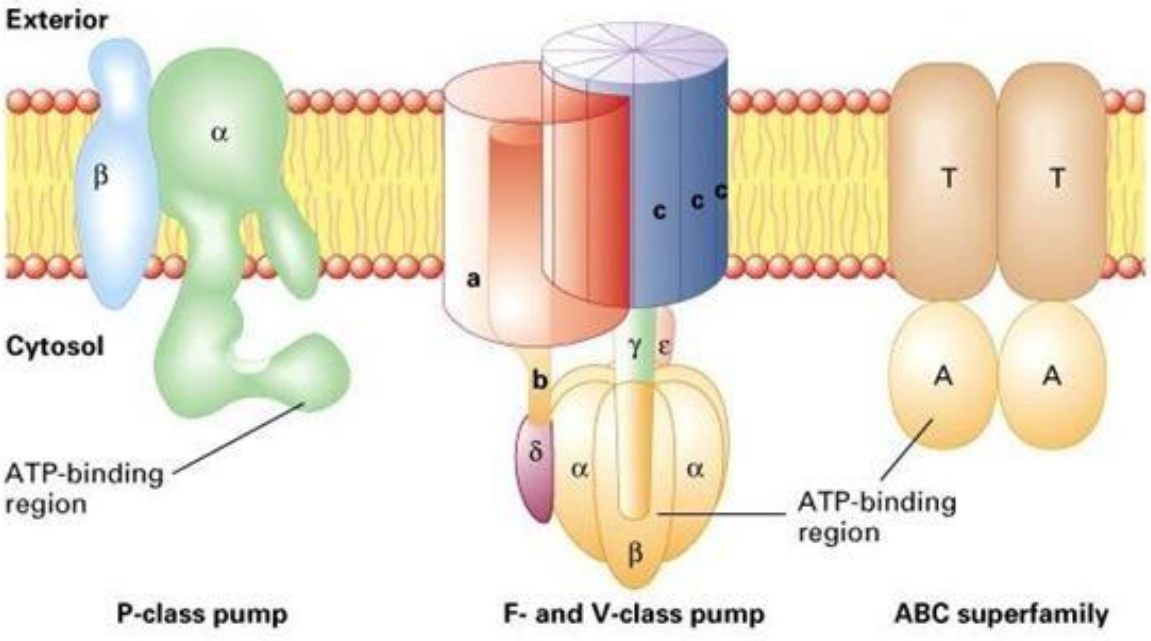

Figure 5. Classes of ATP-consuming ion transporters (13).

1.2.2 P-type ATPases

P-type ATPases are the most intensively studied and best characterized ion-transporting ATPases (14,15). With few exceptions, they are constituted of a single subunit with a molecular mass between 70 and 150 kDa that carries out both ATP hydrolysis and ion transport. Despite a low degree of sequence conservation, they all present a similar tertiary structure. Both the N- and C-terminal sequences are located on the cytoplasmic side of the membrane so that (almost) all P-type ATPases are characterized by an even number of transmembrane segments. The cytoplasmic portion is organized in several domains that play specific roles in coupling ATP hydrolysis and ion transport. During the transport cycle, P-type ATPases assume two different conformations in which the ion-binding sites, located in the transmembrane domain, face one side of the membrane or the other. Moreover, in contrast to the other ion-transporting ATPases, they form a phosphorylated intermediate where the phosphate is covalently bound to an Asp residue. Indeed, the name "P-type" is derived from this distinctive feature.

Based on their sequence homology, the P-type ATPase family can be divided in 5 subclasses (14,15):

- *P1* are the simplest and probably most ancient P-type ATPases. P1A is a small class of bacterial ion pumps; the most important is the KdpB-ATPase of *E. coli* that shows unique features. In contrast to the other P-type ATPases, KdpB is associated in a complex with three additional subunits, KdpF, KdpA, and KdpC. Moreover, ATP hydrolysis and K^+ ions transport occur in two different subunits, KdpB and KdpA, respectively.

P1B-ATPases are a group of heavy metals ion pumps, able to transport both monovalent (Cu^{+}, Ag^{+}) and divalent cations (Cu^{2+}, Zn^{2+}, Co^{2+}, Cd^{2+}, Pb^{2+}). They are responsible for both the uptake of heavy metals required for the maturation of metalloproteins and the extrusion of toxic ions from the cell. They represent the most common P-type ATPases in bacteria, but are also present in eukaryotic cells, where they may have important biological functions. For example, mutations in the human Cu-ATPase causes the Menkes and Wilson diseases, related to disorders in copper metabolism.

- *P2* are the most diverse P-type ATPases. Many of them have fundamental physiological roles in animal cells. P2A and P2B are both groups of Ca-ATPases. P2A Ca-ATPases are common in bacteria, while in animal cells they are localized specifically in the endoplasmic reticulum. In particular, in muscle cells they are located in the sarco(endo)-plasmic reticulum and, thus, are named SERCA, sarcoplasmic reticulum calcium pumps. After muscle contraction, SERCA molecules load Ca^{2+} ions back into the sarcoplasmic reticulum, reducing the intracellular Ca^{2+} concentration and contributing significantly to the muscle relaxation process. P2B Ca-ATPases are localized only in the plasma membrane of animal cells, while they have a wider distribution in plants and fungi. P2C includes the Na,K-ATPase and the gastric H,K-ATPase. They are composed of more than one essential subunit, with the heavily glycosylated, single membrane-spanning β subunit associated to the catalytic α subunit. The Na,K-ATPase is present in virtually all animal cells, where it maintains the Na^{+} and K^{+} ion gradients across the plasma membrane. It is the transport system that mainly contributes to the transmembrane potential of animal cells. The gastric H,K-ATPase is localized specifically in the parietal cells of the stomach mucosa and is responsible for the acidification of the stomach content. The P2D class is a group of eukaryotic Na-ATPases.

- Among *P3*, P3A are H-ATPases found almost exclusively in the plasma membrane of plants and fungi. They maintain an intracellular pH of ~ 6.6 against an extracellular pH of 3.5, generating a transmembrane potential of -180 mV. Indeed, in plant and fungi cells the transmembrane potential is essentially protonic, since the Na,K-ATPase is absent in these organisms. Type P3B corresponds to a small class of bacterial Mg-ATPases.

- *P4*-ATPases have been found so far only in eukaryotic cells, where they are involved in the maintenance of the lipid bilayer asymmetry by promoting phospholipids flipping across the membrane. These enzymes are called *flippases,* and their transport mechanism is still unclear. It has been hypothesized that they are ion pumps working in close association with ion-dependent lipid transporters. In most eukaryotes, they represent the largest class of P-type ATPases.

- Finally, *P5* are eukaryotic ATPases, but their specific substrates and biological roles are still unknown. They can be divided in two subgroups, P5A and P5B, with a different intracellular localization: P5A pumps are found exclusively in the endoplasmic reticulum, whereas P5B are located in lysosomes (humans), vacuoles (yeast), and plasma membrane (*C. elegans*).

  A summarizing overview is presented in Table 1.

Type	Subtype	Transported ions	Distribution
P1	P1A	K^+	*E. coli*
	P1B	Cu^+, Ag^+, Cu^{2+}, Zn^{2+}, Co^{2+}, Cd^{2+}, Pb^{2+}	Bacteria, Eukaryotes
P2	P2A	Ca^{2+}	Bacteria, Animals
	P2B	Ca^{2+}	Eukaryotes
	P2C	Na^+, K^+, H^+	Animals
	P2D	Na^+	Eukaryotes
P3	P3A	H^+	Plants, Fungi
	P3B	Mg^{2+}	Bacteria
P4	-	Lipids (coupled with ions)	Eukaryotes
P5	P5A, P5B	Unknown	Eukaryotes

Table 1. Classification of P-type ATPases.

1.3 The Na,K-ATPase

1.3.1 Function and Physiological Roles

The Na,K-ATPase is an integral membrane protein present in virtually all animal cells, where it actively transports Na^+ and K^+ ions across the plasma membrane. For every ATP molecule hydrolyzed, the enzyme pumps three Na^+ ions out of and two K^+ ions into the cell (Fig. 6).

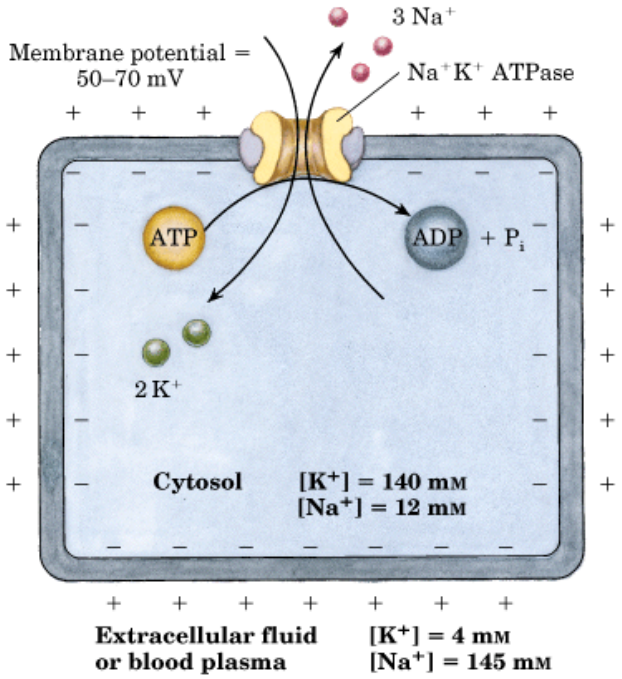

Figure 6. The Na,K-ATPase pumps three Na^+ ions out of and two K^+ ions into the cell using ATP as energy source. The transport generates electrochemical gradients for both sodium and potassium across the plasma membrane, contributing to the creation of a transmembrane potential (7).

The electrogenic transport generates electrochemical gradients for both sodium and potassium across the plasma membrane that are fundamental for cell survival. The sodium gradient is exploited by secondary active transport systems for the uptake of nutrients (glucose, vitamins, amino acids) and neurotransmitters as well as for the extrusion of H^+ and Ca^{2+} ions via the Na/H- and Na/Ca-exchangers. Therefore, the Na,K-ATPase is involved in the regulation of shape and cell volume as well as intracellular pH and calcium concentration. Moreover, the electrochemical gradients of Cl^-, Na^+ and, predominantly, K^+ ions create the transmembrane electric potential, which is essential for the electrical excitability of cells. Considering its importance, a large fraction of the energy consumed in the cell is used to operate this transporter. At rest, about 25% of ATP is consumed by the Na,K-ATPase, a fraction that can increase up to 70% in the nervous system (7).

The Na,K-ATPase plays a fundamental role in many physiological processes. In kidneys, the enzyme regulates the reabsorption of sodium, potassium, and water across the epithelium, maintaining the osmotic equilibrium (Fig. 7). Moreover, the sodium gradient generated by the enzyme is exploited by other transporters for the reabsorption of glucose, vitamins, and Cl^- ions that would be lost otherwise in large amounts by urine excretion. Similar mechanisms for the absorption of the various solutes are present in the intestine.

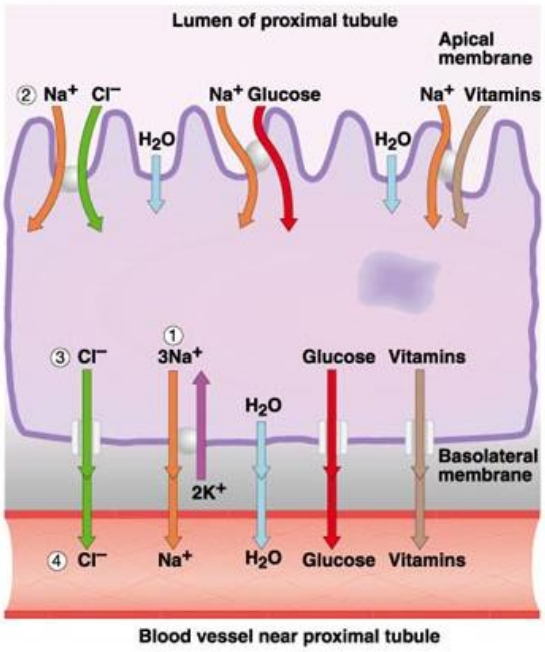

Figure 7. Reabsorption of solutes and water in kidneys (16).

In muscle and neuronal cells, the Na,K-ATPase is required to maintain electrical excitability. Following action potentials, the sodium and potassium gradients across the cell membrane are significantly reduced. If the electrochemical gradients are not re-established by the enzyme, continuous stimulation determines leveling of the gradients and loss of electrical excitability. Moreover, in muscle cells the enzyme acts indirectly as a regulator of contraction, since it affects the intracellular calcium concentration via the Na/Ca-exchanger.

Incorrect function of the Na,K-ATPase can result in severe pathologies. For example, impairment of the enzyme in kidney and small intestine can be associated with hypertension and chronic diarrhoea, respectively (17).

1.3.2 Transport Mechanism

The model for the transport mechanism of the Na,K-ATPase was first proposed by R. W. Albers (18) and R. L. Post (19) and it is therefore known as *Post-Albers cycle* (Fig. 8). During the cycle, the Na,K-ATPase assumes two different conformations, E_1 and E_2, with the ion-binding sites facing the cytoplasmic and the extracellular side of the membrane, respectively. The two conformations show different affinities for Na^+ and K^+ ions (see *4.3*), which are transported sequentially in a so-called *ping-pong mechanism* (6,20). The K^+ ions and the first two Na^+ ions bind to the same ion-binding sites, called *bifunctional*, while the third Na^+ ion binds to a Na^+-specific ion-binding site. During the transport, the ion-binding sites remain more or less in the same position inside the membrane dielectric; the protein movements due to the conformational transitions open and close alternatively the access to the ion-binding sites on the two sides of the membrane (21).

In physiological conditions, the unphosphorylated protein binds ATP that shifts the conformational equilibrium towards E_1. In the E_1 conformation, the enzyme binds three Na^+ ions from the cytoplasmic side. The third Na^+-specific ion-binding site becomes available only after the first two Na^+ ions are bound to the bifunctional ion-binding sites. Binding of the three Na^+ ions allows phosphorylation of the protein by ATP in the presence of Mg^{2+} as cofactor. Phosphorylation induces the conformational transition via the intermediate,

occluded state, $(Na_3)E_1$-P, where the bound ions are unable to exchange with the aqueous media. In the phosphorylated E_2 conformation, the ion-binding sites face the extracellular medium. The enzyme has a significantly lower Na^+-binding affinity and it releases the Na^+ ions at the extracellular side.

$$E_1{\cdot}ATP + 3\ Na^+ \rightarrow Na_3E_1{\cdot}ATP \rightarrow (Na_3)E_1\text{-}P \rightarrow P\text{-}E_2Na_3 \rightarrow P\text{-}E_2 + 3\ Na^+$$

Binding of two K^+ ions at the extracellular side stimulates dephosphorylation, followed by the conformational transition back to E_1 via the intermediate occluded state $E_2(K_2)$. In the E_1 conformation, the enzyme releases the K^+ ions at the cytoplasmic side and is ready to start a new transport cycle.

$$P\text{-}E_2 + 2\ K^+ \rightarrow P\text{-}E_2K_2 \rightarrow E_2(K_2) + Pi \rightarrow K_2E_1 \rightarrow E_1 + 2\ K^+$$

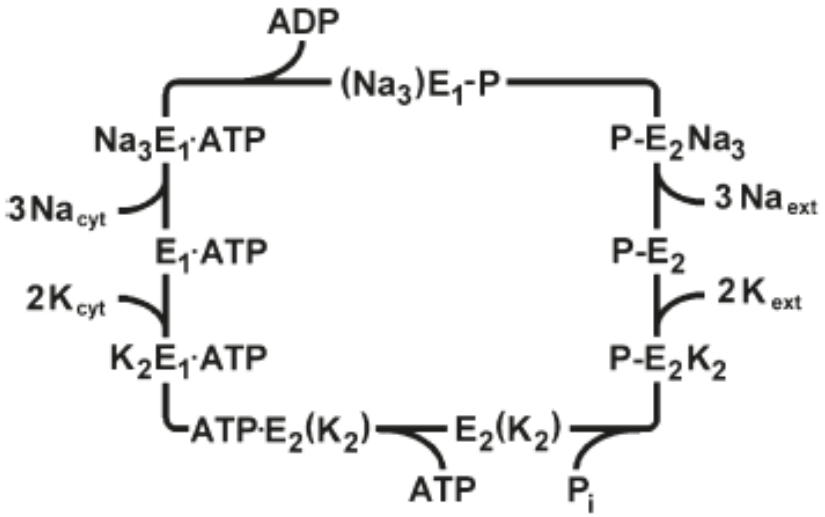

Figure 8. The transport mechanism of the Na,K-ATPase, known as Post-Albers cycle (22).

1.3.3 Structure and Isoforms

The minimal functional unit of the Na,K-ATPase consists of two subunits, the α and the β subunit. The α subunit is responsible for the catalytic activity and contains the binding sites for Na^+ and K^+ ions in the transmembrane domain and for ATP in the cytoplasmic portion. It is homologous to the single subunit of the monomeric P-type ATPases like the SERCA. The β subunit is a glycoprotein unique to the K^+-counter-transporting P-type ATPases, Na,K-ATPase and H,K-ATPase. In addition, a third subunit is present that belongs to the family of FXYD proteins. This subunit is not required for the enzyme function, but modulates its transport properties (see *1.4*).

The α subunit is constituted of about 1000 amino acid residues and has a molecular mass of ~ 112 kDa (23). It is organized in 10 transmembrane α-helices (M1-M10) connected by two large cytoplasmic loops that form three distinct domains: the phosphorylation domain (P), the nucleotide (ATP)-binding domain (N), and the so-called actuator domain (A) (15) (Fig. 9). The P domain is highly conserved among all P-type ATPases and it is formed by the loop between M4 and M5. During each catalytic cycle, it is phosphorylated at the Asp residue located in the conserved sequence Asp-Lys-Thr-Gly (DKTG), corresponding to Asp 369 in the Na,K-ATPase. The N domain is a modular insertion into the P domain. It binds

ATP via interactions with the adenosine part, leaving the three phosphate groups protruding away from the binding site. Finally, the A domain is a globular module connected to M1, M2, and M3 by flexible linkers. It contains the signature motif Thr-Gly-Glu (TGE), common to all P-type ATPases.

Figure 9. Schematic structure of the α subunit of the Na,K-ATPase, showing the transmembrane

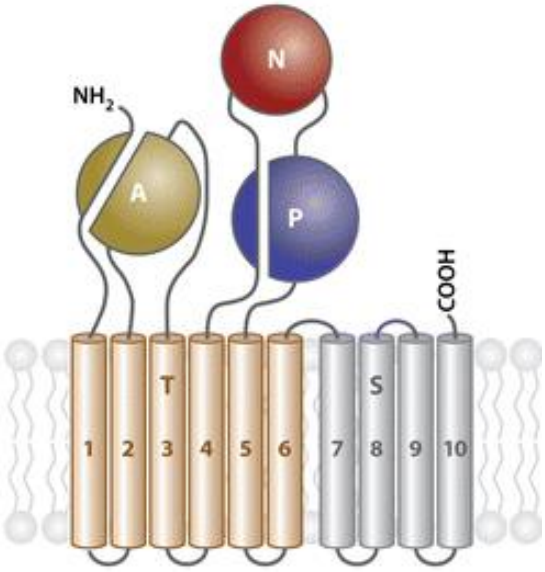

segments and the cytoplasmic domains (15).

The β subunit contains about 300 residues and has a molecular mass between 40 and 60 kDa, depending on the degree of glycosylation (23). It is characterized by a single transmembrane α-helix (βM) and a large extracellular C-terminal domain containing three disulfide bonds and a different number of glycosylation sites depending on the isoform (23). The β subunit is required for the delivery of the α subunit from the endoplasmic reticulum to the plasma membrane as well as its correct membrane integration and packing, necessary for the protection of the enzyme against cellular degradation and for the acquisition of its functional properties (10,24,25). Moreover, the β subunit is involved in the occlusion of K^+ ions during the transport cycle (24-26). Reduction of the disulfide bonds in the extracellular domain results in loss of enzyme activity (10,26), while deglycosylation has little effect, indicating that it is not required for functional activity (10,27).

Overall, the enzyme is extended for at least 4 nm on the cytoplasmic side of the membrane and 2 nm on the extracellular side (7). About 40% of the protein molecular mass is situated in the lipid bilayer, another 40% is in the cytoplasm, and the remaining 20% is on the extracellular side (7).

Four different α and three distinct β isoforms have been identified in mammalian cells (23). The α isoforms vary slightly in length, with α_3 being the smallest and α_4 the largest. The degree of identity across species is ~ 92% between α_1 and α_2, and over 96% between α_1 and α_3. In contrast, α_4 is the most divergent, sharing 78% identity with α_1. The highest structural variability among the isoforms occurs at the N-terminal sequence, while the greatest similarities are in the cytoplasmic region where the ATP-binding and phosphorylation sites are located, in the transmembrane domain, and in the C-terminal sequence. The homology among different β isoforms is lower than that found for the catalytic subunit. Compared with β_1, β_2 exhibits 34% identity and β_3 39%. 49% of the residues are conserved between β_2 and β_3. The transmembrane domain is the most highly conserved region, while the extracellular domain presents a variable number of glycosylation sites depending on isoform and species.

Expression of both α and β isoforms is tissue- and species-dependent (23). In rats, the $\alpha_1\beta_1$ isozyme is found in nearly every tissue and is the principal isozyme in the kidney, where the α_2 and α_3 isoforms correspond to only 0.1% of the total enzyme. In contrast to the broad tissue distribution of α_1 and β_1, the other α and β polypeptides are more restricted in their expression. The α_2 isoform predominates in muscle, heart, brain, and adipocytes, while α_3 is abundant in nervous tissues and α_4 is testis-specific. The β isoforms are also distributed in a tissue-dependent manner. The β_2 isoform is found in skeletal muscle, pineal gland, and nervous tissues, whereas β_3 is present in testis, retina, liver, and lung. The expression pattern of the various isozymes is subjected to developmental as well as hormonal regulation and can be altered during pathological states.

The different isozymes of the Na,K-ATPase show distinct functional properties. The specific properties of the various human αβ isozymes have been investigated recently upon expression in *X. oocytes* (28). The distinct functional properties and the specific localization of the Na,K-ATPase isozymes contribute to differentiate the enzyme function.

Recently, the crystal structure of the pig kidney Na,K-ATPase ($\alpha_1\beta_1$FXYD2) has been published with a resolution of 3.5 Å (29), followed by the one of the ion pump from shark rectal glands ($\alpha_1\beta_1$FXYD10) at 2.4 Å resolution (30) (Fig. 10). Both ion pumps have been crystallized in the presence of the phosphate analogue MgF_4^{2-} and two bound Rb^+ or K^+ ions, respectively. Therefore, both structures represent the occluded state $Pi{\cdot}E_2(K_2)$.

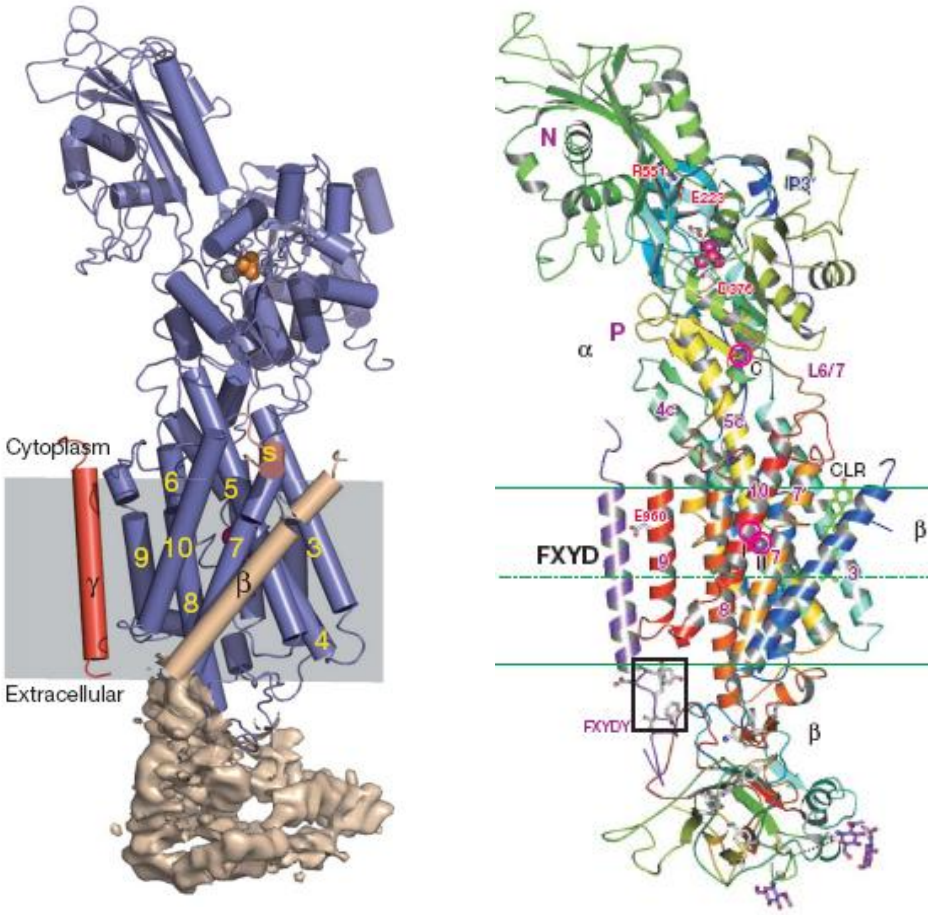

Figure 10. Crystal structures of the pig kidney (left) and the shark (right) Na,K-ATPase. In the first structure (29), the α subunit is shown in blue, the β subunit in pink, and FXYD2 (γ) in red. The phosphate analogue MgF_4^{2-} is orange and grey, and the two bound Rb^+ ions are purple. In the second structure (30), the β subunit is shown in blue, and FXYD10 in violet. The phosphate analogue MgF_4^{2-} is purple, and the two bound K^+ ions are violet.

The high resolution of the second structure has allowed the identification of the amino acid residues involved in K^+ binding. The two K^+ ions are bound in the transmembrane domain between helices M4, M5, and M6 of the α subunit, inside the same cavity. Site I is made of five oxygen atoms, provided by one main chain carbonyl (Thr 779), three side chain oxygen atoms (Ser 782, Asn 783, and Asp 811), and one water molecule. Site II is shifted of 1.3 Å toward the extracellular side. The K^+ ion is coordinated by three main chain carbonyls (Val 329, Glu 786, Asp 811, and possibly Val 332), and three or four side chain oxygen atoms (Asn 783, Glu 786, Asp 811, and possibly Glu 334).

According to the alternate access model, these two sites represent also two of the three binding sites for Na^+ ions. The third Na^+-selective ion-binding site is not visualized in the crystal structures. Previously, site-specific mutagenesis experiments proposed Tyr 771 (M5), Thr 807 (M6), and Glu 954 (M9) as ligands for the third Na^+ ion (29). In the first crystal structure, these residues are found to cluster with Asp 808 (M6) and Gln 923 (M8) that could be also part of the third ion-binding site (Fig. 11).

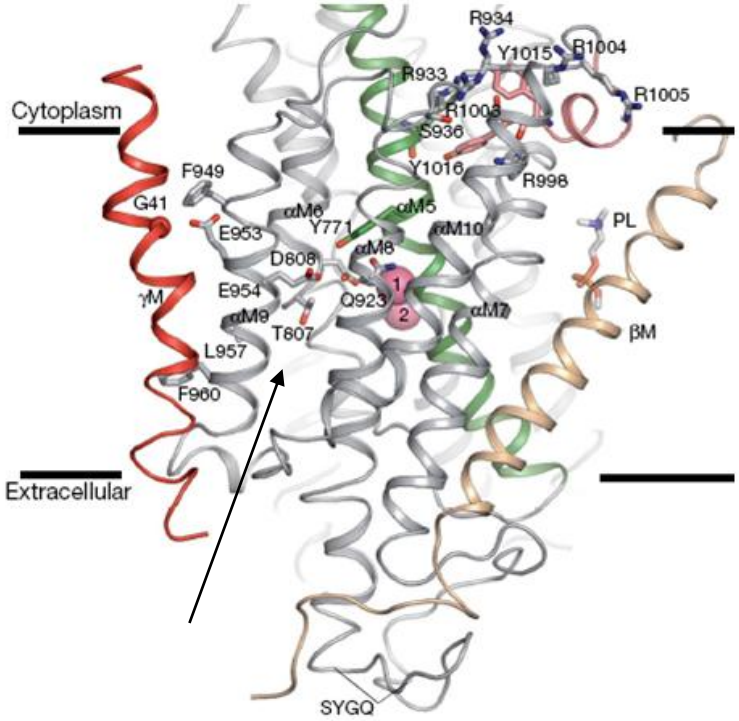

Figure 11. Side view of the transmembrane domain showing the putative location of the third Na^+-specific ion-binding site between helices M5, M6, M8 and M9 (29).

In both crystal structures, the transmembrane segment of the FXYD protein presents a mostly α-helical structure. It runs approximately perpendicular to the membrane plane and interacts almost exclusively with M9. In FXYD10, the extracellular motif FXYD interacts with both the α and the β subunit via hydrogen bonds and aromatic interactions (Fig. 12). The cytoplasmic segment could not be resolved in either structure, indicating that it is not specifically attached to the enzyme but highly flexible.

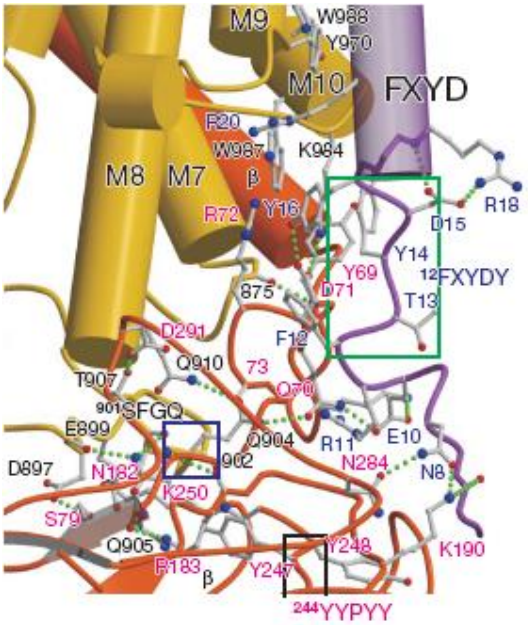

Figure 12. Cartoon highlighting the interactions between the extracellular segment of FXYD10 (violet) and the α (yellow) and β (orange) subunits; view approximately parallel to the membrane (30).

1.3.4 Molecular Mechanism

ATP hydrolysis and ion translocation occur in the cytoplasmic and in the transmembrane portion, respectively. Therefore, coupling of chemical reaction and transport must occur via conformational transitions involving the complete enzyme molecule (14,15). As already mentioned in the previous paragraph (*1.3.3*), the cytoplasmic portion of the α subunit is organized in P domain, N domain, and A domain. During the catalytic cycle of all P-type ATPases, the P domain interacts with the N domain and the A domain, leading to phosphorylation and dephosphorylation, respectively. These domains undergo large movements that, thanks to the connection with individual helices in the transmembrane portion, are transmitted to the transmembrane domain. In particular, rotational movements of the A domain cause the transmembrane helices M1-M4 to shift up and down, opening and closing alternatively the cytoplasmic and extracellular access channels to the ion-binding sites.

In physiological conditions, the unphosphorylated Na,K-ATPase binds ATP at the N domain. As a result, the conformational equilibrium is shifted towards E_1. The phosphate groups of ATP are close to the P domain, with the γ-phosphate approaching Asp 369. Phosphorylation is hindered, however, by the electrostatic repulsion between the γ-phosphate and the negatively charged lateral chains on the surface of the P domain. Binding of the third Na^+ ion induces a helix rearrangement in the transmembrane domain that is transmitted to the P domain, with the generation of a Mg^{2+}-binding site near Asp 369. Coordination of a Mg^{2+} ion by two conserved sequences of this domain, Thr-Gly-Asp-Asn (TGDN) and Gly-Asp-Gly-X-Asn-Asp (GDGXND), reduces the electrostatic repulsion, allowing phosphorylation to occur (Fig. 13). In this way a strict coupling between sodium binding and enzyme phosphorylation is obtained.

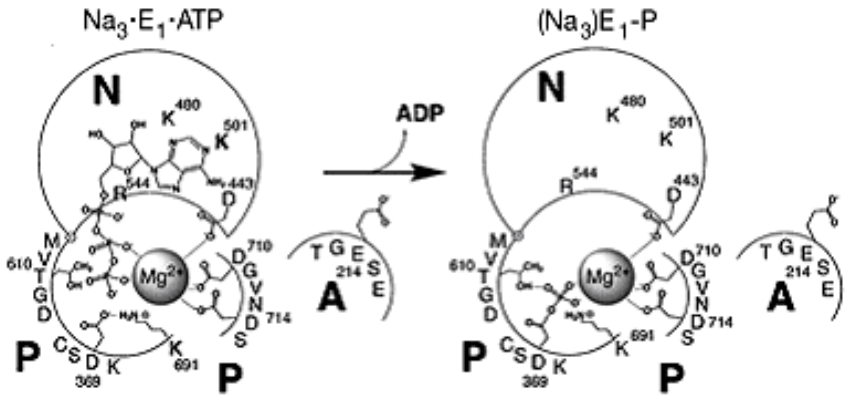

Figure 13. Coordination of Mg^{2+} and phosphorylation of the enzyme (31).

During phosphorylation, the A domain pulls helices M1 and M2 toward the cytoplasmic site, closing the cytoplasmic access channel to the ion-binding sites with the formation of the $(Na_3)E_1$-P occluded state. At this point, the A domain is able to rotate by about 90 ° on its vertical axis. This movement is transmitted to the transmembrane domain, where it leads to the opening of the extracellular access channel to the ion-binding sites and to a reorientation of the coordinating residues, changing the ion-binding affinities. These conformational changes correspond to the transition from E_1-P to P-E_2 (Fig. 14). The Na^+ ions are released on the extracellular side in exchange for two K^+ ions. Binding of K^+ ions induces a helix rearrangement in the transmembrane domain. This movement is transmitted to the P domain and causes a slight further rotation of the A domain, which shifts its conserved TGE motif in close proximity to the phosphorylated Asp. Substitution of the coordinating residues from the P domain with the TGE loop destabilizes the Mg^{2+}-binding site.

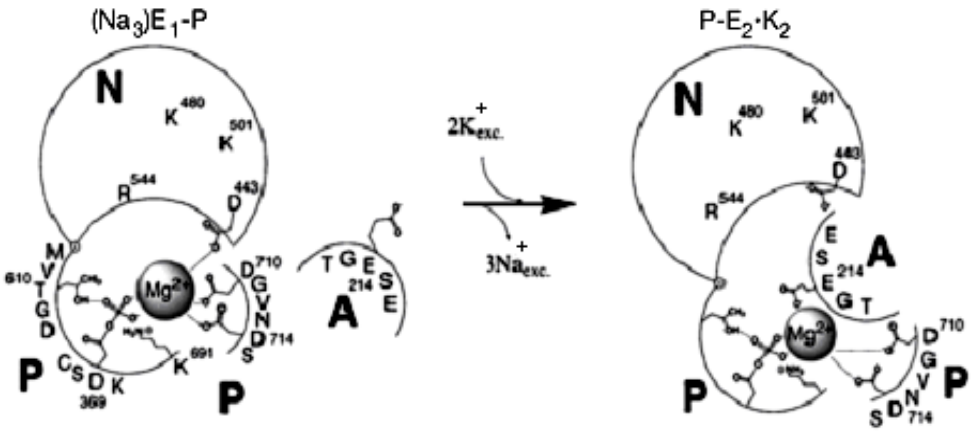

Figure 14. Conformational transition from E_1-P to P-E_2. Upon rotation of the A domain, the TGE motif of the A domain substitutes the residues from the P domain in the coordination of the Mg^{2+} ion (31).

As a result, a water molecule is able to carry out a nucleophilic attack on the phosphate bond, dephosphorylating the enzyme. Therefore, as binding of Na^+ ions is coupled to phosphorylation, binding of K^+ ions is coupled to dephosphorylation of the enzyme. Dephosphorylation results in ion occlusion. Release of phosphate and binding of ATP at the N domain lead to a rotation of the A domain away from the P domain, which then can interact again with the N domain. This reaction sequence is associated with helical movements in the transmembrane domain that change the ion-binding affinities and open the cytoplasmic

access channel. The enzyme is again in the E_1 conformation and can start a new transport cycle. This molecular mechanism is similar for all P-type ATPases (Fig. 15).

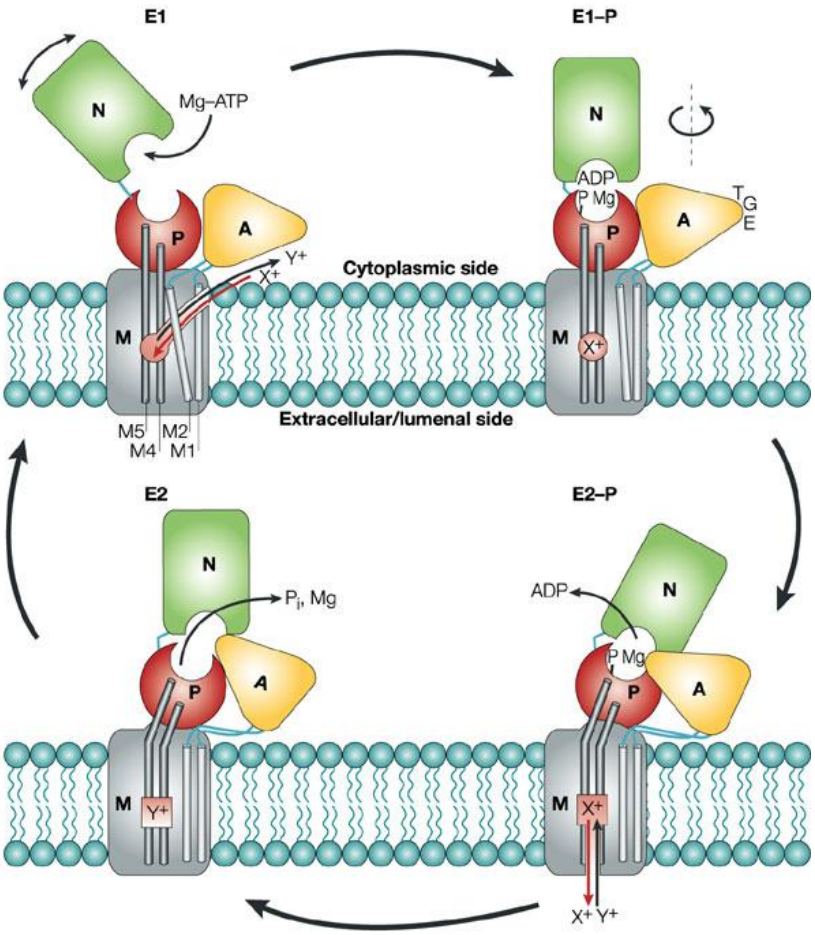

Figure 15. Schematic model of the molecular mechanism of a P-type ATPase. In the E_1 conformation, the N domain is docked onto the P domain, with the A domain displaced to one side. In the E_2 conformation, the A domain rotates and docks between the N and P domains, interfering with their interaction (15).

1.3.5 Transport Electrogenicity

For every ATP molecule hydrolyzed, the Na,K-ATPase pumps three Na^+ ions out of and two K^+ ions into the cell. As a consequence, the transport is overall electrogenic. The electrogenicity is detectable in partial reactions of the transport cycle where net electric charge is moved across the membrane dielectric. As mentioned in *1.3.2*, during the transport cycle the ion-binding sites remain more or less in the same position inside the membrane dielectric. Therefore, the conformational transitions are essentially electro-neutral, while ion binding and ion release are the steps that mainly contribute to the transport electrogenicity (21).

In Fig. 16, the electrogenic steps are marked by Greek letters. Each letter represents the dielectric coefficient of the specific step, corresponding to the value of the equivalent charge translocated across the whole membrane dielectric (20,21).

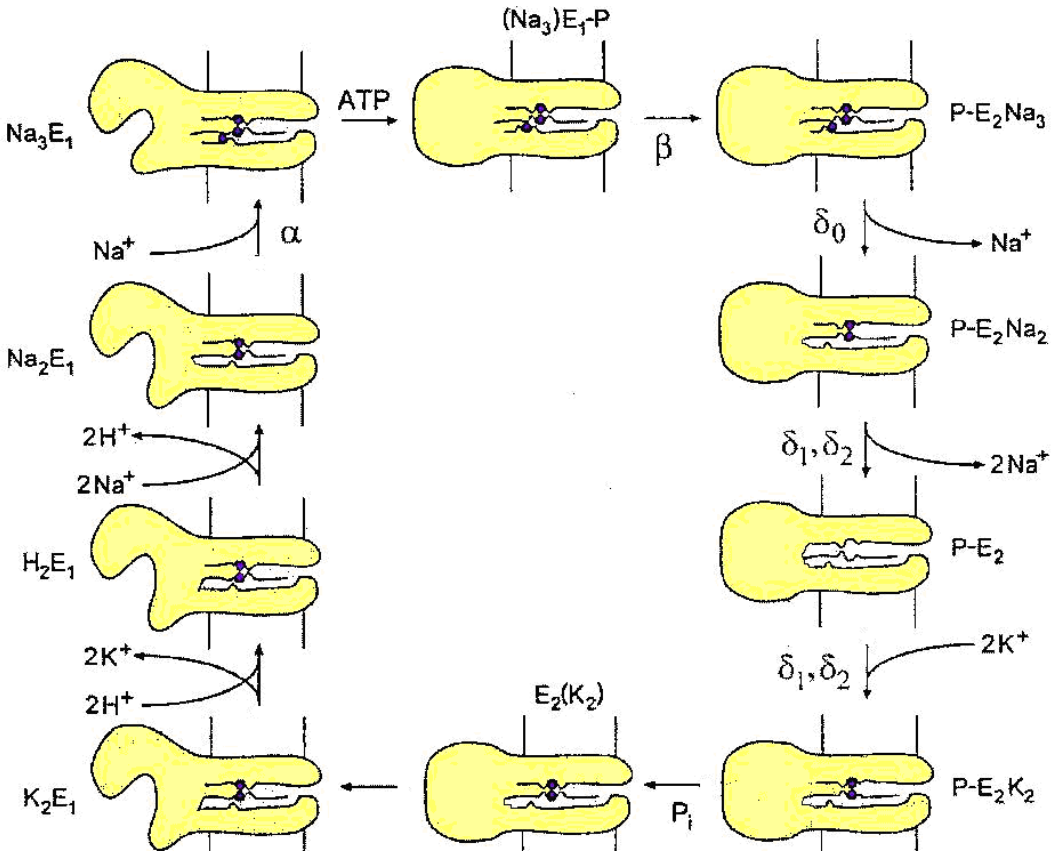

Figure 16. Model of the functional mechanism of the Na,K-ATPase including the H^+ ions. The Greek letters indicate the electrogenic steps of the transport cycle and represent the dielectric coefficients: $\alpha = 0{,}25$; $\beta \leq 0{,}1$; $\delta_0 = 0{,}7$; $\delta_1 = \delta_2 = 0{,}1\text{-}0{,}2$ (21).

At the physiological pH of 7.2, the two bifunctional ion-binding sites in the E_1 conformation are protonated for more than 83% in the absence of Na^+ and K^+ ions (32). As a consequence, binding of the first two Na^+ ions is accompanied by the release of almost two protons and this step appears only slightly electrogenic. Instead, binding of the third Na^+ ion to the Na^+-selective ion-binding site is electrogenic (α).

The conformational transition with all three binding sites loaded is of only minor electrogenicity (β). The release of the first Na^+ ion on the extracellular side is the main electrogenic step of the transport cycle (δ_0). This ion moves through about 65-70% of the protein dielectric, in a narrow and deep channel between the third ion-binding site and the extracellular medium. The release of this cation induces a conformational relaxation that widens the access channel between the ion-binding sites and the extracellular aqueous medium. Therefore, both remaining ions have to cross only about 10-20% of the membrane dielectric to be released (δ_1, δ_2). In conclusion, all Na^+ ions are released electrogenically, to a different extent.

In the $P\text{-}E_2$ conformation, the enzyme binds both K^+ ions in an electrogenic manner (δ_1, δ_2). After dephosphorylation, the protein undergoes the conformational transition back to E_1 and releases the K^+ ions in the cytosol. As explained for the binding of the first two Na^+ ions, the release of K^+ ions at the intracellular side is compensated by the binding of two Na^+ ions or, if sodium is absent, protons so that this step appears to be electroneutral.

1.3.6 Regulation of the Na,K-ATPase

Because of its important physiological roles, the Na,K-ATPase activity has to be regulated carefully. The protein can be modulated by both short- and long-term mechanisms. Short-term modulation involves direct effects on the enzyme activity or on the protein translocation between plasma membrane and its intracellular stores. Long-term mechanisms, instead, are related to protein synthesis and degradation.

The enzyme activity depends first of all on the substrate concentrations, but a more accurate regulation can be obtained by interaction with membrane-associated components or endogenous inhibitors circulating in the bloodstream. Moreover, the enzyme can be modulated by a variety of hormones. The various control mechanisms are often specific for different tissues. Besides endogenous mechanisms of regulation, several exogenous substances can interfere with the Na,K-ATPase activity.

1.3.6a Membrane-associated Components

The most important membrane-associated components that modulate the Na,K-ATPase activity are the FXYD proteins. This family of proteins will be discussed more in detail in paragraph *1.4*.

Specific cytoskeletal proteins, like adducin, actin, ankyrin, spectrin, and pasin, can interact with the Na,K-ATPase either directly or indirectly (33). The main consequence of these interactions is supposed to be the correct targeting of the enzyme molecules to the appropriate membrane compartment. Moreover, some of these proteins have been shown to regulate enzyme activity. For example, monomeric actin can activate the Na,K-ATPase by a mechanism mediated by the cAMP-dependent protein kinase (PKA), while mutants of adducin can stimulate the enzyme activity in kidneys by increasing the apparent affinity for ATP.

Membrane lipids can affect the Na,K-ATPase activity significantly. In general, their main effects are related to thickness and fluidity of the lipid bilayer: lipids promoting the formation of a membrane with a physiological thickness (5-10 nm) and increasing its fluidity stimulate the enzyme activity. In addition, specific effects of different lipids have been reported. The importance of negatively charged phospholipids (phosphatidylserine, phosphatidylinositol, phosphatidylglycerol) in preserving the Na,K-ATPase activity has been documented extensively (34-38). Moreover, cholesterol has been shown to affect some partial reactions of the transport cycle in a specific way (39), while free fatty acids have been reported to inhibit the enzyme (40).

1.3.6b Hormonal Regulation

The Na,K-ATPase is subjected to both short- and long-term regulation by a wide variety of hormones (33). Hormones can be classified in lipophilic (thyroid and steroid hormones) and hydrophilic (catecholamines and peptide hormones). Lipophilic hormones are able to cross the lipid bilayer and interact with intracellular receptors. Hormone/receptor complexes can behave as transcription factors, binding DNA and influencing the transcription of specific genes. In contrast, hydrophilic hormones are unable to penetrate inside the cell and can interact with membrane receptors only. As a consequence of the interaction, an intracellular signal transduction cascade is activated that generally results in the stimulation or inhibition of specific proteins.

Several steroid hormones, especially corticosteroids, have specific effects on the Na,K-ATPase. Both aldosterone and dexamethasone have been shown to stimulate the expression of the enzyme in several tissues. Moreover, aldosterone exhibits also two short-term effects that may be mediated by specific membrane receptors: on the one hand, it increases the cytoplasmic concentration of Na^+ ions, stimulating the translocation of protein molecules to the plasma membrane; on the other hand, it may stimulate the enzyme activity by increasing its Na^+-binding affinity. The overall effect of aldosterone is to increase reabsorption of ions and water in the kidney, increasing blood volume and, therefore, blood pressure.

Dopamine, epinephrine, and norepinephrine are catecholamines with different effects on the Na,K-ATPase: dopamine inhibits the enzyme, while epinephrine and norepinephrine stimulate its activity. The different action of these hormones depends on the interaction with specific membrane receptors and the initiation of different intracellular signaling cascades. The signal transduction involves often the activation of protein kinases or phosphatases that phosphorylate/dephosphorylate the enzyme (or the FXYD protein associated to it) at specific Ser, Thr, and Tyr residues with different effects on its activity. Alternatively, the signaling cascade may end with the activation of phospholipases that cut phospholipids in specific positions, releasing fatty acid molecules. Inhibition of the Na,K-ATPase by dopamine in kidneys represents a physiologically important mechanism for regulating salt readsorption during high salt intake. Instead, stimulation by epinephrine and norepi-nephrine in neural tissue helps to re-establish quickly the electrochemical sodium and potassium gradients across the membrane after the transmission of electrical impulses.

Protein hormones comprise a major class of Na,K-ATPase regulators. Among them, the effects of insulin on the enzyme have been characterized extensively. Insulin is a pancreatic hormone responsible for the regulation of the blood glucose level and also involved in potassium homeostasis. Increased potassium uptake by various tissues is a well-known effect of insulin and it has been ascribed mainly to stimulation of the Na,K-ATPase. There are several mechanisms of short-term regulation by insulin on the Na,K-ATPase. One example is the insulin-mediated translocation of protein molecules from their intracellular stores to the plasma membrane. In addition, the hormone can stimulate the enzyme activity by increasing the cytoplasmic sodium concentration via ion channels and ion exchangers or, in kidneys, by increasing the Na^+-binding affinity. As for catecholamines, the mechanisms for the insulin-mediated short-term effects on the Na,K-ATPase involve signaling cascades. Besides short-term mechanisms of regulation, insulin has also long-term effects on the Na,K-ATPase. These effects are complex and can result in either an increase or decrease in enzyme activity, the latter being particularly relevant to diabetes. Many other peptide hormones have specific regulatory effects on the enzyme, like the parathyroid hormone, angiotensin II, vasopressin, the insulin-like growth factor I, and the epithelial growth factor.

1.3.6c Cardiac Glycosides

Cardiac glycosides are steroid compounds bound to a sugar moiety that specifically inhibit the Na,K-ATPase. They are synthesized by both plants and animals, and are classified in cardenolides (ouabain, digoxin, digitoxin) and bufadienolides depending on their chemical structure. These molecules bind to the extracellular side of the enzyme, blocking it in the $P\text{-}E_2$ conformation and impeding the conformational transition back to E_1 (6). They show different selectivity for the α isoforms of the enzyme, mainly due to their sugar moiety (41). In particular, they present an up to 4-fold selectivity for α_2 and α_3 over α_1 that is supposed to have an important physiological meaning (41).

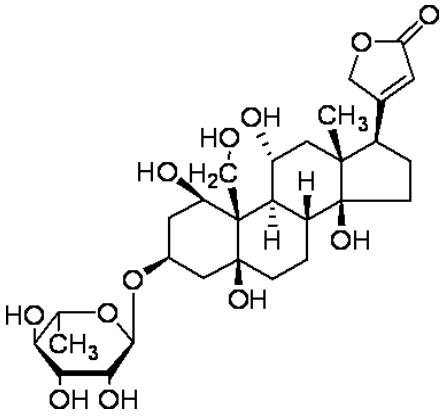

Ouabain

Plants-derived cardiac glycosides have been used for a long time to treat heart failure, and new drugs derived from them are still in use. Inhibition of the Na,K-ATPase by cardiac glycosides in cardiac myocytes leads to an increase in the cytoplasmic Na^+ concentration and, therefore, also in the cytoplasmic calcium concentration due to a less efficient transport by the Na/Ca-exchanger. This change results in greater and sustained contractions of the cardiac muscle fibers and, consequently, in an increase in blood pressure. However, excessive inhibition of the Na,K-ATPase can lead to calcium overload and cardiac arrhythmias.

Five different cardiac glycosides have been identified in mammals, including the cardenolides ouabain and digoxin and the bufadienolides marinobufagenin, telocinobufagin, and 19-norbufalin (41). They are present at very low concentrations in the bloodstream and are believed to be synthesized by the adrenal gland. It has been hypothesized that these molecules act as endogenous modulators of the Na,K-ATPase, consequently regulating blood pressure with the above mechanism (33).

1.3.6d Other Exogenous Molecules

Besides cardiac glycosides, the Na,K-ATPase can be modulated by several exogenous molecules. Among them, orthovanadate and oligomycin are the most well known. Orthovanadate (VO_4^{3-}) inhibits all P-type ATPases binding to the phosphorylation site with a higher affinity compared to phosphate and blocking the enzyme in the state $V\text{-}E_2{\cdot}X_n$ (42). Oligomycine, a specific inhibitor of the Na,K-ATPase, decreases its turnover rate of about 20% binding to the state $(Na_3)E_1$-P and blocking the conformational transition to $P\text{-}E_2$ (6).

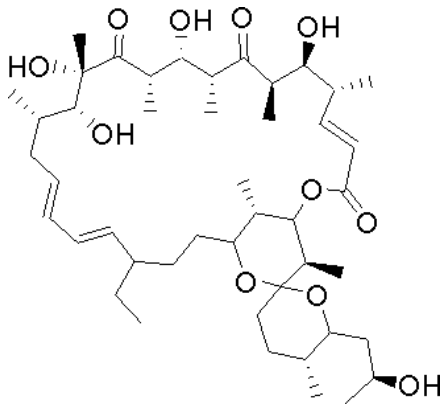

Oligomycin

1.4 The FXYD Protein Family

FXYD proteins are short transmembrane polypeptides named after the invariant extracellular motif FXYD. The gene family of FXYD proteins has been defined 12 years ago (43) and contains seven mammalian members: FXYD1 (or phospholemman, PLM), FXYD2 (or γ-subunit), FXYD3 (or mammary tumor marker, Mat-8), FXYD4 (or corticosteroid hormone-induced factor, CHIF), FXYD5 (or related to ion channel, RIC), FXYD6 (or phosphohippolin), and FXYD7. A FXYD1-like protein has been identified in shark rectal glands, FXYD10 (44), while more recently several FXYD proteins have been discovered in salmon (45).

For over 30 years, the renal Na,K-ATPase has been known to be associated to a short polypeptide that was named γ-subunit (FXYD2) (46). However, the physiological role of this third subunit, not required for the enzyme activity, was unknown. Only recently FXYD2 has been demonstrated to modulate the enzyme activity (47). Similarly, FXYD1 has been identified first as the major substrate of protein kinases A (PKA) and C (PKC) in the heart (48-50) and only later it has been shown to associate with and modulate the Na,K-ATPase (51). These findings prompted an intense research over FXYD proteins and their physiological role. Several studies have demonstrated that all mammalian FXYD proteins as well as the shark FXYD10 associate with the Na,K-ATPase in a tissue- and isozyme-specific way, and regulate its activity depending on the physiological requirements of the different cells.

Many extensive reviews have been published on the topic (52-58). In the following paragraphs, the features of the mammalian FXYD members and their functional effects on the Na,K-ATPase will be summarized with particular focus on FXYD1.

1.4.1 Structure and Post-translational Modifications

All mammalian FXYD proteins contain 61 to 95 amino acids with the only exception of FXYD5, which has 178 amino acids due to an atypically long N-terminal sequence (Fig. 17). Except FXYD2 and FXYD7, all proteins contain a signal peptide. In FXYD1, FXYD4, and FXYD5, the signal peptide is cleaved post-translationally, but not in FXYD3. Besides the extracellular motif FXYD, two intramembrane Gly, and a Ser residue at the membrane-cytoplasm interface are conserved in all family members and species. In mammals, an invariant Pro residue just before the FXYD motif is found as well (59). Residue X in the FXYD motif is typically Tyr, but can also be Thr, Glu, or His (43,59).

All FXYD proteins are type I single-span membrane proteins, with an extracellular N-terminus and a cytoplasmic C-terminus. FXYD3 is the only member that may have a second transmembrane segment. Marked homology among family members is observed in a stretch of 35 amino acids in and around the transmembrane domain, but not outside this region. However, the extracellular N-terminal sequence is always acidic, while the cytoplasmic C-terminal sequence is basic, particularly in the segment close to the membrane-cytoplasm interface (59).

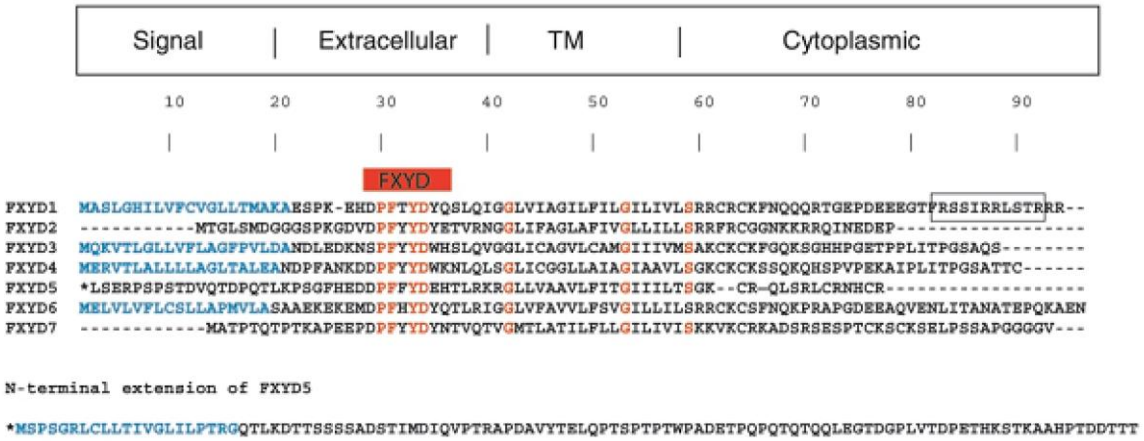

Figure 17. Alignment of the primary sequences of the currently known 7 human FXYD proteins. The conserved residues are shown in red, and the cleavable N-terminal signal sequences in blue (53).

Recently, the structure of FXYD1 as a free monomer in SDS micelles has been determined by NMR spectroscopy (60) (Fig. 18). FXYD1 appears to be organized in four α-helices: H1 at the extracellular side (Asp 12-Gln 17), H2 as transmembrane domain (Ile 18-Leu 36), H3 (Ser 37-Lys 43) and H4 (Thr 59-Ser 68) on the cytoplasmic side. The FXYD motif forms a disordered segment preceding H1. H1, H2, and H3 are rigidly connected and show similar backbone dynamics, while helix H4 is linked to the others by a long flexible loop. Both cytoplasmic helices H3 and H4 are associated to the micelle surface so that, overall, FXYD1 adopts an L-shaped conformation. So far this is the only complete structure available for a FXYD protein, since both crystal structures of the Na,K-ATPase (29,30) could not resolve the cytoplasmic sequence of FXYD2 and FXYD10, respectively.

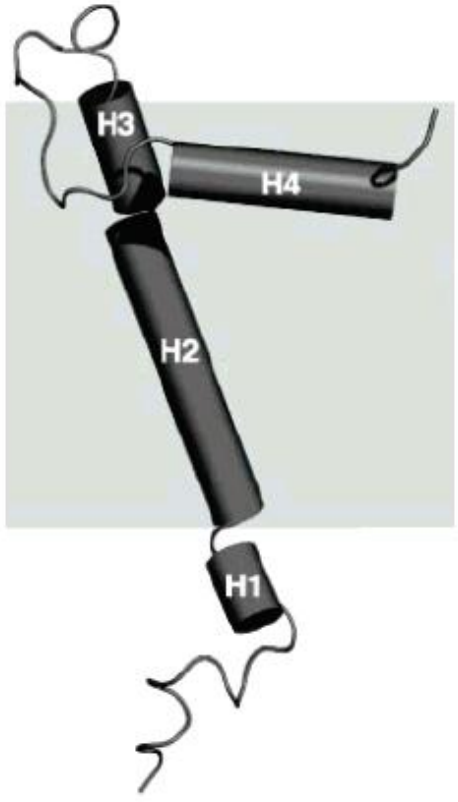

Figure 18. Tube representation of FXYD1 as a free monomer in SDS micelles (60).

In the NMR structure, the transmembrane segment of FXYD1 runs approximately perpendicular to the plane of the membrane, similarly to the transmembrane segments of FXYD2 and FXYD10 associated to the Na,K-ATPase in the crystal structures (29,30). Solid-state NMR data of FXYD1 as a free monomer in lipid bilayers (DOPC/DOPG 4:1) indicate that the transmembrane segment is tilted only by ~ 15 ° relative to the membrane normal (61). A sequence of small residues (Gly 20, Ala 24, Gly 25, Gly 31, Val 35) runs along one side of the H2 helix interrupted only by the aromatic ring of Phe 28, which protrudes from the transmembrane segment near the center of the lipid bilayer. The marked homology observed in the transmembrane segment of all FXYD proteins suggests that these residues may be involved in specific interactions with the Na,K-ATPase.

The cytoplasmic helix H3 is buried in the SDS micelle, with the charged Arg and Lys side chains (Arg 38, Arg 39, Arg 41, and Lys 43) pointing away from the micelle interior and into the aqueous phase. Helix H4 is associated to the micelle surface oriented almost parallel to it. According to its amphiphilic nature, it is organized with the apolar residues (Phe 60, Ile 64, and Leu 67) facing the micelle interior and the charged residues (Arg 61, Arg 65, and Arg 66) facing the aqueous medium (Fig. 19). Solid-state NMR data of FXYD1 in lipid bilayers (DOPC/DOPG 4:1) also indicate the association of these helices with the membrane (61).

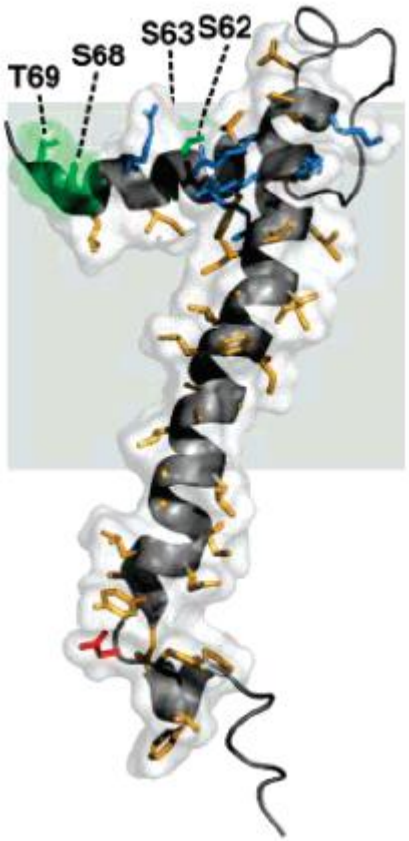

Figure 19. Molecular backbone of FXYD1 as a free monomer in SDS micelles. In the helical regions, basic side chains are shown in blue, acidic side chains in red, and apolar side chains in yellow. The established (S63, S68) and putative (S62, T69) phosphorylation sites in the cytoplasmic helix H4 are shown in green (see text) (60).

The presence of several basic residues in helices H3 and H4 helps explaining their propensity to interact with the negatively charged SDS micelle surface and with lipid bilayers containing 25% of the anionic phospholipid DOPG. Indeed, isothermal titration calorimetric experiments have shown that a 35-amino acid peptide representing the FXYD1

cytoplasmic sequence ($FXYD1_{38–72}$) strongly associates with anionic phospholipid head groups in the membrane (62). However, this interaction is weakened significantly when the fraction of negatively charged phospholipids is reduced to represent a more physiological environment (Fig. 20).

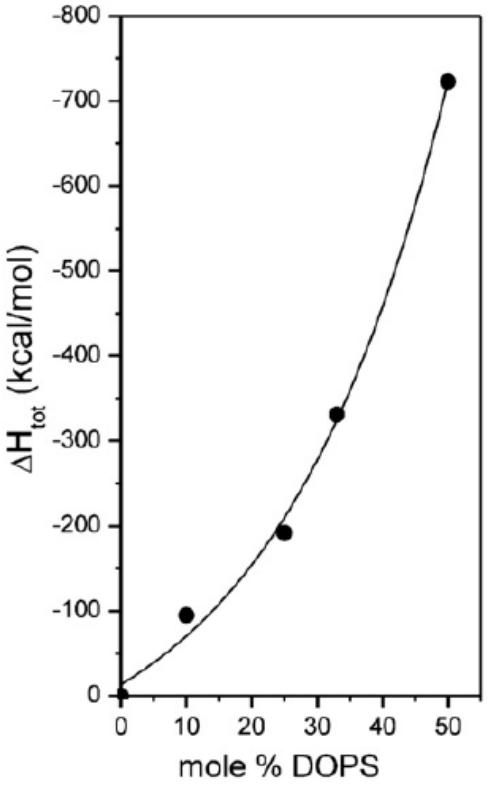

Figure 20. Isothermal calorimetry experiments show the interaction of a peptide representing the cytoplasmic segment of FXYD1 ($FXYD1_{38–72}$) with membranes containing different amounts of the anionic phospholipid dioleoylphosphatidyserine (DOPS) (62).

The emerging structures of FXYD3 and FXYD4 indicate a helix-break-helix structural organization in both SDS micelles and lipid bilayers similar to the one detected for FXYD1 (61,63). Such organization is supposed to be common to all FXYD members. It is interesting to notice that, although FXYD proteins are relatively small, they are encoded by genes with six to nine exons (43). Their secondary structure seems to mirror the intron-exon structure of the corresponding gene, suggesting that these proteins are assembled from discrete structured domains (63). While the structural organization in and around the membrane is supposed to be similar in all FXYD proteins, the cytoplasmic sequences show peculiar features for each member (61,63).

FXYD1 is phosphorylated by PKA and PKC in cardiac myocytes (48-50). The established target residues *in vivo* are Ser 63 (PKC) and Ser 68 (PKA, PKC) (64,65), both located in the cytoplasmic helix H4 and exposed to the aqueous medium (60). Recently, also Thr 69 has been demonstrated to be phosphorylated by PKC *in vitro* and in adult rat cardiac myocytes (65).

The NMR structure of the monomeric FXYD1 in SDS micelles after *in vitro* phosphorylation at Ser 68 by PKA has been published recently (66). In the same paper, also the structure of the S68D mutant mimicking PKA phosphorylation has been investigated. Interestingly, neither the *in vitro* phosphorylation nor the S68D mutation cause major changes in the conformation of FXYD1. Indeed, both appear to induce only a modest

increase in the mobility of helix H4, with no influence on its helical structure and association to the micelle surface (Fig. 21).

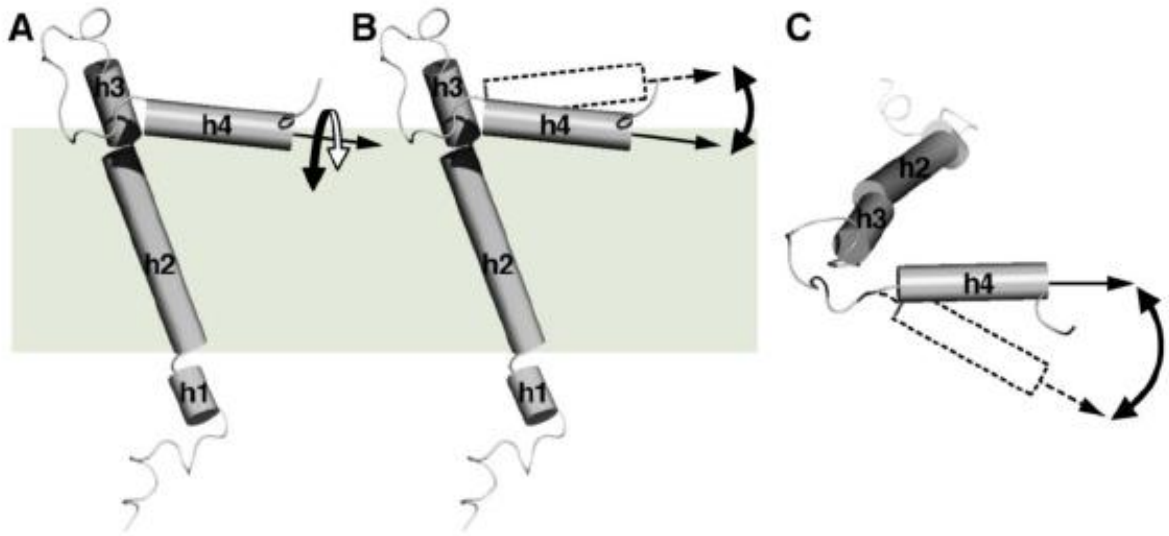

Figure 21. Possible reorientation of helix H4 in SDS micelles upon phosphorylation at S68: (A) rotation around the helix axis; (B) reorientation perpendicularly to the micelle surface; (C) reorientation in the plane of the micelle surface (view from the cytoplasm) (66).

Experiments measuring the fluorescence resonance energy transfer (FRET) between fluorescent probes covalently bound to the C-terminus of FXYD1 and to the N-terminus of the enzyme have indicated an increase in distance of about 4 Å upon phosphorylation (67-69). Other FXYD members contain putative phosphorylation sites, but so far only FXYD2 and the shark FXYD10 have been shown to be phosphorylated by protein kinases *in vitro* (44,70).

Recently FXYD1 expressed in rat cardiac myocytes has been reported to be partially palmitoylated at Cys 40 and Cys 42, modification that seems to protect the protein against cellular degradation (71). Interestingly, unpalmitoylatable FXYD1, which is correctly delivered to the plasma membrane, fails to inhibit the Na,K-ATPase (see *1.4.4*). Moreover, phosphorylation at Ser 68 has been shown to increase the degree of palmitoylation. Since all FXYD proteins contain Cys residues in their cytoplasmic segment, palmitoylation could be a common post-translational modification. However, so far it has not been detected for any other member of the FXYD family. Investigation of the post-translational modifications of FXYD7 has revealed that this member is O-glycosylated at three Thr residues, but no palmitoylation has been observed (72).

1.4.2 Association with the Na,K-ATPase: Localization and Isozyme Specificity

FXYD proteins associate with the Na,K-ATPase in a tissue- and isozyme-specific way. In mammals, they are localized in tissues involved in solute and fluid transport (kidney, colon, pancreas, mammary gland, liver, lung, prostate, and placenta) or that are electrically excitable (heart, skeletal muscle, and neural tissues) (73). All members interact with the α_1 isoform in native membranes, but many of them are known to associate also with other isoforms *in vivo* or upon co-expression in heterologous systems.

Association between FXYD1 and the Na,K-ATPase is supposed to occur post-translationally, either in the Golgi apparatus or in the plasma membrane (51). A 1:1 stoichiometric association of the complex with the α subunit has been indicated by several studies detecting FXYD1 and the α subunit with specific antibodies (38,51,74), and has been proved later on by FRET experiments (68). It is unclear whether the association is altered upon phosphorylation of FXYD1, since no change has been detected using specific antibodies (75-77), but experiments measuring FRET have hypothesized a partial dissociation of the complex (67,69).

FXYD1 is widely distributed, with the highest expression level in heart and skeletal muscle, where it is the only FXYD member expressed (78). In cardiac myocytes, it has been detected in all regions exposed to the extracellular space: sarcolemma, intercalated disks, and t-tubules (79,80). Moreover, FXYD1 is highly expressed in selected structures of the central nervous system. In particular, it is most abundant in cerebellum and in choroid plexus, where it has been detected both in neurons and glia (81). Finally, FXYD1 has been localized also in kidneys, specifically in the extraglomerular mesangial cells and in the afferent arterioles, but not in nephrons (82).

In the heart, FXYD1 associates with different isozymes of the Na,K-ATPase depending on the species. In particular, it has been detected with $\alpha_1\beta$, $\alpha_2\beta$, and $\alpha_3\beta$ in human and rabbit (76), with $\alpha_1\beta$ and $\alpha_2\beta$ in mouse (68,83) and bovine (51), but only with $\alpha_1\beta$ in rat (75). Human and rabbit hearts are known to express all three α isoforms, while rodent hearts express only α_1 and α_2 (73,79,84,85). In cardiac myocytes, the α isoforms have a specific subcellular distribution. The association of FXYD1 with all or some α isoforms may have a precise physiological meaning. In the central nervous system, FXYD1 associates with $\alpha_1\beta$, $\alpha_2\beta$, and $\alpha_3\beta$ (81), while in kidney it has been found specifically with $\alpha_2\beta_2$ (82). Upon co-expression in *X. oocytes*, FXYD1 associates stably with $\alpha_1\beta_1$, $\alpha_2\beta_1$, $\alpha_3\beta_1$, $\alpha_1\beta_2$, $\alpha_2\beta_2$, and $\alpha_3\beta_2$, although less efficiently with the $\alpha\beta_2$ than with the $\alpha\beta_1$ isozymes (51).

A recent study in different human tissues has evidenced an abundant FXYD1 expression not only in heart, skeletal muscle, and kidney, but also in placenta, gastric mucosa, small intestine, and colon. Lower expression levels have been detected in uterine, intestinal and bladder smooth muscle, choroid plexus, liver, spleen, gallbladder, breast, prostate, and epididymis (86). These results suggest that FXYD1 may not only be involved in the physiological regulation of contractile tissues and urinary epithelial tissues, but also in regulating the Na,K-ATPase, or other ion transporters in reproductive, gastrointestinal, hepatic, and pancreatobiliary systems.

Localization and *in situ* isozyme specificity of the other mammalian FXYD members is summarized in Table 2. It is interesting to notice that all FXYD proteins have unique and complementary patterns of expression with low overlap. This is particularly evident in kidney, where four members (FXYD1, FXYD2, FXYD4, and FXYD5) are expressed in specific, distinct cells. Their unique expression pattern and functional effects on the Na,K-ATPase (see *1.4.4*) reflect the different physiological conditions and needs in the various parts of the kidney that are of relevance for the Na^+ reabsorption process. Both FXYD3 and FXYD5 have been detected in several cancer tissues and are believed to play a role in tumor progression.

	Tissue	Isozyme
FXYD1	Heart, Skeletal Muscle, Brain (cerebellum, choroid plexus), Kidney (extraglomerular mesangium, afferent arterioles)	$\alpha_1\beta$, $\alpha_2\beta$, $\alpha_3\beta$
FXYD2	Kidney (proximal convoluted tubule, ascending loop of Henle, distal convoluted tubule)	$\alpha_1\beta_1$
FXYD3	Uterus, Stomach, Colon, Skin Tumors (murine and human breast tumors, prostate tumors, colorectal cancer cell lines)	$\alpha_1\beta_1$
FXYD4	Kidney (collecting duct), Colon, Papilla	$\alpha_1\beta_1$
FXYD5	Kidney (basolateral membrane of the collecting tubule, connecting tubule, intercalated cells of the collecting duct), Intestine, Lung, Heart, Spleen Tumors	
FXYD6	Brain	
FXYD7	Brain (neurons, glial cells)	$\alpha_1\beta_1$

Table 2. Tissue and isozyme specificity of mammalian FXYD proteins.

So far FXYD proteins are known to associate *in situ* only with the Na,K-ATPase. The only exception is FXYD1, which has been reported to interact with and modulate the Na/Ca-exchanger (87) and the L-type Ca-channels (88). In contrast, it does not associate with SERCA2a (51,76).

FXYD1 have been demonstrated to form ion channels upon overexpression in *X. oocytes* (89,90) or reconstitution into planar lipid bilayer (91). FRET experiments indicate that FXYD1 may oligomerize and form tetramers (69). The channels show high permeability to many ions, both monoatomic and polyatomic, and in particular to taurine. Since taurine efflux is associated with changes in cell volume, these observations have suggested a role of PLM in cell volume regulation. However, so far there are no data indicating the formation of ion channels in vivo.

1.4.3 Functional and Structural Interactions with the Na,K-ATPase

Modulation of the Na,K-ATPase by FXYD proteins is achieved by intermolecular interactions between the two proteins. Multiple structural and functional sites of interaction exist, which involve both the transmembrane and the cytoplasmic domain. In principle, interactions at the transmembrane level are likely to affect mostly the intrinsic enzyme affinity for Na^+ and K^+ ions. In contrast, interactions of the cytoplasmic domains may influence the conformational equilibrium of the enzyme and, as a consequence, its apparent affinity for Na^+ and K^+ ions as well as for ATP.

The crystal structures of the Na,K-ATPase have revealed that the transmembrane segment of FXYD2 and FXYD10, and probably of all FXYD proteins, interacts specifically

with helix M9 of the α subunit (29,30). Important residues for the interaction of FXYD proteins with the enzyme have been individuated in this α-helix (92). Leu 964 and Phe 967 contribute to the stable interaction with FXYD2, FXYD4, and FXYD7, but do not influence the functional effect of these FXYD proteins on the apparent K^+-binding affinity of the enzyme. On the other hand, Phe 956 and Glu 960 do not contribute to the complex association, but transmit, to a different extent, their effect on the apparent K^+-binding affinity.

Experiments with FXYD2/FXYD4 chimeras have shown that specific amino acids in the transmembrane segment of these FXYD proteins are responsible for both the stability of their association with the Na,K-ATPase and their effects on the apparent Na^+-binding affinity (93). Similarly, experiments with FXYD4/FXYD5 chimeras have demonstrated an analogous crucial importance of the transmembrane domain of FXYD5 (94). The two conserved Gly residues in the transmembrane segment of FXYD proteins appear to be implicated both in the association with and in the regulation of the enzyme, as shown by mutagenesis experiments on FXYD2 (95) and FXYD7 (96). A detailed study on the specific contribution of each residue in the transmembrane segment of FXYD7 has shown that most of the residues involved in structural and/or functional interactions are clustered in a face of the transmembrane helix containing the two conserved Gly residues, evidently facing helix M9 of the α subunit (97).

The extracellular segment of FXYD proteins contains the motif FXYD. Despite its conservation among all family members, so far no specific function could be revealed for it: it is required for the stable interaction of the α subunit with FXYD2 and FXYD4 (98), but not with FXYD7 (96). Cross-linking experiments between FXYD2 and the α or the β subunit have located the extracellular segment near the site of the α/β interaction (99), similarly to what detected in the crystal structure of the $\alpha_1\beta_1$FXYD10 complex (30) (Fig. 12). Analogous experiments with FXYD4 have indicated that the extramembrane segment of FXYD4 comes also into proximity with both the α and the β subunit, but the specific sites of interaction are unknown (100).

FXYD proteins show the highest variability in length and sequence in the cytoplasmic part. Such variability partly reflects their different functional effects on the Na,K-ATPase. For example, the use of an antibody against the cytoplasmic segment of FXYD2 (101,102) or the deletion of this segment (103) abolishes the effect of FXYD2 on the apparent affinity for ATP, demonstrating that the cytoplasmic segment is responsible for such an effect. In FXYD4, mutation of the positively charged amino acids at the membrane-cytoplasm interface results in enzyme inhibition and increase of the apparent K^+-binding affinity (98). Therefore, the cytoplasmic segment of FXYD4 is at least in part responsible for the effect on the apparent K^+-binding affinity of the enzyme.

Despite their importance, the structural interactions of the cytoplasmic segment of FXYD proteins with the enzyme are largely unknown. The published crystal structures of the Na,K-ATPase could not resolve the cytoplasmic segments of FXYD2 (29) and FXYD10 (30), indicating that they are not arrested in specific positions on the enzyme or on the membrane surface. Cross-linking experiments between FXYD2 and α or β have located the cytoplasmic segment of FXYD2 close to loops L6/7 and L8/9 of the α subunit (99). Moreover, in FXYD2 and, to a lesser extent, in FXYD4, the positively charged amino acids close to the membrane-cytoplasm interface have been found to be necessary for the stable association with the enzyme (98).

Extensive investigations on the structural and functional interactions of FXYD1 with the Na,K-ATPase are still lacking. Experiments with a FXYD1/FXYD4 chimera containing the transmembrane segment of FXYD1 have shown that this segment is responsible for an increase in the apparent Na^+-binding affinity of the enzyme (74). The importance of the interaction with the cytoplasmic segment of FXYD1 is attested by the effect of FXYD1

phosphorylation on the enzyme transport properties (see *1.4.4*). In this regard, experiments with a peptide representing the cytoplasmic segment of FXYD1 ($FXYD1_{54-72}$) have shown that this segment inhibits and stimulates the Na,K-ATPase depending on its phosphorylation state similarly to the complete FXYD1 (104).

The structural interactions of the cytoplasmic segment of FXYD1 with the cytoplasmic domains of the enzyme as well as its alteration upon phosphorylation are still unclear. Recently, a model of the $\alpha_1\beta_1$FXYD1 complex has been generated (66) by replacing the coordinates of the endogenous FXYD2 in the crystal structure of the Na,K-ATPase from pig kidney (29) with those of the unphosphorylated FXYD1 determined by NMR (60) (Fig. 22). In this model, the cytoplasmic helix H4 is associated to the membrane surface and can interact with two different regions of the Na,K-ATPase at the cytoplasm-membrane interface, depending on its orientation.

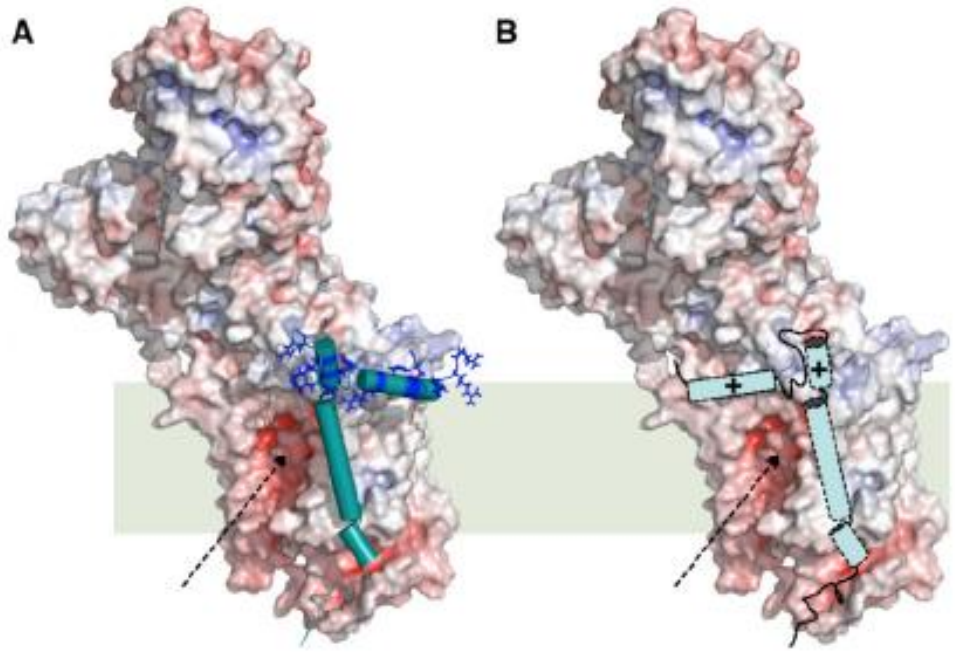

Figure 22. Structural model of the $\alpha_1\beta_1$FXYD1 complex and potential alternative orientation of helix H4 (66).

Whether this model represents a correct interaction of FXYD1 with the enzyme has to be determined. Indeed, despite several observations showing that helix H4 of the monomeric FXYD1 associates with the membrane surface (60-62,66), so far there are no data indicating a similar propensity when it is associated to the enzyme.

1.4.4 Functional effects on the Na,K-ATPase

FXYD proteins modulate the transport properties of the Na,K-ATPase in a complex and distinct way. Several reviews report and compare the functional effects of the different members on the Na,K-ATPase (52-58) that are summarized in Table 3.

	Na^+-binding Affinity	K^+-binding Affinity	ATP-binding Affinity	Maximum Turnover Rate
FXYD1 (unphosphorylated)	↓	↓	-	-
FXYD2	↓	-	↑	-
FXYD3	↓	↓	-	-
FXYD4	↑	↓	-	-
FXYD5	-	-	-	↑
FXYD6	↓	↓	-	-
FXYD7	-	↓	-	-

Table 3. Functional properties of the mammalian FXYD proteins. The arrows pointing up or down indicate an increase or a decrease of the indicated transport property, respectively. A dash indicates that no difference in the transport property has been detected so far.

The functional effects of FXYD1 on the Na,K-ATPase have been studied extensively in native cells, mainly cardiac myocytes, and heterologous systems like *X. oocytes* and HeLa cells. Several studies have attested that unphosphorylated FXYD1 inhibits the enzyme (104,105) by reducing its apparent affinity for intracellular Na^+ ions (51,74,77,106,107). Moreover, a FXYD1-induced decrease in the apparent affinity for extracellular K^+ ions has been reported in *X. oocytes* (51,77) and mouse cardiac myocytes (108). The extent of the reduction in intracellular Na^+-binding affinity varies slightly among the studies. In *X. oocytes*, a 30-40% reduction has been reported (51,77), while in HeLa cells FXYD1 induces a decrease of about 20% (74) or 30% (107). Moreover, the comparison of cardiac myocytes from wild-type (WT) and FXYD1 knockout (KO) mice shows a FXYD1-induced decrease of about 30% (106). A different decrease in extracellular K^+-binding affinity has also been reported, specifically of about 20-30% in *X. oocytes* (51,77) and almost 50% in mouse cardiac myocytes (108).

Phosphorylation of FXYD1 by PKA stimulates the enzyme activity (75,79,104) thanks to the abolition of the functional effect of FXYD1 on the intracellular Na^+-binding affinity (68,77,106). Phosphorylation of FXYD1 by PKC has been shown to induce an increase of about 40-60% in the maximum turnover rate of the enzyme in mouse cardiac myocytes (68,109) and *X. oocytes* (77), but not in HeLa cells (107). In some studies, also a partial abolition of the functional effect of FXYD1 on the intracellular Na^+-binding affinity has been detected (68,107), similarly to what has been observed upon phosphorylation by PKA. The extracellular apparent K^+-binding affinity is not altered upon phosphorylation by either PKA (77,108) or PKC (77).

Phosphorylation by PKA or PKC seems to induce distinct effects, despite the close proximity of their target residues. FRET experiments have shown a similar increase in the distance between the C-terminus of FXYD1 and the N-terminus of the enzyme upon phosphorylation by either PKA or PKC (67-69). Moreover, it has been demonstrated recently that phosphorylation at either Ser 63 or Ser 68 is sufficient to restore the apparent Na^+-binding affinity of the enzyme and relieve its FXYD1-dependent inhibition (107).

Therefore, the distinct effects of PKA and PKC phosphorylation may be related mainly to a change in the electrostatic of the cytoplasmic segment rather than to a major conformational change. Further studies are required to elucidate the molecular mechanism underneath the specific effects of PKA and PKC phosphorylation.

Considering the observations above, the following mechanism of interaction can be proposed. The unphosphorylated cytoplasmic segment of FXYD1 may interact with the cytoplasmic domains of the α subunit, restricting their movements and leading to inhibition of the enzyme. In particular, the interaction may stabilize the E_2 conformation, which would lead indirectly to a lower Na^+-binding affinity. Upon phosphorylation, the interaction would be impaired, resulting in stimulation of the enzyme activity. Instead, the effect of FXYD1 on the K^+-binding affinity could be mediated by its transmembrane segment and induce an effect on the intrinsic binding affinity for potassium. This would explain why it is not affected by FXYD1 phosphorylation.

Experiments with ventricular myocytes from WT and FXYD1 KO mice using a peptide representing the cytoplasmic segment of FXYD1 ($FXYD1_{54-72}$) have shown that this segment inhibits and stimulates the Na,K-ATPase similarly to the complete FXYD1 (104). The unphosphorylated peptide inhibits the enzyme, while the peptide phosphorylated at Ser 68 stimulates it in both WT and KO mice. However, the effects on the apparent Na^+- and K^+-binding affinities were not investigated.

Experiments with a FXYD1/FXYD4 chimera containing the transmembrane segment of FXYD1 have shown that this segment is responsible for an increase of about 20% in the intracellular Na^+-binding affinity of the enzyme (74). This is likely to arise from an effect on the intrinsic binding affinity for sodium. Whether it also affects the K^+-binding affinity has not been tested. In the same study, the transport properties of the human detergent-solubilized, purified $\alpha_1\beta_1$FXYD1 complex have been investigated. The complex has been obtained after co-expression in *P. pastoris* or *in vitro* reconstitution following separate expression in the same heterologous system. Interestingly, a FXYD1-induced increase of about 30% in the apparent Na^+-binding affinity of the enzyme has been detected, but no change in the apparent K^+-binding affinity and in the maximum turnover rate has been revealed. FXYD1 expressed in *P. pastoris* was found to be partially phosphorylated at Ser 68. Considering the results with the FXYD1/FXYD4 chimera and with the detergent-solubilized purified $\alpha_1\beta_1$FXYD1 complex, the authors have concluded that the transmembrane segment of FXYD1 induces an increase in affinity for Na^+ ions (74). Therefore, the different segments of FXYD1 may affect the Na^+-binding affinity of the Na,K-ATPase in a distinct way: on the one hand, the unphosphorylated cytoplasmic segment could decrease the apparent Na^+-binding affinity by stabilizing the enzyme in the E_2 conformation, on the other hand the transmembrane segment may increase the intrinsic Na^+-binding affinity. This second effect could be masked by a decrease induced by the unphosphorylated cytoplasmic segment and be revealed only upon phosphorylation of it, depending on the degree of phosphorylation. However, so far this is the only study supporting this hypothesis, since all the other studies have reported abolition of the FXYD1-induced decrease of intracellular Na^+-binding affinity, but no further increase of it.

As described in paragraph *1.3.3*, different tissues express distinct isozymes of the Na,K-ATPase. In particular, $\alpha_1\beta_1$ and $\alpha_2\beta_1$ are both present in human, rabbit, and rodent cardiac myocytes (73,79,84,85). Whether and how FXYD1 modulates the functional properties of the different isozymes of the Na,K-ATPase is still unclear. In guinea pig cardiac myocytes, PKA activation affects specifically the α_1 isoform of the enzyme (79,85), while the PKC-dependent pathway targets only α_2 (85). Upon co-expression in *X. oocytes*, phosphorylation of FXYD1 by PKA has been shown to reverse the FXYD1-induced effect on the intracellular Na^+-binding affinity of both $\alpha_1\beta_1$ and $\alpha_2\beta_1$, while phosphorylation by PKC induces an increase in the maximum turnover rate of $\alpha_2\beta_1$ only (77). In mouse cardiac myocytes, both

PKA- and PKC-mediated phosphorylation of FXYD1 reverses the Na^+-binding affinity of the α_1 and α_2 isoforms, but PKC activation increased the maximum turnover rate of the α_2 isoform only (68). The complex and distinct regulation of the Na,K-ATPase isozymes by phosphorylation of FXYD1 may be important for the efficient control of heart contractility and excitability.

Pathological states can have a strong influence on the expression level of the different isozymes of the Na,K-ATPase and of FXYD1 as well as on the phosphorylation state of FXYD1. For example, the expression of α_1, α_2, and α_3 as well as of FXYD1 is drastically reduced in heart failure, but the fraction of FXYD1 phosphorylated at Ser 68 is dramatically increased (68). Therefore, the reduced Na,K-ATPase expression in heart failure may be functionally offset by a lower inhibition by FXYD1.

Finally, few studies have published different observations from those reported above. For example, the comparison of cardiac sarcolemmal membranes from WT and FXYD1 KO mice has shown no difference in apparent Na^+-binding affinity, but a lower maximum turnover rate in KO mice (110). Moreover, in bovine choroid plexus membranes an antibody against the cytoplasmic segment of FXYD1 reduces the maximum turnover rate without affecting the Na^+-binding affinity (81). An explanation for these observations is still lacking.

1.5 Aim of the Project

As reported in the above paragraph, the effects of FXYD1 on the Na,K-ATPase have been investigated mainly in intact cells, both heterologous systems and native cells. These systems allow a better characterization of the physiological effects of FXYD1, but are of limited use for the investigation of the functional and structural interactions between FXYD1 and the enzyme. The availability of the purified, detergent-solubilized recombinant Na,K-ATPase with and without FXYD1 described in (74) enables us to apply the biophysical techniques available in our lab to characterize the transport cycle of the ion pump. These preparations provide a system that allows us to work under well defined conditions and without interference by other cellular components. Unlike in native cells, the effects of FXYD1 on the different isozymes of the Na,K-ATPase can be investigated separately. Moreover, the phosphorylation state of FXYD1 in the purified preparations is easily controllable. Therefore, when the transport properties of the enzyme with and without FXYD1 are compared, the specific effects of FXYD1 can be defined.

CHAPTER 2

MATERIALS AND METHODS

2.1 Preparation of the Purified, Detergent-solubilized Human α_1/His$_{10}$-β_1, α_2/His$_{10}$-β_1, and α_1/His$_{10}$-β_1/FXYD1

The purified, detergent-solubilized human α_1/His$_{10}$-β_1, α_2/His$_{10}$-β_1, and α_1/His$_{10}$-β_1/FXYD1 have been prepared according to a procedure developed by the group of Steven Karlish at the Weizmann Institute of Science (27,37,38,74,111). The human α_1/His$_{10}$-β_1 and α_2/His$_{10}$-β_1 isozymes of the Na,K-ATPase have been expressed in the methylotrophic yeast *P. pastoris*, while human FXYD1 has been expressed in *E. coli*. After detergent-solubilization and purification, the α_1/His$_{10}$-β_1/FXYD1 complex has been obtained by *in vitro* reconstitution. The protein-containing *P. pastoris* and *E. coli* cells have been provided by Steven Karlish.

2.1.1 Purification of α_1/His$_{10}$-β_1 and α_2/His$_{10}$-β_1 Expressed in P. pastoris

The human α_1/His$_{10}$-β_1 and α_2/His$_{10}$-β_1 isozymes of the Na,K-ATPase have been expressed in yeast *P. pastoris* as described previously (27,37,38,74,111). A His10 tag has been added to the N-terminus of the β subunit to allow purification by metal chelate affinity chromatography. In this position, the His tag has been shown not to significantly affect expression level or protein activity (37).

The detergent-solubilized preparations have been obtained in a two step procedure (27,38,111). In the first step, the *P. pastoris* cells are broken with glass beads and urea-treated membranes are prepared. In the second step, the membranes are solubilized with the non-ionic detergent n-dodecyl-β-maltoside (DDM) at a protein:detergent ratio of 1:2 (w/w), and the proteins are purified by Co^{2+}-chelate affinity chromatography with BD-Talon Beads. During the purification procedure, 1-stearoyl-2-oleoyl-phosphatidylserine (SOPS) and cholesterol are added to preserve enzyme activity. This procedure yields about 80% pure, functional, and stable enzyme in mixed protein/lipid/detergent complexes without further purification steps. Approximately 100 μg of purified enzyme are obtained from 100 mg of membrane protein.

Both the cells and the membranes have been stored at -80 °C, and thawed overnight in the fridge before use.

Materials

- MOPS (Sigma, ≥99,5%)
- Tricine (Serva, ≥99%, analytical grade)
- Tris (MP Biomedicals, UltraPure)
- Imidazole (Merck, buffer substance, ACS)
- EDTA (Merck, Titriplex® II, for analysis, ACS)
- D-Sorbitol (Sigma, BioUltra, ≥99,5%)

- Glycerol (VWR, 99,3%)
- Urea (AnalaR NORMAPUR®, ≥99,5%, for analysis, ACS)
- NaCl (Roth, ≥99,5%, for analysis, ACS)
- Phenylmethylsulfonyl fluoride (PMSF) (Sigma, ≥98,5%)
- Pepstatin A (Sigma, microbial)
- Leupetin hydrochloride (Sigma, microbial, ≥90%)
- Chymostatin (Sigma, microbial)
- DDM (Anatrace, ≥99%)
- Octaethylene glycol monododecyl ether ($C_{12}E_8$) (Sigma, ≥98%)
- SOPS disodium salt (Avanti Polar Lipids, ≥99%)
- Cholesterol (Sigma, ≥99%)
- EtOH (Merck, for spectroscopy)
- $CHCl_3$ (Merck, for spectroscopy)

2.1.1a Part 1 – Preparation of the P. pastoris Membranes

Solutions

All solutions are ice-cold, unless indicated otherwise. The PMSF solution is prepared directly before use.

- *Lysis Buffer*: 10 mM MOPS, 1.4 M sorbitol, 1 mM EDTA, pH 7.4 (Tris)
- *Buffer A*: 20 mM MOPS, 1 mM EDTA, pH 7.4 (Tris)
- 10 M urea (25 °C)
- *Buffer B*: 10 mM MOPS, 25% glycerol, pH 7.4 (Tris)
- 200 mM PMSF in EtOH
- 2 mg/ml pepstatin in 70% EtOH (-30 °C)
- 2 mg/ml leupeptin (-30 °C)
- 2 mg/ml chymostatin in DMSO (-30 °C)

Procedure

All steps are performed on ice.

1- About 20 g of *P. pastoris* cells containing either the α_1/His_{10}-β_1 or the α_2/His_{10}-β_1 isozyme of the Na,K-ATPase are suspended in 200 ml Lysis Buffer and then transferred in the chamber of a Glass Bead Beater (BioSpec Products, Inc.) containing glass beads (BioSpec Products, Inc., 0.5 mm) for 2/3 of its volume. The cooling jacket of the Glass Bead Beater is filled with 50% glycerol at -20 °C and dry ice to keep the temperature between -5 and -20 °C during cell disruption. The cells are disrupted by 7 x 1-min plus 1 x 2-min cycles, waiting 1 min in between each cycle to allow cooling of the system.

2- The glass beads are washed with 150 ml Lysis Buffer for maximum membrane recovery. Unbroken cells and organelles are removed by centrifugation at 10,000 g, 4 °C, for 15 min. Subsequently, the cell membranes are collected by ultracentrifugation at 100,000 g, 4 °C, for 1 h 46 min.

3- The pellet is suspended in 40 ml Buffer A, homogenized with a glass tissue grinder, and transferred in an Erlenmeyer flask. Urea is added dropwise while shaking up to a final concentration of 2 M and the membranes are incubated for 30 min, 6 °C, stirred at 20 rpm. This washing procedure removes about 50% membrane-associated proteins without affecting the Na,K-ATPase activity. After the incubation, urea is diluted with 150 ml Buffer A and the membranes are collected by ultracentrifugation at 100,000 g, 4 °C, for 1 h 46 min.

4- The pellet is finally suspended in 40 ml Buffer B containing 1 mM PMSF, 0.01 mg/ml pepstatin, 0.01 mg/ml leupeptin, and 0.01 mg/ml chymostatin. The protease inhibitors are added to the buffer directly before use. The membranes are homogenized with a glass tissue grinder and stored at -80 °C.

5- The membrane protein concentration is determined with the Lowry assay (*2.3.1*).

2.1.1b Part 2 – Solubilization and Purification of the α_1/His$_{10}$-β_1 and α_2/His$_{10}$-β_1 Isozymes

Solutions

All solutions are ice-cold, unless indicated otherwise. Solutions containing DDM or lipids (except the stock solutions of lipids in $CHCl_3$) are prepared directly before use.

- 20% DDM
- 200 mM PMSF in EtOH
- 200 mM EDTA, pH 7.5 (Tris)
- 20 mg/ml SOPS in $CHCl_3$ (-30 °C)
- 5 mg/ml cholesterol in $CHCl_3$ (-30 °C)
- *Solubilization Buffer 2x*: 40 mM Tricine, 500 mM NaCl, 10 mM imidazole, 20% glycerol, pH 7.4 (Tris)
- *Wash Buffer*: Solubilization Buffer 1x, 0.05% DDM
- *Beads Buffer 2x*: 40 mM Tricine, 200 mM NaCl, 20 mM imidazole, 20% glycerol, pH 7.4 (Tris)
- *Lipids 50x*: 2.5 mg/ml SOPS, 0.5 mg/ml cholesterol, 5 mg/ml $C_{12}E_8$
- *NaTGI Buffer*: Beads Buffer 1x, Lipids 1x
- *Elution Buffer*: Beads Buffer 1x, Lipids 1x, 180 mM imidazole

The Lipid 50x solution is prepared by mixing SOPS and cholesterol in a glass tube, evaporating $CHCl_3$ under a gentle flux of N_2, and solubilizing the lipids in 5 mg/ml $C_{12}E_8$. The lipid/detergent mixture is kept under N_2 atmosphere to prevent lipid peroxidation.

Procedure

All steps are performed on ice.

1- A volume of *P. pastoris* membranes containing 200 mg membrane proteins is suspended in 50 ml Solubilization Buffer 1x containing 0.5 mM PMSF and transferred into an Erlenmeyer flask. DDM is added dropwise while shaking up to a final concentration of 0.8%. The membranes are then transferred in a glass tissue grinder with

a Teflon pestle and homogenized 30 times in 15 min (α_1/His_{10}-β_1) or 15 times in 5 min (α_2/His_{10}-β_1) avoiding the formation of foam. The non-solubilized material is removed by ultracentrifugation at 100,000 g, 4 °C, for 36 min.

2- In two falcons, 1 ml of BD-Talon beads is washed in each falcon with 15 ml distilled water and then with 10 ml Wash Buffer. After each washing step, the beads are spun down at 700 g, 4 °C, for 5 min and the supernatant is discarded. The supernatant of the ultracentrifugation containing the solubilized enzyme is divided in two parts and each part is incubated with 1 ml BD-Talon beads in the presence of 150 μM EDTA for 5 h, 6 °C, stirred at 5 rpm. During the incubation, the solubilized enzyme binds to the BD-Talon beads via the His tag. The low concentration of EDTA improves the purity by reducing the binding of contaminant proteins.

3- At the end of the incubation, the BD-Talon beads are spun down at 700 g, 4 °C, for 5 min and the supernatant is discarded. The beads are washed twice with 5 ml NaTGI Buffer by gentle mixing for 10 min to remove possible bound impurities. After each washing step, the beads are spun down at 700 g, 4 °C, for 5 min and the supernatant is discarded.

4- Finally, the beads-bound enzyme is eluted by incubating the beads with 1 ml Elution Buffer for 30 min, 6 °C, stirred at 5 rpm. At the end of the incubation, the beads are spun down at 700 g, 4 °C, for 5 min, and the protein-containing supernatant is centrifuged again at maximum speed for 30 sec to spin down any BD-Talon beads left. The eluted protein is carefully removed avoiding the beads.

5- To perform the biophysical experiments in the desired conditions, the elution buffer is replaced by a solution of 20 mM tricine and 25% glycerol, pH 7.4 (Tris), and the sample is concentrated to 0.7-1.1 mg/ml protein with Amicon Ultra Centrifugal Filters 100 K (exclusion size 100 kDa).

6- The protein concentration of the concentrated sample is determined with the Lowry assay (*2.3.1*) and the specific ATPase activity is tested with the pyruvate kinase/lactate dehydrogenase assay (*2.3.2*). The purity of the preparation is estimated by SDS-PAGE (*2.3.3*). The sample is stored at 0 °C or at -80 °C after freezing with liquid N_2.

2.1.2 Purification of FXYD1 Expressed in E. coli

Human FXYD1 has been expressed in *E. coli* cells with a His6 tag at the N-terminus followed by a TEV protease cleavage site as described in (111).

In the first part of the project, FXYD1 has been purified in a two-steps procedure similar to the one described for the purification of the α_1/His_{10}-β_1 and α_2/His_{10}-β_1 isozymes of the Na,K-ATPase (111,112). The *E. coli* cells are broken with a French Press; afterwards, the membranes are solubilized with the non-ionic detergent n-dodecyl-β-maltoside (DDM) at a protein:detergent ratio of 1:2 (w/w) and FXYD1 is purified by Co^{2+}-chelate affinity chromatography with BD-Talon Beads. Approximately 50 μg of purified FXYD1 are obtained from 100 mg of membrane protein.

Subsequently, FXYD1 has been found to be mainly expressed in inclusion bodies inside the cell. To obtain maximum FXYD1 yield, after cell disruption the membranes are

incubated with 8 M urea in addition to DDM. This way approximately 0.8 mg of purified FXYD1 are obtained from 1 g of cells in a single step.

Both the cells and the membranes have been stored at -80 °C, and thawed overnight in the fridge before use.

Materials

- K_2HPO_4 trihydrate (Merck, for analysis)
- Tricine (Serva, ≥99%, analytical grade)
- Tris (MP Biomedicals, UltraPure)
- Imidazole (Merck, buffer substance, ACS)
- EDTA (Merck, Titriplex® II, for analysis, ACS)
- Glycerol (VWR, 99,3%)
- Urea (AnalaR NORMAPUR®, ≥99,5%, for analysis, ACS)
- $MgSO_4$ heptahydrate (Merck, for analysis)
- $MgCl_2$ (Merck, for analysis, EMSURE®, ACS)
- NaCl (Roth, ≥99,5%, for analysis, ACS)
- PMSF (Sigma, ≥98,5%)
- Pepstatin A (Sigma, microbial)
- Leupetin hydrochloride (Sigma, microbial, ≥90%)
- Chymostatin (Sigma, microbial)
- DDM (Anatrace, ≥99%)
- $C_{12}E_8$ (Sigma, ≥98%)
- SOPS disodium salt (Avanti Polar Lipids, ≥99%)
- Cholesterol (Sigma, ≥99%)
- EtOH (Merck, for spectroscopy)
- $CHCl_3$ (Merck, for spectroscopy)
- Deoxyribonuclease I from bovine pancreas (DNase) (Sigma, Type IV, lyophilized powder, ≥2,000 kU/mg protein)
- AcTEV™ protease (Invitrogen, 10 U/µl)

2.1.2a Procedure 1, Part 1 – Preparation of the E. coli Membranes

Solutions

All solutions are ice-cold, unless indicated otherwise. The PMSF solution is prepared directly before use.

- *Lysis Buffer*: 50 mM K_2HPO_4, 2 mM $MgSO_4$, pH 7.4 (HCl)
- 10 mg/ml DNase in 20 mM Tricine, 10% glycerol, pH 7.4 (Tris)
- *Beads Buffer 2x*: 40 mM Tricine, 200 mM NaCl, 20 mM imidazole, 20% glycerol, pH 7.4 (Tris)
- 200 mM PMSF in EtOH
- 2 mg/ml pepstatin in 70% EtOH (-30 °C)
- 2 mg/ml leupeptin (-30 °C)
- 2 mg/ml chymostatin in DMSO (-30 °C)

Procedure

All steps are performed on ice.

1- About 15 g of *E. coli* cells are suspended in 150 ml Lysis Buffer containing 0.5 mM PMSF and 10 μg/ml DNase, and disrupted with 2 cycles of a French Press treatment at 1,000 psi.

2- Unbroken cells and organelles are removed by centrifugation at 10,000 g, 4 °C, for 15 min. Subsequently, the cell membranes are collected by ultracentrifugation at 130,000 g, 4 °C, for 1h 30 min.

3- The pellet is suspended in 30 ml Beads Buffer 1x containing 1 mM PMSF, 0.01 mg/ml pepstatin, 0.01 mg/ml leupeptin, and 0.01 mg/ml chymostatin. The protease inhibitors are added to the buffer directly before use. The membranes are homogenized with a glass tissue grinder and stored at -80 °C.

4- The membrane protein concentration is determined with the Lowry assay (*2.3.1*).

2.1.2b Procedure 1, Part 2 – Solubilization and Purification of FXYD1

Solutions

All solutions are ice-cold, unless indicated otherwise. Solutions containing DDM or lipids (except the stock solutions of lipids in $CHCl_3$) are prepared directly before use.

- 20% DDM
- 200 mM PMSF in EtOH
- 200 mM EDTA, pH 7.5 (Tris)
- 20 mg/ml SOPS in $CHCl_3$ (-30 °C)
- 5 mg/ml cholesterol in $CHCl_3$ (-30 °C)
- *Solubilization Buffer 2x*: 40 mM Tricine, 500 mM NaCl, 10 mM imidazole, 20% glycerol, pH 7.4 (Tris)
- *Wash Buffer*: Solubilization Buffer 1x, 0.05% DDM
- *Beads Buffer 2x*: 40 mM Tricine, 200 mM NaCl, 20 mM imidazole, 20% glycerol, pH 7.4 (Tris)
- *Lipids 50x*: 2.5 mg/ml SOPS, 0.5 mg/ml cholesterol, 5 mg/ml $C_{12}E_8$
- *NaTGI Buffer*: Beads Buffer 1x, Lipids 1x
- *Elution Buffer*: Beads Buffer 1x, Lipids 1x, 180 mM imidazole

The Lipid 50x solution is prepared by mixing SOPS and cholesterol in a glass tube, evaporating $CHCl_3$ under a gentle flux of N_2, and solubilizing the lipids in 5 mg/ml $C_{12}E_8$. The lipid/detergent mixture is kept under a N_2 atmosphere to prevent lipid peroxidation.

Procedure

All steps are performed on ice.

1- A volume of *E. coli* membranes containing 200 mg membrane proteins is suspended in 50 ml Solubilization Buffer 1x containing 0.5 mM PMSF and transferred in an Erlenmeyer flask. DDM is added dropwise while shaking up to a final concentration of

0.8%. The membranes are then transferred in a glass tissue grinder with a Teflon pestle and homogenized 30 times avoiding the formation of foam. The non-solubilized material is removed by ultracentrifugation at 120,000 g, 4°C, for 30 min.

2- In two falcons, 1 ml of BD-Talon beads is washed in each falcon with 15 ml water and then 10 ml Wash Buffer. After each wash, the beads are spun down at 700 g, 4°C, for 5 min and the supernatant is discarded. The supernatant of the ultracentrifugation is divided in two parts and each part is incubated with 1 ml BD-Talon beads in the presence of 160 μM EDTA for 5 h, 6 °C, stirred at 5 rpm. During the incubation, the solubilized FXYD1 binds to the BD-Talon beads via the His tag. A small concentration of EDTA improves the purity by reducing the binding of contaminant proteins.

7- At the end of the incubation, the BD-Talon beads are spun down at 700 g, 4°C, for 5 min and the supernatant is discarded. The beads are washed twice with 5 ml NaTGI Buffer by gentle mixing for 10 min to remove possible bound impurities. After each wash, the beads are spun down at 700 g, 4°C, for 5 min and the supernatant is discarded.

8- Finally, the beads-bound FXYD1 is eluted by incubating the beads with 1 ml Elution Buffer for 30 min, 6 °C, at 5 rpm. At the end of the incubation, the beads are spun down at 700 g, 4°C, for 5 min and the protein-containing supernatant is centrifuged again at maximum speed for 30 sec to spin down any BD-Talon beads left. The eluted protein is carefully removed avoiding the beads.

9- The protein concentration of the sample is determined with the Lowry assay (*2.3.1*) and the purity of the preparation is estimated by SDS-PAGE (*2.3.3*). The sample is stored at 0 °C and used for *in vitro* reconstitution with α_1/His_{10}-β_1 in within 24 h. Before the *in vitro* reconstitution, FXYD1 is incubated with 1 μl AcTEV™ protease/30 mg protein overnight at RT to remove the His tag.

2.1.2c Procedure 2 – Purification of FXYD1 from E. coli Cells

Solutions

All solutions are ice-cold, unless indicated otherwise.

- *Lysis Buffer*: 50 mM Tricine, 250 mM NaCl, 5 mM $MgCl_2$,1 mM EDTA, pH 7.4 (Tris)
- 10 mg/ml DNase in 20 mM Tricine, 10% glycerol, pH 7.4 (Tris)
- *Solubilization Buffer* (25 ^{o}C): 50 mM Tricine, 10% glycerol, 250 mM NaCl, 2 mg/ml DDM, 8 M urea, pH 7.4 (Tris)
- *Urea Dilution Buffer* (25 ^{o}C): 50mM Tricine, 250 mM NaCl, 10% glycerol, pH 7.4 (Tris)
- *Beads Buffer*: 50 mM Tricine, 10% glycerol, 250 mM NaCl, 1 mg/ml DDM, 4 M urea, 40 mM imidazole, pH 7.4 (Tris)
- *Elution Buffer*: 50 mM Tricine, 10% glycerol, 500 mM NaCl, 0.1 mg/ml $C_{12}E_8$, 4 M urea, 250 mM imidazole, pH 7.4 (Tris)
- *Dialysis Buffer*: 50 mM Tricine, 10% glycerol, 500 mM NaCl, 3 M urea, pH 7.4 (Tris)

- *Dialysis Dilution Buffer*: 50 mM Tricine, 10% glycerol, 500 mM NaCl, pH 7.4 (Tris)

Procedure

All steps are performed on ice, unless indicated otherwise.

1- About 1.5 g of *E. coli* cells are washed with 7.5 ml Lysis Buffer and then centrifuged at 10,000 g, 4ºC, for 30 min. The pellet is suspended with 50 ml Lysis Buffer containing 1 mM PMSF and 10 µg/ml DNase, and the cells are disrupted with 2 cycles of a French Press treatment at 1,000 psi.

2- The membranes are collected by ultracentrifugation at 200,000 g, 4 °C, for 90 min, suspended with 30 ml Solubilization Buffer, homogenized 30 times at RT in a glass tissue grinder with a Teflon pestle, and incubated for 30 min, RT, at 5 rpm.

3- Urea is diluted 2 fold by the addition of Urea Dilution Buffer and the non-solubilized material is removed by ultracentrifugation at 200,000 g, 4 °C, for 30 min.

4- In two falcons, 3 ml of BD-Talon beads are washed in each falcon with 30 ml Beads Buffer. The beads are spun down at 700 g, 4 °C, for 5 min and the supernatant is discarded. The supernatant of the ultracentrifugation containing the solubilized protein is divided in two parts and each part is incubated with 3 ml BD-Talon beads for 1 h, 6 °C, stirred at 5 rpm. During the incubation, the solubilized FXYD1 binds to the BD-Talon beads via the His tag.

5- At the end of the incubation, the BD-Talon beads are spun down at 700 g, 4 °C, for 5 min and the supernatant is discarded. The beads are washed three times with 9 ml Beads Buffer by gentle mixing for 10 min to remove possible bound impurities. After each wash, the beads are spun down at 700 g, 4 °C, for 5 min and the supernatants is discarded.

6- Finally, the beads-bound FXYD1 is eluted by incubating the beads with 3 ml Elution Buffer for 30 min, 6 °C, stirred at 5 rpm. At the end of the incubation, the beads are spun down at 700 g, 4 °C, for 5 min and the protein-containing supernatant is centrifuged again at maximum speed for 30 sec to spin down any BD-Talon beads left. The eluted protein is carefully removed avoiding the beads.

7- The protein concentration of the sample is determined with the Lowry assay (*2.3.1*) and the purity of the preparation is estimated by SDS-PAGE (*2.3.3*). The sample is stored at -20 °C. Before *in vitro* reconstitution with α_1/His_{10}-β_1, FXYD1 is dialyzed to reduce the urea concentration up to 0.5 M. At lower urea concentrations, FXYD1 oligomerizes rapidly (approximately 48 h at RT). The dialysis is performed in four 2 h-steps against x100 volumes of different buffers: Dialysis Buffer to get 3 M urea, 1/3 Dialysis Buffer exchanged with Dialysis Dilution Buffer to get 2 M urea, 1/2 Dialysis Buffer exchanged with Dialysis Dilution Buffer to get 1 M urea, and finally again 1/2 Dialysis Buffer exchanged with Dialysis Dilution Buffer to get 0.5 M urea. FXYD1 is then incubated with 1 µl AcTEV™ protease/15 mg protein overnight at RT to remove the His tag.

2.1.3 In Vitro Reconstitution of the α_1/His$_{10}$-β_1/FXYD1 Complex

The *in vitro* reconstitution of the α_1/His$_{10}$-β_1/FXYD1 complex has been conducted during the purification of the α_1/His$_{10}$-β_1 isozyme as described in (111,112). After incubating the solubilized α_1/His$_{10}$-β_1 with BD-Talon beads as described in *2.1.1b*, one part of the BD-Talon beads is incubated with a 10 fold molar excess of purified FXYD1 for 3 h, 6 °C, stirred at 5 rpm. Upon incubation, the purified FXYD1 spontaneously associates with the beads-bound α_1/His$_{10}$-β_1 at an enzyme:FXYD1 ratio of 1:1. Afterwards, the BD-Talon beads are washed to remove the non-reconstituted FXYD1, and the complex is eluted as described in *2.1.1b*. With this procedure it is possible to obtain α_1/His$_{10}$-β_1 and α_1/His$_{10}$-β_1/FXYD1 simultaneusely starting form the same yeast membranes. Therefore, the direct comparison of the properties of the enzyme with and without FXYD1 allows the definition of the specific effects of FXYD1 on the ion pump.

To perform the biophysical experiments in the desired conditions, the elution buffer is replaced by a solution of 20 mM tricine and 25% glycerol, pH 7.4 (Tris), and the samples are concentrated to 0.7-1.1 mg/ml protein with Amicon Ultra Centrifugal Filters 100 K (exclusion size 100 kDa). The protein concentration of the concentrated sample is determined with the Lowry assay (*2.3.1*) and the specific ATPase activity is tested with the pyruvate kinase/lactate dehydrogenase assay (*2.3.2*). The purity of the preparation is estimated by SDS-PAGE (*2.3.3*).

To verify reconstitution, the enzyme:FXYD1 ratio has been checked by quantitative protein determination with SDS-PAGE (*2.3.3*) for $\alpha_1\beta_1$ and with Western Blot (*2.3.4*) for FXYD1. Since the molecular weight ratio between FXYD1 and $\alpha_1\beta_1$ is ~ 1:20, an amount of $\alpha_1\beta_1$ about 20 times the amount of FXYD1 indicates a 1:1 enzyme:FXYD1 ratio. Calibration curves have been obtained with known amounts of purified α_1/His$_{10}$-β_1 or FXYD1. The range has been chosen calculating the relative amount of $\alpha_1\beta_1$ and FXYD1 in a purified α_1/His$_{10}$-β_1/FXYD1 sample of known concentration assuming a ratio of 1:1. Gels and Western Blots have been elaborated with USI-Gel V.5.1.

2.2 Preparation of Proteoliposomes

Lipid vesicles containing the native Na,K-ATPase from rabbit kidney, or the purified recombinant α_1/His_{10}-β_1 or α_1/His_{10}-β_1/FXYD1, have been prepared with a method similar to the one described before for the reconstitution of bacteriorhodopsin (113). Since DDM cannot be efficiently removed by dialysis due to its low critical micelle concentration (0.01% at 25 °C), the proteoliposomes are obtained by adsorption of the detergent onto SM2 Bio-Beads (BioRad, 20-50 mesh). In summary, the addition of an excess of SM2 Bio-Beads to a solution containing a mix of DDM-solubilized native Na,K-ATPase or purified recombinant enzyme and lipid/DDM micelles leads to the fast adsorption of the detergent by the beads and the formation of active unilamellar proteoliposomes with an average diameter of 110 nm (113). Typically, half of the protein molecules are reconstituted with the ATP-binding site facing outward.

The lipid composition of the vesicles has been optimized to obtain proteoliposomes with a low membrane conductance and a high enzyme activity. The vesicles are formed by a mixture of dieicosenoylphosphatidylcholine (DEPC), L-α-phosphatidylcholine from soybean (SBPC), and cholesterol in the ratio of 50:49:1 mol/mol. SBPC provides a mix of phospholipids with a broad fatty acid chains distribution, creating a lipid environment comparable to a cell membrane. To investigate the effect of anionic phospholipids on the interaction of FXYD1 with the enzyme, in some experiments the zwitterionic DEPC has been replaced with 10, 20, 35 and 50 mol % of the anionic dioleoylphosphatidylserine (DOPS).

Materials

- Imidazole (Merck, buffer substance, ACS)
- EDTA (Merck, Titriplex® II, for analysis, ACS)
- $MgSO_4$ heptahydrated (Merck, for analysis)
- K_2SO_4 (Merck, for analysis, ACS)
- Na_2SO_4 anhydrous (Merck, for analysis, ACS)
- DDM (Anatrace, ≥99%)
- L-α-phosphatidylcholine from soybean (Sigma, Type II-S, 14-23% choline basis)
- DEPC (Avanti Polar Lipids, >99%)
- DOPS (Avanti Polar Lipids, >99%)
- Cholesterol (Sigma, ≥99%)
- $CHCl_3$ (Merck, for spectroscopy)
- H_2SO_4 (Backer, 95-97%)

Solutions

All solutions are stored at -30 °C, unless indicated otherwise.

- *Buffer H*: 25 mM imidazole, 1 mM EDTA, 5 mM $MgSO_4$, 5 mM Na_2SO_4, 70 mM K_2SO_4, pH 7.2 (H_2SO_4) (4 °C)
- 100 mg/ml SBPC in $CHCl_3$
- 50 mg/ml DEPC in $CHCl_3$
- 20 mg/ml DOPS in $CHCl_3$
- 5 mg/ml cholesterol in $CHCl_3$
- 10% DDM in Buffer H

Procedure

1- Appropriate amounts of the lipid stock solutions are mixed in a glass vessel and $CHCl_3$ is evaporated at RT for 30 min under vacuum while rotating.

2- The thin lipid film is dissolved in a volume of 2% DDM in Buffer H to obtain a lipid concentration of 8 mg/ml. The lipid/DDM mixture is sonicated for 1-2 minutes and kept at RT until a clear solution is obtained, indicating complete solubilization of the lipids. To avoid lipid peroxidation, the mixture is kept always under N_2 atmosphere.

3- An amount of SM2 Bio-Beads equal to 1 mg beads/2 ml lipid/DDM mixture is equilibrated in Buffer H and degassed for 30 min under vacuum while rotating. At the end of the incubation, Buffer H is removed with capillary tips (Biozym).

4- To obtain proteoliposomes with the native Na,K-ATPase from rabbit kidney, protein-containing membrane fragments prepared according to (114) are solubilized with DDM at a protein:detergent ratio 1:2 (w/w). The solubilized native Na,K-ATPase or the purified recombinant enzyme is diluted with Buffer H to get a protein concentration of 0.1 mg/ml and mixed with the lipid/DDM mixture at a ratio 1:1 v/v. The beads are added and the mixture is incubated overnight, 6 °C, stirred at maximum speed.

5- The solution containing the vesicles is separated from the beads with capillary tips and stored at 0 °C. When kept on ice for a minimum of 3 h, tight vesicles are obtained. Assuming that all the enzyme molecules reconstitute inside the lipid membrane, the final enzyme:lipid ratio is about 1:15000, meaning 6-7 ion pumps per vesicle.

The specific ATPase activity of the native Na,K-ATPase before and after solubilization of the membrane fragments as well as after reconstitution in lipid vesicles has been determined with the pyruvate kinase/lactate dehydrogenase assay (*2.3.2*).

2.3 Assays, SDS-PAGE and Western Blot

2.3.1 Determination of the Total Protein Concentration - Lowry Assay

The protein concentration of the *P. pastoris* and *E. coli* membranes as well as of the purified α_1/His_{10}-β_1, α_2/His_{10}-β_1, FXYD1, and α_1/His_{10}-β_1/FXYD1 samples has been determined with the Lowry assay (115). The Lowry assay is a colorimetric method for the determination of the total protein concentration in a sample. It is based on the reaction of Cu^+-protein complexes with the Folin-Ciocalteu Phenolreagent, a mixture of phosphor-tungstic acid and phosphomolybdic acid, that develops a blue color measured spectro-photometrically at 700 nm. The absorbance is proportional to the protein concentration. Using a calibration curve obtained with a protein standard of known concentration, usually bovine serum albumin (BSA), it is possible to obtain the unknown total protein concentration of the sample.

Material

- BSA (BioRad, Protein Standard I, lyophilized)
- NaOH (Riedel-de Haën, for analysis)
- $CuSO_4$ pentahydrated (Riedel-de Haën, for analysis, ACS)
- Disodium tartrate dihydrated (Merck, for analysis, EMSURE®)
- Na_2CO_3 anhydrous (Riedel-de Haën, for analysis, ACS)
- Folin-Ciocalteu Phenolreagent (Merck)

Solutions

- 3 mg/ml BSA
- 0,5 M NaOH
- 1% $CuSO_4$
- 2% disodium tartrate
- 4% Na_2CO_3
- Reagent D (250 µl 1% $CuSO_4$, 250 µl 2% disodium tartrate, 24.5 ml 4% Na_2CO_3)
- 1:10 Folin-Ciocalteu Phenolreagent

Procedure

The assay is carried out in disposable glass vials.

1- To obtain the calibration curve, different vials containing amounts of BSA between 0 and 30 µg are prepared. For the determination of the unknown protein concentration in a sample, two vials are prepared: one with the protein-containing sample and one with the sample buffer, used as background. For the measurement of the *P. pastoris* and *E. coli* membrane protein concentration, 1 µl of sample is used, while for the purified α_1/His_{10}-β_1, α_2/His_{10}-β_1, FXYD1, and α_1/His_{10}-β_1/FXYD1, 10 µl are used. Equal volumes of the respective buffers are used as background. In each vial, distilled water is added up to 10 µl.

2- At the beginning of the assay, 400 µl of 0.5 M NaOH are added to each vial and incubated at 37 °C for 30 min.

3- At the end of the incubation, 1 ml of Reagent D is added to each vial and incubated at RT for 15 min. The unfolded protein molecules react with Reagent D in alkali conditions to form Cu^{+}-protein complexes.

4- Finally, 1 ml of 1:10 Folin-Ciocalteus Phenolreagent is added to each vial and incubated at RT for 30 min. The Cu^{+}-protein complexes react with the Folin-Ciocalteu Phenolreagent developing a blue color.

5- The absorbance of each vial is measured at 700 nm in a Perkin-Elmer Lambda40 UV/VIS Spectrometer using a cuvette made of special glass (Hellma, type 100-OS). Distilled water is used as reference. The sample concentration is obtained by interpolation on the calibration curve of the sample absorbance corrected for the background absorbance.

2.3.2 Determination of the Specific ATPase Activity – PK/LDH Assay

The specific ATPase activity of the purified recombinant α_1/His_{10}-β_1, α_2/His_{10}-β_1, and α_1/His_{10}-β_1/FXYD1 preparations as well as of the native Na,K-ATPase in membrane fragments, in solubilized form, and in lipid vesicles has been determined with an enzymatic method exploiting the enzymes pyruvate kinase (PK) and lactate dehydrogenase (LDH) (116). The method is based on the following reactions:

$$\mathrm{ATP} \xrightarrow{\text{Na,K–ATPase / other ATPases}} \mathrm{ADP} + \mathrm{P_i}$$

$$\mathrm{Phosphoenolpyruvate} + \mathrm{ADP} \xrightarrow{\text{PK}} \mathrm{Pyruvate} + \mathrm{ATP}$$

$$\mathrm{Pyruvate} + \mathrm{NADH} \xrightarrow{\text{LDH}} \mathrm{Lactate} + \mathrm{NAD^{+}}$$

By measuring the NADH consumption at 340 nm it is possible to evaluate the total ATPase activity of the sample. Besides the Na,K-ATPase, also other ATP-consuming systems (e.g. other ATPases) contribute to the total activity. To obtain the specific activity of the Na,K-ATPase, the enzyme is selectively inhibited by 125 µM ouabain at the end of the experiment. The NADH consumption detected after ouabain addition corresponds to the residual activity, due only to the other ATP-consuming systems in the sample. Therefore, the total activity corrected for the residual activity provides the specific activity of the Na,K-ATPase in the sample.

Material

- NaCl (Roth, ≥99,5%, for analysis, ACS)
- KCl (Riedel-de Haën, for analysis)
- $MgCl_2$ hexahydrate (Merck, for analysis, EMSURE®, ACS)
- Imidazole (Merck, buffer substance, ACS)
- ATP disodium salt (Sigma, ≥99%)
- Phosphoenolpyruvic acid tris(cyclohexylamine) salt (PEP) (Sigma, ≥98%)
- EDTA (Merck, Titriplex® II, for analysis, ACS)
- Tris (MP Biomedicals, UltraPure)

- NADH disodium salt (Roche, grade II, approx. 98%)
- PK/LDH enzymes from rabbit muscle (Sigma, buffered aqueous glycerol solution, 600-1,000 U/ml PK, 900-1400 U/ml LDH)
- Ouabain octahydrate (Sigma, ≥95%)

Solutions

The solution containing NADH is prepared directly before use.

- *NaK Buffer*: 100 mM NaCl, 10 mM KCl, 5 mM $MgCl_2$, 25 mM imidazole, 3 mM ATP, 2 mM PEP, 1 mM EDTA, pH 7.2 (HCl)
- 60 mg/ml NADH in 1 mM EDTA, pH 7.2 (Tris)
- 5 mM ouabain

Procedure

The experiment is performed at 37 ± 0.5 °C in a Perkin-Elmer Lambda40 UV/VIS Spectrometer. The absorbance is recorded at 340 nm for a period of 10 min. After every addition, the solution is carefully mixed with a small spatula.

1- A cuvette made of quartz SUPRASIL® (Hellma, type 104B-QS) is filled with 800 µl of NaK Buffer and equilibrated for 10 min inside the instrument to stabilize the desired temperature.

2- At the beginning of the experiment, 6 µl of the PK/LDH suspension are added to the cuvette and the resulting absorbance is recorded as background absorbance.

3- After starting the measurement, 2.5 µl of the NADH solution are added. The absorbance increases up to a stable value corresponding to zero ATPase activity.

4- Upon addition of 10 µl protein sample or 60 µl vesicles, a steep absorbance decrease, corresponding to NADH consumption, is recorded for a few minutes.

5- Finally, 125 µM ouabain is added to specifically inhibit the Na,K-ATPase activity. A slower absorbance decrease, corresponding to the residual consumption of NADH, is recorded until the end of the experiment.

The specific activity of the Na,K-ATPase is obtained with the following formula:

$$\text{Specific Activity} = \frac{(\text{Absorbance Decrease} / \text{min}) \cdot V \cdot 770{,}4}{m \cdot 60} = \mu\text{mol } P_i / (mg \cdot \text{min})$$

with

Absorbance Decrease/min = slope of the signal before ouabain addition minus slope of the signal after ouabain addition

V = volume in the cuvette (ml)

m = protein in the cuvette (µg)

2.3.3 SDS-PAGE

The purity of the purified α_1/His_{10}-β_1, α_2/His_{10}-β_1, FXYD1, and α_1/His_{10}-β_1/FXYD1 has been estimated by SDS-PAGE prepared according to Lämmli (117). As explained in *2.1.3*, the enzyme:FXYD1 ratio in the purified α_1/His_{10}-β_1/FXYD1 complex has been checked by quantitative protein determination with SDS-PAGE for $\alpha_1\beta_1$ and with Western Blot following SDS-PAGE for FXYD1.

Material

- Rotiphorese® Gel 30% Acrylamide/Bisacrylamide 37.5:1 (Roth)
- PageRuler™ Prestained Protein Ladder 10-170 kDa (Fermentas)
- Ammonium Persulfate (APS) (BioRad)
- Temed (BioRad)
- Tris (MP Biomedicals, UltraPure)
- Glycine (Roth, ≥99%, for analysis)
- SDS (Pierce, electrophoresis grade)
- Glycerol (VWR, 99,3%)
- β–Mercaptoethanol (Merck, for analysis)
- Bromophenol blue (Fluka)
- Coomassie Blue R-250 (BioRad, electrophoresis purity)
- Isopropanol (Baker, ACS)
- Acetone (Baker, ACS)
- Isobutanol (Fluka, ≥99,5%)
- MeOH (Sigma, ≥99,9%, for HPLC)
- Acetic Acid (Merck, ≥96%, for analysis)

Solutions

Tris Buffer for Stacking Gel 4x, Tris Buffer for Separating Gel 4x, and Running Buffer 10x are stored at 4 °C and equilibrated at RT before use. All other solutions are stored at RT. Solutions containing APS and/or Temed are prepared directly before use.

- 1:1 Isopropanol/Acetone
- *Tris Buffer for Stacking Gel 4x*: 0.5 M Tris, 0.4% SDS, pH 6.8 (HCl)
- *Tris Buffer for Separating Gel 4x*: 1.5 M Tris, 0.4% SDS, pH 8.8 (HCl)
- 10% APS
- *Stacking Gel Solution*: 4% Acrylamide/Bisacrylamide, Tris Buffer for Stacking Gel 1x, 0.1% APS, 0.1% Temed
- 90% Isobutanol
- *Separating Gel Solution*: 12% Acrylamide/Bisacrylamide, Tris Buffer for Separating Gel 1x, 0.5% Glycerol, 0.1% APS, 0.04% Temed
- *Sample Buffer 3x*: Tris Buffer for Staking Gel 1.5x, 9% SDS, 30% Glycerol, 1.5 mM β–Mercaptoethanol, 0.01% Bromophenol Blue
- *Running Buffer 10x*: 250 mM Tris, 2 M Glycine, 1% SDS
- *Fixing Solution*: 10% Acetic Acid, 40% MeOH
- *Staining Solution*: 10% Acetic Acid, 50% MeOH, 0.1% Coomassie Blue R-250
- *Destaining Solution*: 7% Acetic Acid, 20% MeOH

Procedure

The gels are run in a BioRad Mini-PROTEAN II electrophoresis cell connected to a Consort electrophoresis power supply.

1- The glass plates are cleaned with 1:1 Isopropanol/Acetone and left to dry. The glass plate sandwiches are assembled in the clamp assembly with 1 mm spacers according to the instruction manual and transferred to the casting slots of the casting stand.

2- About 4.5 ml of Separating Gel Solution are poured into the glass plate sandwiches avoiding the formation of air bubbles. The solution is overlaid with about 1 ml 90% Isobutanol and left to polymerize at RT for 1 h. This way a straight, regular interface between Separating Gel and Stacking Gel is obtained.

3- The overlay solution is rinsed carefully with distilled water. The Stacking Gel Solution is poured into the glass plate sandwiches to fill them completely avoiding the formation of air bubbles. A 10 well x 1 mm comb is placed in each sandwich and the solution is left to polymerize at RT for 30 min.

4- The combs are removed carefully. The wells are rinsed with Running Buffer 1x and covered with it. Protein samples are prepared with 5 µl Sample Buffer 3x, various amounts of purified protein, and distilled water up to 15 µl. For α_1/His_{10}-β_1, α_2/His_{10}-β_1, and α_1/His_{10}-β_1/FXYD1, 3-7 µg purified protein are used. If SDS-PAGE is followed by Western Blot, 0.1-0.5 µg purified FXYD1 are used, otherwise 2 µg. 8 µl PageRuler™ Prestained Protein Ladder or 10 µl protein sample are loaded carefully in each well with a Hamilton syringe. The protein samples are not heated to avoid aggregation of membrane proteins.

5- The glass plate sandwiches are placed into the running apparatus according to the instruction manual. The upper buffer chamber is filled with Running Buffer 1x until the buffer reaches a level halfway between the short and long plates. The lower buffer chamber is filled with Running Buffer 1x to cover at least 1 cm of the bottom of the gel and ensure electrical contact. The equipment is closed and connected to the power supply. The gels are run at the constant voltage of 85 V in the Stacking Gel and 110 V in the Separating Gel.

6- At the end of the run, the gels are removed carefully from the glass plate sandwiches and incubated 15 min with Fixing Solution while shaking gently.

7- Afterwards, the gels are incubated with Staining Solution for 2 h while shaking gently.

8- Finally, the gels are incubated with Destaining Solution for 15 min and then overnight while shaking gently.

2.3.4 Western Blot

The fraction of FXYD1 in the purified α_1/His_{10}-β_1/FXYD1 complex has been estimated by Western Blot following SDS-PAGE as explained in *2.1.3*. In this case, the gels have not been stained as described in points 6-8 of *2.3.3*. An antibody raised against the C-terminal sequence CRSSIRRLSTRRR of FXYD1, provided by Steven Karlish, has been used as primary antibody to recognize the unphosphorylated FXYD1.

Material

- NaCl (Roth, ≥99,5%, for analysis, ACS)
- KCl (Riedel-de Haën, for analysis)
- $MgCl_2$ hexahydrate (Merck, for analysis, EMSURE®, ACS)
- Na_2HPO_4 dihydrate (Merck, for analysis, EMSURE®, ACS)
- K_2HPO_4 trihydrate (Merck, for analysis)
- Tris (MP Biomedicals, UltraPure)
- Glycine (Roth, ≥99%, for analysis)
- SDS (Pierce, electrophoresis grade)
- Non-Fat Dry Milk (BioRad, blotting grade blocker)
- Tween® 20 (Fluka)
- Triton X-100® (Fluka, BioXtra)
- MeOH (Sigma, ≥99,9%, for HPLC)
- Anti-Rabbit IgG (whole molecule) Alkaline Phosphatase, produced in goat (Sigma)
- Western Blue® Stabilized Substrate for Alkaline Phosphatase (Promega)

Solutions

Milk Blocking Solution is prepared just before use. All other solutions are stored at 4 °C and equilibrated at RT before use.

- *Transfer Buffer*: 25 mM Tris, 192 mM Glycine, 0.02% SDS, 20% MeOH, pH 8.3
- *PBS Buffer 10x*: 1.37 M NaCl, 27 mM KCl, 100 mM Na_2HPO_4, 20 mM KH_2PO_4, pH 7.4 (HCl)
- *Milk Blocking Solution*: PBS Buffer 1x, 0.05% Tween® 20, 5% Non-Fat Dry Milk
- *PBSTT Buffer*: PBS Buffer 1x, 0.05% Tween® 20, 0.2% Triton X-100®
- *Alkaline Phosphatase Buffer*: 100 mM NaCl, 10 mM $MgCl_2$, 100 mM Tris, pH 9.5 (HCl)

Procedure

The transfer is performed in a BioRad Mini Trans-Blot® cell connected to a Consort electrophoresis power supply.

1- Before the transfer, the gels are incubated 15 min with Transfer Buffer while shaking gently. Extra thick Blot paper mini blot size (BioRad) is wet with Transfer Buffer; Roti®-PVDF membranes (Roth, 0.45 µm) are activated a few sec in MeOH and then in Transfer buffer. The sandwiches are assembled according to the instruction manual.

2- The sandwiches are placed into the running apparatus together with a cooling unit and a magnetic stirrer, and the chamber is filled with Transfer Buffer. The equipment is closed and connected to the power supply. The transfer is performed for 16 h at the constant voltage of 30 V under magnetic stirring.

3- At the end of the transfer, the PVDF membranes are removed carefully and incubated 1 h with Milk Blocking Solution while shaking gently. At the end of the incubation, the membranes are washed three times for 10 min with PBSTT Buffer while shaking gently.

4- Afterwards, the membranes are incubated 1 h with the primary antibody 1:10,000 in PBSTT Buffer while shaking gently, and then washed as described above.

5- Subsequently, the membranes are incubated 1 h with anti-Rabbit IgG 1:20,000 in PBSTT Buffer while shaking gently, and then washed as described above.

6- Finally, the membranes are equilibrated twice for 10 min with Alkaline Phosphatase Buffer while shaking gently and then incubated with Western Blue® Stabilized Substrate for Alkaline Phosphatase diluted 1:1 with Alkaline Phosphatase Buffer until clear bands are visible.

2.4 Investigation of the Na,K-ATPase with Fluorescent Dyes

Luminescence is a process where an excited molecule relaxes via the emission of light. There are several types of luminescence, named according to the source of excitation. *Fluorescence* is a form of photoluminescence, since the molecule is excited by the absorption of photons. The absorbed energy is re-emitted in a few nanoseconds, unlike *phosphorescence*, also a type of photoluminescence, in which the relaxation process occurs on a scale of seconds to hours. The emission of radiation with the same wavelength of the absorbed radiation is defined *resonance fluorescence*. In most cases, the wavelength of the emitted radiation is longer (red-shifted) than the one of the exciting radiation, meaning that it has a lower energy.

Several methods based on fluorescence have been developed for the investigation of proteins. Such methods can exploit the natural fluorescence of proteins, named *intrinsic fluorescence*, or the fluorescence of exogenous dyes, called *extrinsic fluorescence*. Detailed information about the transport mechanism of P-type ATPases can be obtained, including the affinity for the various substrates and the rate of the conformational transitions.

2.4a Intrinsic Fluorescence

The intrinsic fluorescence of proteins is due to the fluorescence of their aromatic residues. In particular, Tryptophan (Trp) presents a strong fluorescence due to the indole ring. It shows a maximum of absorption at 280 nm and a *solvatochromic* emission peak at 350 nm, whose intensity and position depend on the polarity of the environment surrounding the residue (118). Tryptophan fluorescence can be exploited to detect the conformational states of a protein. If the Trp residues of the protein experience different polar environments in the different conformations, a conformational transition induces a change in intensity as well as a red- or blue-shift of the solvatochromic peak. In particular, water has a strong fluorescence quenching effect: it promotes relaxation of the excited molecule via non-radiating processes, thus reducing the intensity of the emitted radiation. When the conformational transition results in a higher exposition of the Trp residues to water, the fluorescence intensity decreases strongly.

2.4b Extrinsic Fluorescence

Protein-bound as well as membrane-bound dyes can be used to investigate the function of proteins. The first dyes applied to the study of the transport properties of the Na,K-ATPase have been fluorescein derivatives covalently bound to the side chains of specific residues in the protein. Among them, fluorescein-5-isothiocyanate (FITC) and 5-iodoacetamide fluorescein (5-IAF) are the most popular.

FITC responds with significant fluorescence changes to the conformational transitions of the enzyme (119-121). Since it binds to Lys 501 within the ATP-binding site, it prevents ATP binding and enzyme phosphorylation (122), allowing the investigation of the transitions between E_1 and E_2, but not between E_1-P and P-E_2 (120,121). Moreover, FITC is able to report binding of the third Na^+ ion to the Na,K-ATPase in the E_1 conformation (123). Since the ATP-binding site of P-type ATPases is highly conserved, FITC can be used also to study the Ca-ATPase and the H,K-ATPase.

5-IAF binds to Cys 457 of the Na,K-ATPase, far from the phosphorylation site. Therefore, it allows the enzyme to be phosphorylated and undergo the complete transport

cycle, thus overcoming the FITC limitation (21). However, it shows significant differences in the fluorescence response depending on the animal source of the enzyme (21).

The underlying mechanism of the fluorescein labels is that of a pH indicator that responds to the small pH changes in the surrounding environment. A conformational transition induces a small variation of the protein surface shape near the dye. The charged residues side chains affect the local ion concentration on the protein surface and, consequently, the local pH. Therefore, when the pH in the bulk of the solution is buffered, the fluorescence intensity of the dye is modulated by the protein conformational changes (21).

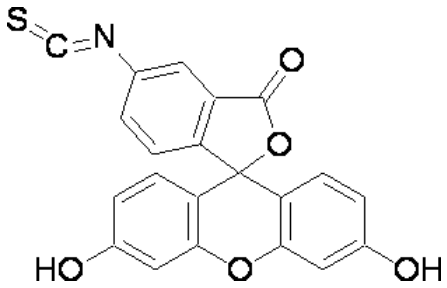

Fluorescein-5-isothiocyanate (FITC)

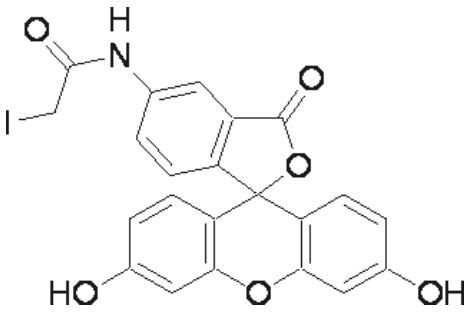

5-iodoacetamide fluorescein (5-IAF)

A second important set of dyes used to investigate the ion transport of ATPases are the voltage-sensitive dyes. These dyes are not covalently bound to the protein, but insert in the membrane containing the enzyme. Voltage-sensitive dyes allow the optical recording of membrane potentials and, thus, can be used to study the enzyme-mediated charge translocation processes. Depending on their response mechanism, they can be subdivided into slow dyes (response time ~ 300 ms) and fast dyes (response time $t \leq 1$ ms) (6). The RH styryl dyes belong to the family of fast dyes (124), while Oxonols are slow dyes (125).

The voltage-sensitive dyes RH421 and Oxonol VI have been exploited in the current study to characterize the transport properties of the purified α_1/His_{10}-β_1, α_2/His_{10}-β_1, and α_1/His_{10}-β_1/FXYD1 preparations. Therefore, they are discussed in detail in the following paragraphs.

2.4.1 The electrochromic styryl dye RH421

Originally synthesized by Rina Hildesheim, the RH dyes are dialkylaminophenylpolyenylpyridinium compounds (126). The RH421 is characterized by a terminal sulfobutyl chain bound to the nitrogen atom in the pyridine ring (Fig.23). A negative charge is localized on the terminal sulfo group, while a positive charge is delocalized on the pyridinium moiety.

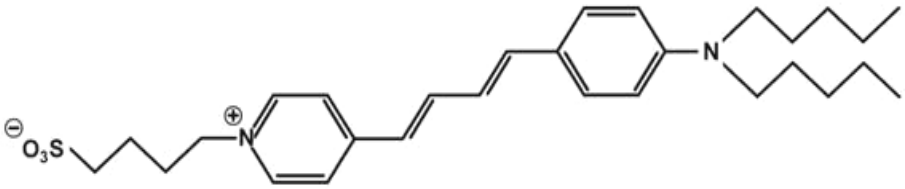

Figure 23. Structure of the electrochromic styryl dye RH421.

According to their amphiphilic structure, the RH421 molecules insert into the membrane oriented perpendicularly to the membrane surface, with the sulfo group facing the aqueous solution and the rest of the molecule in the apolar interior of the lipid bilayer (127-128). Thanks to an electrochromic effect, the dye is able to monitor the changes of the local electric field strength inside the membrane dielectric with spectral shifts (Fig. 24). The electrochromic effect derives from a dependence of the energy difference between the ground state and the excited state of the dye on the electric field strength (127). In the excited state, the delocalized positive charge on the pyridinium moiety of the dye is shifted to the aniline moiety in the membrane interior. As a consequence, a positive electric field strength inside the membrane dielectric leads to a blue-shift of the adsorption spectrum of the dye. This affects, in turn, the fluorescence spectrum of the dye.

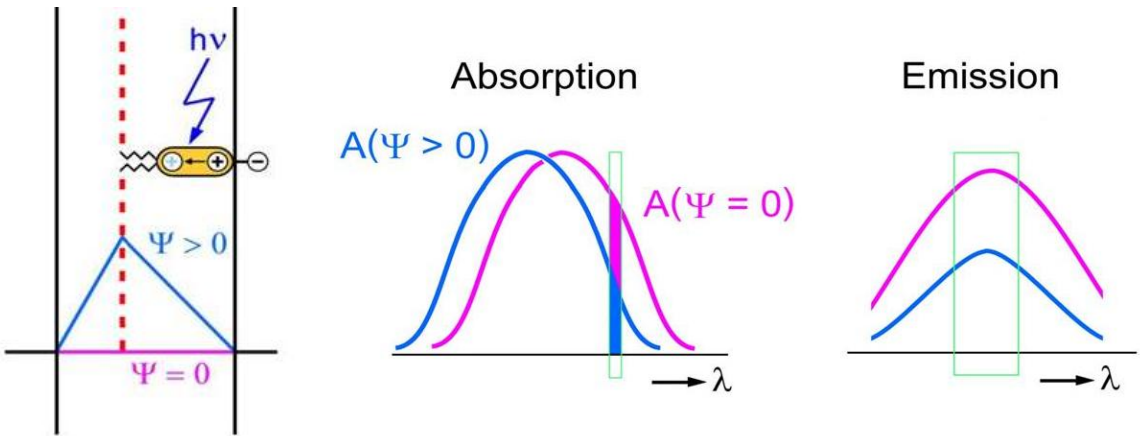

Figure 24. Electrochromic effect of the styryl dye RH421. A change in the electric field strength Ψ in the membrane dielectric affects the adsorption and the emission spectra of the dye.

When the dye molecules are inserted into open membrane fragments suspended in an aqueous solution, the two sides of the membrane are short-circuited by the electrically conducting medium. The transmembrane voltage is always zero under quasi-stationary conditions. If the membrane fragments contain a high density of Na,K-ATPase molecules, the dye reports the charge movements inside the enzyme during the transport cycle (128) (Fig. 25).

Since the detection mechanism is based on the movement of the delocalized positive charge from the pyridinium to the aniline moiety of the dye, the time resolution is significantly higher than the time constants of the ion movements between the aqueous media and the ion-binding sites of the enzyme (124). Therefore, the dye RH421 can be exploited for the detection of the electrogenic steps of the Na,K-ATPase transport cycle, mainly ion binding and ion release (*1.3.5*) (127,128). The fluorescence response of the styryl dye depends linearly on the electric field strength in the membrane dielectric and, thus, on the number of charges in the ion-binding sites of the enzyme (128).

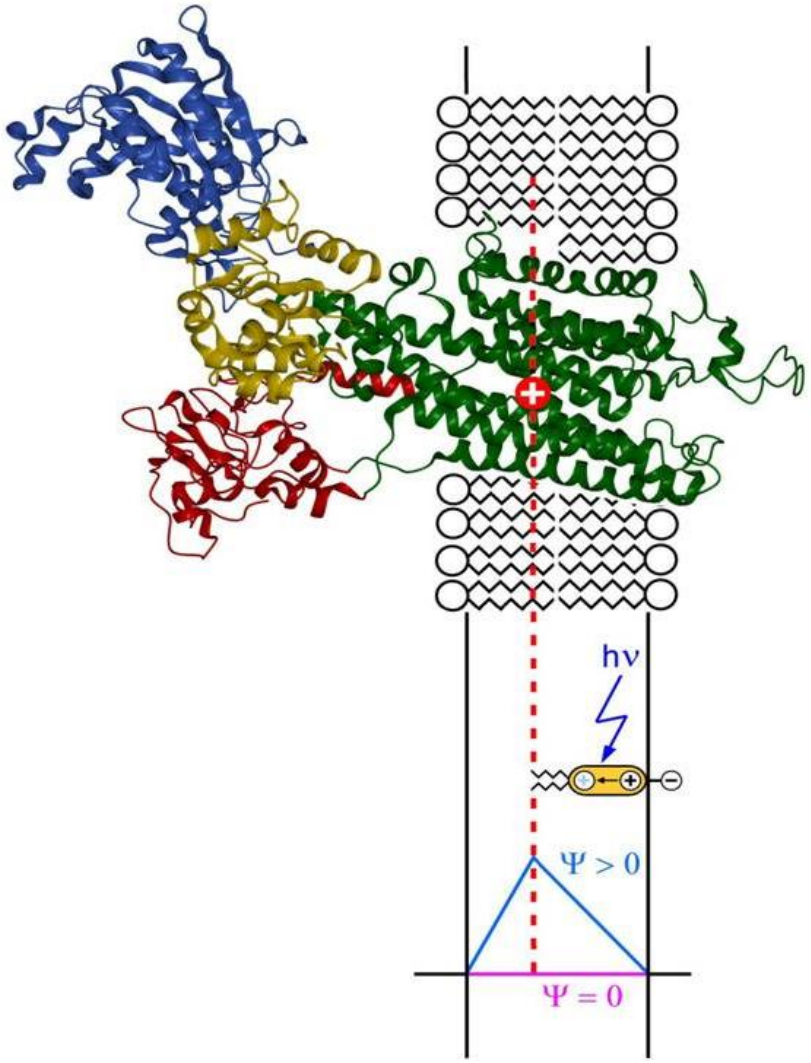

Figure 25. Thanks to the electrochromic effect, the styryl dye RH421 is able to report the charge movements inside the enzyme during the transport cycle.

The dye RH421 has been widely and successfully used to characterize the electrogenic partial reactions in the transport cycle of the native Na,K-ATPase in open membrane fragments (32,123,127-144). The main limitation of the methods exploiting this dye is related to the requirement of a high density of purified active protein in the membrane (10^3-10^4 enzyme molecules/μm^2) so that all dye molecules are close to the transmembrane domain of the ion pumps and significant fluorescence signals are detected (127). The expression level of recombinant Na,K-ATPase in *P. pastoris* membranes is about 0.1% (27), too low for this purpose. Recently, we have demonstrated that it is possible to overcome this limitation and extend the methods exploiting the dye RH421 to the detergent-solubilized native Na,K-

ATPase (145). In the current study, the transport properties of the purified recombinant α_1/His$_{10}$-β_1, α_2/His$_{10}$-β_1, and α_1/His$_{10}$-β_1/FXYD1 have been investigated with a steady-state fluorescence method and with time-resolved kinetic measurements after photochemical release of ATP. Steady-state fluorescence measurements allow the evaluation of the ion-binding affinities in the E_1 and P-E_2 conformations as well as the study of the so-called *backdoor phosphorylation* reaction. Time-resolved kinetic experiments after photochemical release of ATP enable the estimation of the ATP-binding affinity and the time constant of the conformational transition (Na_3)E_1-P → P-E_2Na_3.

2.4.1a Steady-state Fluorescence Measurements

The steady-state fluorescence measurements have been carried out in a Perkin-Elmer LS 50B fluorescence spectrophotometer (Fig. 26). The optical system of the instrument consists of a xenon flash lamp, monochromators on the excitation and emission sides, a stirred cell holder, a photomultiplier for the detection of the fluorescence emission, and a system of mirrors. To correct the fluctuations of the light source, a minor portion of the exciting radiation is deviated by a beam splitter to a reference photomultiplier. The temperature of the cell holder is controlled by an external thermostat.

The excitation wavelength has been set to 580 nm and the emission wavelength to 660 nm, with slit widths of 15 and 20 nm, respectively. At these wavelengths, the binding of cations to the ion-binding sites of the enzyme induces a decrease in the fluorescence intensity of the dye, whereas the release of cations induces a fluorescence increase. Monochromators transmit not only the selected wavelength, but also multiples of it. To avoid the detection of these wavelengths, for example 330 nm, a cut-off filter at 430 nm has been placed before the photomultiplier.

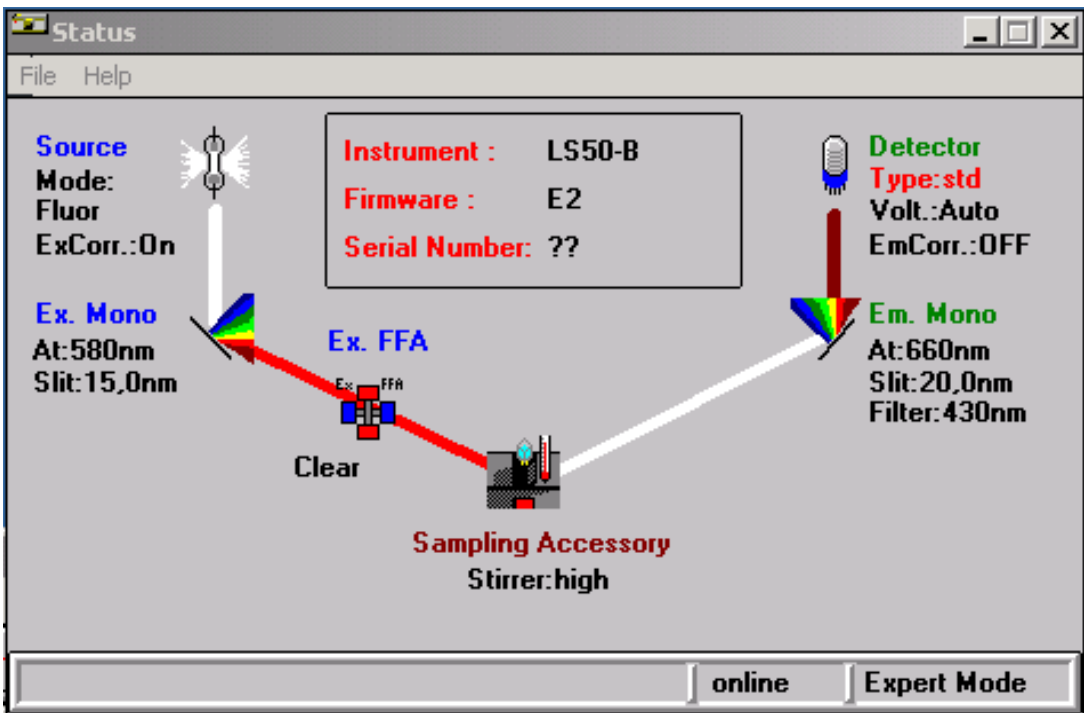

Figure 26. Scheme of the optical system of the Perkin-Elmer LS 50B fluorescence spectrophotometer, set on the conditions used for the steady-state fluorescence measurements.

The basic experiment of the steady-state technique is the so-called *standard experiment*. In this experiment, the fluorescence response of the dye RH421 is monitored upon different substrate additions in saturating concentrations (Fig. 27). The additions stabilize specific stationary states of the enzyme during the transport cycle. The experiment enables the detection of electrogenic ion binding and release (127).

Materials

- Imidazole (Merck, buffer substance, ACS)
- EDTA (Merck, Titriplex® II, for analysis, ACS)
- $MgCl_2$ hexahydrate (Merck, for analysis, EMSURE®, ACS)
- NaCl (Merck, for analysis)
- ATP disodium salt (Roche, 100%)
- KCl (Merck, for analysis, Suprapur)
- RH421 (MoBiTec)
- EtOH (Merck, for spectroscopy)

Solutions

- *Buffer*: 25 mM imidazole, 1 mM EDTA, pH 7.2 (HCl)
- 1 M $MgCl_2$
- 200 µM RH421 in EtOH
- 5 M NaCl
- 0.5 M ATP
- 2 M KCl

Procedure

The experiment is performed at 20 ± 0.5 °C under magnetic stirring.

1- A cuvette made of special optical glass (Hellma, type 109.004F-OS) is filled with 1 ml of Buffer containing 5 mM $MgCl_2$ and equilibrated for 10 min inside the instrument to stabilize the desired temperature.

2- At the beginning of the experiment, 200 nM RH421 is added to the cuvette. With this dye concentration it is possible to obtain a sufficiently high fluorescence intensity during the experiment and avoid the formation of dye aggregates in the membrane.

3- After 3 min, 9 µg of purified protein are added, causing a strong fluorescence increase due to the insertion of the dye molecules in the membrane. The partition coefficient of the dye is very high (~250,000); >90% of the dye molecules insert in the membrane (127). In the absence of substrates, the Na,K-ATPase is mainly in the E_1 conformation with the ion-binding sites occupied by protons in a pH-dependent manner (32). This state is indicated as H_nE_1; at pH 7.2, n ~ 1.8 (32).

4- When a stable steady-state is reached, 50 mM NaCl is added to the cuvette. The enzyme undergoes the transition to the state Na_3E_1, exchanging about two H^+ with three Na^+ ions. Since the binding of the first two Na^+ ions is mostly counterbalanced by the release of protons, only the binding of the third Na^+ ion is electrogenic.

Therefore, the transition induces a fluorescence decrease that reflects the binding of the last Na^+ ion only.

$$H_nE_1 + 3\ Na^+ \rightarrow Na_3E_1 + n\ H^+$$

5- Upon addition of 0.5 mM ATP, the protein is phosphorylated and undergoes the conformational transition to $P\text{-}E_2$. In this conformation, the protein has a lower Na^+-binding affinity and releases the Na^+ ions on the extracellular side of the membrane. In the absence of K^+ ions, dephosphorylation is very slow (130) and the enzyme is trapped in the $P\text{-}E_2$ state with virtually empty ion-binding sites, since the release of Na^+ ions is not counterbalanced by binding of protons (32). Therefore, a fluorescence increase is detected that reflects the electrogenic release of all three Na^+ ions and that, thus, is about three times the previous fluorescence decrease.

$$Na_3E_1 + ATP \rightarrow Na_3E_1{\cdot}ATP \rightarrow (Na_3)E_1\text{-}P \rightarrow P\text{-}E_2Na_3 \rightarrow P\text{-}E_2 + 3\ Na^+$$

6- Finally, after the addition of 20 mM KCl all substrates are present to maintain the enzyme under turnover conditions. The fluorescence level represents mainly a mixture of the occluded states $(Na_3)E_1\text{-}P$ and $E_2(K_2)$ preceding the conformational transitions, which are the rate-limiting steps of the transport cycle.

$$P\text{-}E_2 + 2\ K^+ \rightarrow P\text{-}E_2K_2 \rightarrow E_2(K_2) + Pi \rightarrow K_2E_1 \rightarrow E_1 + 2\ K^+ \rightarrow Na_3E_1{\cdot}ATP \rightarrow \ldots$$

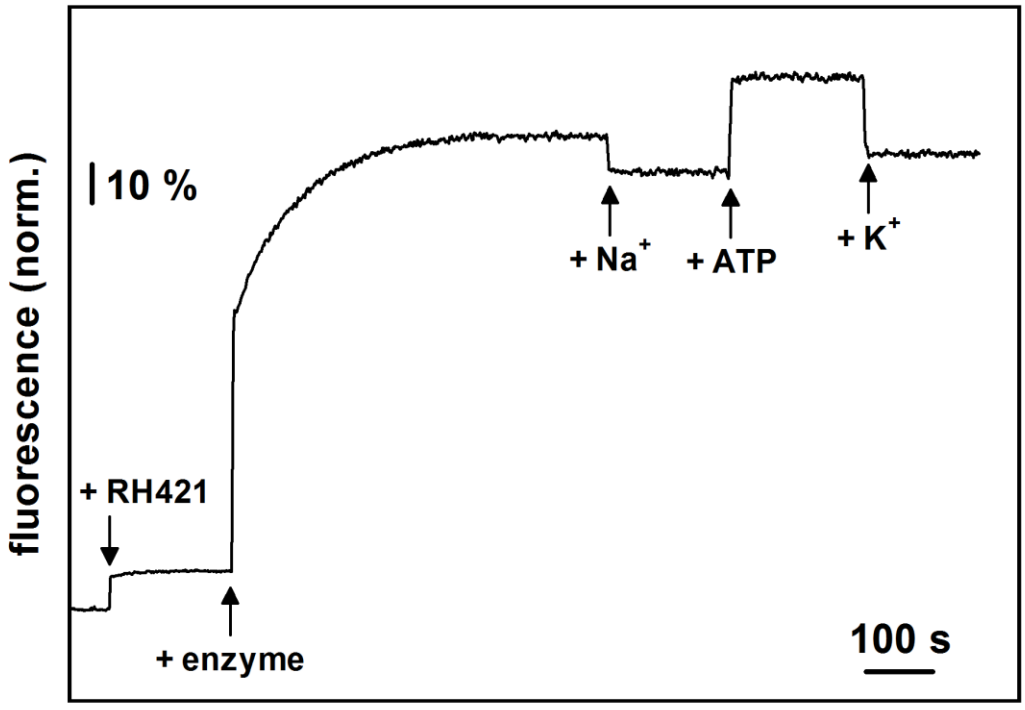

Figure 27. The standard experiment of the steady-state technique.

To allow the comparison between different experiments, the fluorescence changes are normalized with respect to the fluorescence level after the addition of the protein, when the dye is equilibrated inside the membrane.

Starting from the standard experiment it is possible to investigate the electrogenic partial reactions of the transport cycle and evaluate the affinities for the different substrates in the

E_1 and P-E_2 conformations. For example, the fluorescence drop induced by the addition of 50 mM NaCl in the state H_nE_1 (point 4) can be divided into small steps by the addition of small aliquots of NaCl (Fig. 28).

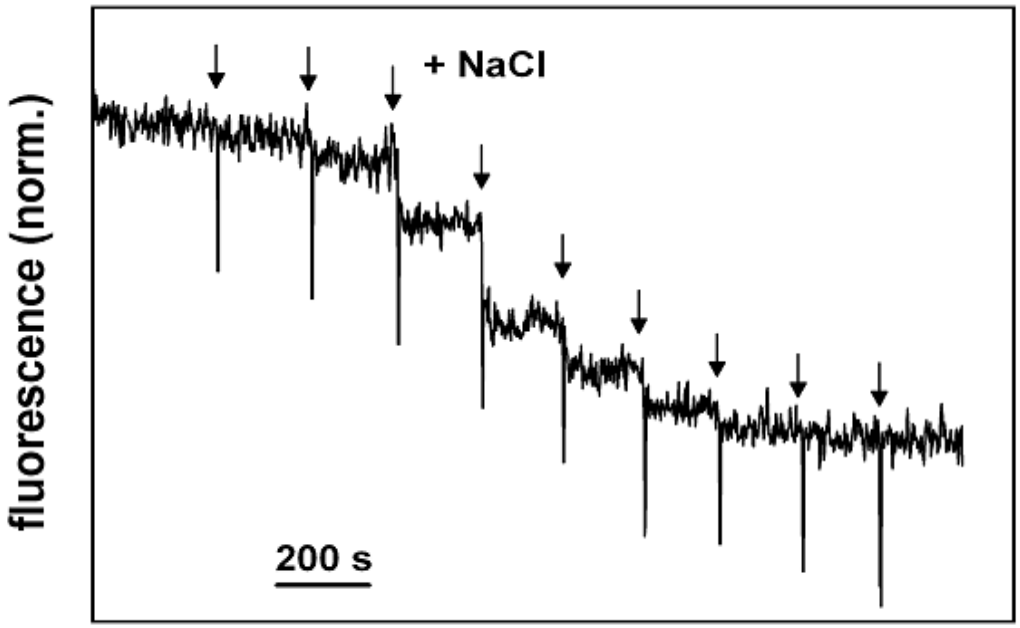

Figure 28. The initial fluorescence drop induced by the addition of 50 mM NaCl in the standard experiment can be divided in small steps by the addition of small aliquots of NaCl.

Fitting of the concentration-dependent normalized fluorescence decrease with a Hill function (Eq. 1) allows the determination of the half-saturating Na^+ concentration, $K_{1/2}$, and, thus, of the Na^+-binding affinity in the E_1 conformation (123).

Equation 1

$$F_{norm} = \frac{F_{\max}}{1 + \left(\frac{K_{1/2}}{[x]} \right)^n}$$

with

F_{norm} = normalized fluorescence
$F_{\max}$ = normalized fluorescence level at the end of the titration
$[x]$ = substrate concentration
$K_{1/2}$ = half-saturating concentration of the substrate
n = Hill coefficient

In the current study, the Na^+-binding affinity of the purified enzymes in the E_1 conformation has been investigated also at different Mg^{2+} and Ca^{2+} concentrations. Mg^{2+} and Ca^{2+} ions are known to compete with Na^+ ions for a binding site on the cytoplasmic domain of the protein, in the loop between M6 and M7 (146). This binding site is close to the entrance of the cytoplasmic access channel to the ion-binding sites in the transmembrane domain. Occupation of this site by a Mg^{2+} or Ca^{2+} ion is assumed to impede Na^+-entrance at the cytoplasmic side (146), thus affecting the Na^+-binding affinity in the E_1 conformation.

Similarly to what explained for the evaluation of the Na^+-binding affinity in the E_1 conformation, titration experiments with KCl or RbCl provide the K^+- and Rb^+-binding affinity

in the E_1 conformation, respectively. Rb^+ ions are known to be congeners of K^+ ions and to bind to the enzyme with a slightly higher affinity (140). Both Na^+, K^+, and Rb^+ ions are able to bind to the two bifunctionl ion-binding sites, but only Na^+ ions can occupy the third Na^+-specific ion-binding site. However, since at pH 7.2 less than two protons are bound to the enzyme in the initial state H_nE_1, the exchange with 2 K^+ or Rb^+ ions is accompanied by a small electrogenic component. Therefore, the binding of K^+ or Rb^+ ions induces a small but measurable fluorescence decrease (132,140).

$$H_nE_1 + 2\ K^+ \rightarrow K_2E_1 + n\ H^+$$

$$H_nE_1 + 2\ Rb^+ \rightarrow Rb_2E_1 + n\ H^+$$

In the standard experiment, upon addition of 1 mM ATP in the presence of 50 mM NaCl (point 5) the enzyme molecules undergo the conformational transition $(Na_3)E_1$-P $\rightarrow$ P-E_2Na_3. After releasing the Na^+ ions at the extracellular side, the enzyme is trapped preferentially in the P-E_2 state with virtually empty binding sites. Thus, titration experiments with NaCl enable the evaluation of the Na^+-binding affinity in the P-E_2 conformation (133). Also in this conformation, the enzyme is able to bind 3 Na^+ ions.

$$P\text{-}E_2 + 3\ Na^+ \rightarrow P\text{-}E_2Na_3$$

The addition of KCl to the P-E_2 state promotes dephosphorylation and, as a consequence, turnover occurs (point 6). However, at concentrations lower than 1 mM KCl, K^+ binding is the rate-limiting reaction step and, therefore, potassium-titration experiments allow the evaluation of the K^+-binding affinity in the P-E_2 conformation (131).

$$P\text{-}E_2 + 2\ K^+ \rightarrow P\text{-}E_2K_2$$

Besides the evaluation of the ion-binding affinities in the E_1 and P-E_2 conformations, the steady-state technique described allows the investigation of the so-called backdoor phosphorylation reaction. The addition of inorganic phosphate (Pi) in the initial state H_nE_1 triggers a H^+-transferring partial reaction.

$$(H_nE_1 \rightarrow)\ H_2E_1 + Pi \rightarrow P\text{-}E_2H_2 \rightarrow P\text{-}E_2 + 2\ H^+$$

Because of the lower H^+-binding affinity in the P-E_2 conformation (32), at pH 7.2 the two bound protons are electrogenically released on the extracellular side. As a consequence, a fluorescence increase can be detected. The steady-state distribution between states H_nE_1 and P-E_2 is controlled by the Pi concentration in the buffer and, thus, titration experiments with Pi allow the evaluation of the apparent Pi-binding affinity (134).

In the various titration experiments performed in the current study, small aliquots of NaCl, KCl, or RbCl (Fluka, >99%) have been added in the H_nE_1 or P-E_2 states, obtained as described in the standard experiment, from concentrated stock solutions until signal saturation. The normalized fluorescence decrease has been fitted with Eq. 1. The apparent Pi-binding affinity has been evaluated by addition in the H_nE_1 state, obtained as described in the standard experiment, of small aliquots of a solution of Tris Phosphate (Fluka, >99%), pH 7.1 (HCl) until signal saturation. The normalized fluorescence increase has been fitted with the Michaelis-Menten function (Eq. 2):

Equation 2

$$F_{norm} = \frac{F_{\max}[Pi]}{K_M + [Pi]}$$

with

F_{norm} = normalized fluorescence
$F_{\max}$ = normalized fluorescence level at the end of the titration
[Pi] = concentration of inorganic phosphate Pi
K_M = half-saturating Pi concentration

The Na^+-binding affinity in the E_1 conformation at different Mg^{2+} and/or Ca^{2+} concentrations has been obtained by adding different amounts of $MgCl_2$ and/or $CaCl_2$ (Merck, Suprapur) before starting the experiment. The sodium-titration experiments in these conditions have been performed as described above.

The normalization of the experiments, as well as the volume and drift corrections, has been performed with the program Drifter. The fitting procedure of the titration experiments has been performed with the data elaboration program FigP 2.98. The error is expressed as standard error of the mean (SEM).

2.4.1b Measurement of Transient Fluorescence Signals after Photochemical Release of ATP

The dye RH421 can be exploited also in time-resolved measurements with caged ATP to obtain kinetic information. Caged ATP is an inactive, photolabile precursor of ATP; upon exposure to an intense light flash, ATP is released and an ATP-concentration jump is created (Fig. 29). At pH 7.0, ATP is released from caged ATP with a time constant of 4.6 ms, allowing the detection of reactions with time constants of 10 ms or higher (147,148).

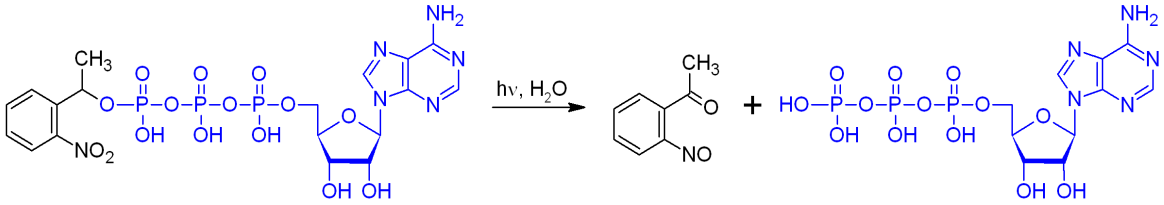

Figure 29. Photochemical release of ATP from caged ATP (P3-[1-(2-Nitrophenyl)ethyl]-ATP).

The time-resolved fluorescence signals induced by photochemical release of ATP have been measured with a home-made instrumental setup as described recently in (22) (Fig. 30). The photochemical release of ATP is triggered by a UV flash generated by an EMG 100 excimer laser (Lambda Physics, Göttingen, Germany; wavelength 351 nm, duration 14 ns, maximum power 6 MW). A UV cut-off filter reduces the effect of the UV flash. The dye RH421 is excited by a HeNe laser set at 594 nm. A quartz lens widens the laser beam to illuminate the whole solution almost homogeneously. The emitted light is collected by an ellipsoidal mirror and converged onto the cathode of a photomultiplier (Mod. R928, Hamamatsu Photonics, Japan). An interference filter (663 ± 18 nm) selects the emitted light of the styryl dye before it enters the photomultiplier. The output current is amplified and digitized by a 12-bit data acquisition board of a PC with sampling frequencies between 1 and 500 kHz. The bottom of the cuvette is in contact with a thermostated copper socket that also stops the incident light.

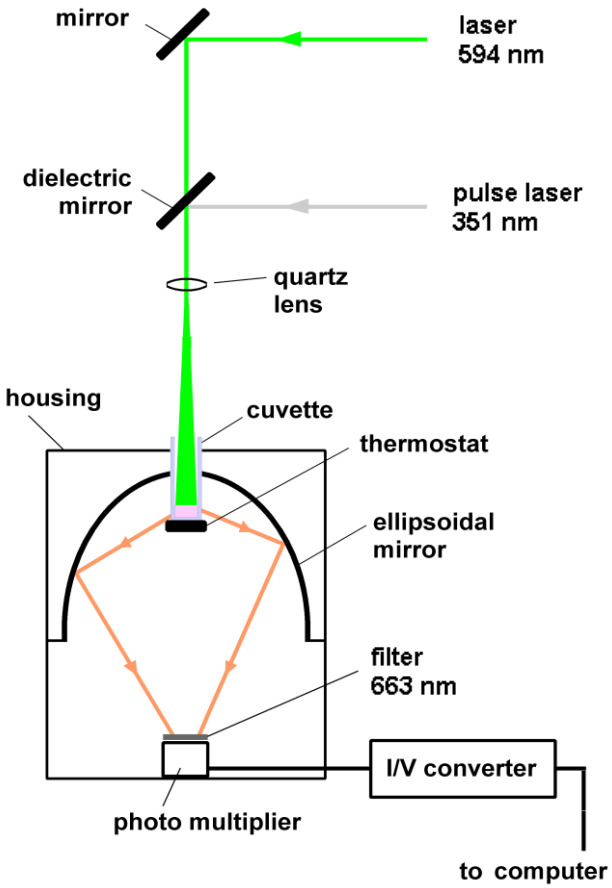

Figure 30. Scheme of the home-made instrumental setup used for the measurements of transient fluorescence signals after photochemical release of ATP.

The measurement of the time-dependent fluorescence signal after photochemical release of ATP at saturating concentrations of Na^+ ions and ATP enables the evaluation of the time constant of the E_1-P → P-E_2 conformational transition (128-130). At 50 mM NaCl, the enzyme is in the state Na_3E_1; ATP release triggers the reaction Na_3E_1 → Na_3E_1·ATP → (Na_3)E_1-P → P-E_2Na_3 → P-E_2 + 3 Na^+. A fluorescence increase is recorded, corresponding to the translocation and then the release of the Na^+ ions at the extracellular side of the membrane (Fig. 31). At saturating ATP concentrations, ATP-binding and phosphorylation are fast compared to the conformational transition. Thus, the time constant of the fluorescence increase reflects the rate of the conformational transition.

Materials

- Imidazole (Merck, buffer substance, ACS)
- EDTA (Merck, Titriplex® II, for analysis, ACS)
- $MgCl_2$ hexahydrate (Merck, for analysis, EMSURE®, ACS)
- NaCl (Merck, for analysis)
- NPE-caged-ATP disodium salt (Molecular Probes)
- Apyrase VI (Sigma)
- RH421 (MoBiTec)
- EtOH (Merck, for spectroscopy)

Solutions

- *Buffer*: 25 mM imidazole, 1 mM EDTA, pH 7.2 (HCl)
- 1 M $MgCl_2$
- 200 µM RH421 in EtOH
- 5 M NaCl
- 10 mM cg-ATP

To remove traces of free ATP from the sample of caged ATP, Apyrase VI (1.4×10^{-3} Units/ml) and 1.4 mM $MgCl_2$ are added to the stock solution.

Procedure

The experiment is performed in a darkened environment at 20 ± 0.5 °C.

1- A cylindrical quartz cuvette (internal diameter 7.8 mm) is filled with 300 µl of Buffer containing 5 mM $MgCl_2$, 200 nM RH421, 50 mM NaCl, 9 µg/ml of protein, and 100 µM caged ATP. The cuvette is equilibrated for 10 min inside the instrument to stabilize the desired temperature. During this time, it is protected from light by a cover to prevent unintended photochemical release of ATP.

2- The cuvette is uncovered and the experiment is started. The generation of a light flash by the excimer laser is controlled by the program DASYLab9, which also records the fluorescence signal. After photochemical release of ATP, the enzyme is phosphorylated and undergoes the conformational transition to $P\text{-}E_2$. In this conformation, the protein releases the Na^+ ions on the extracellular side of the membrane. In the absence of K^+ ions, dephosphorylation is very slow (130) and the enzyme is trapped in the $P\text{-}E_2$ state with virtually empty ion-binding sites since the release of Na^+ ions is not counterbalanced by binding of protons (32). Therefore, a rapid fluorescence increase is detected corresponding to the electrogenic release of all three Na^+ ions.

To allow the comparison between different experiments, the fluorescence increase is normalized with respect to the fluorescence level before ATP release. The normalized transient can be fitted with a single exponential function (Eq. 3) to obtain the corresponding time constant, τ.

Equation 3

$$F_{norm} = F_{\max} \cdot (1 - e^{-t/\tau})$$

with

F_{norm} = normalized fluorescence

$F_{\max}$ = normalized fluorescence level of the steady-state after ATP release

τ = time constant of the normalized fluorescence increase after ATP release

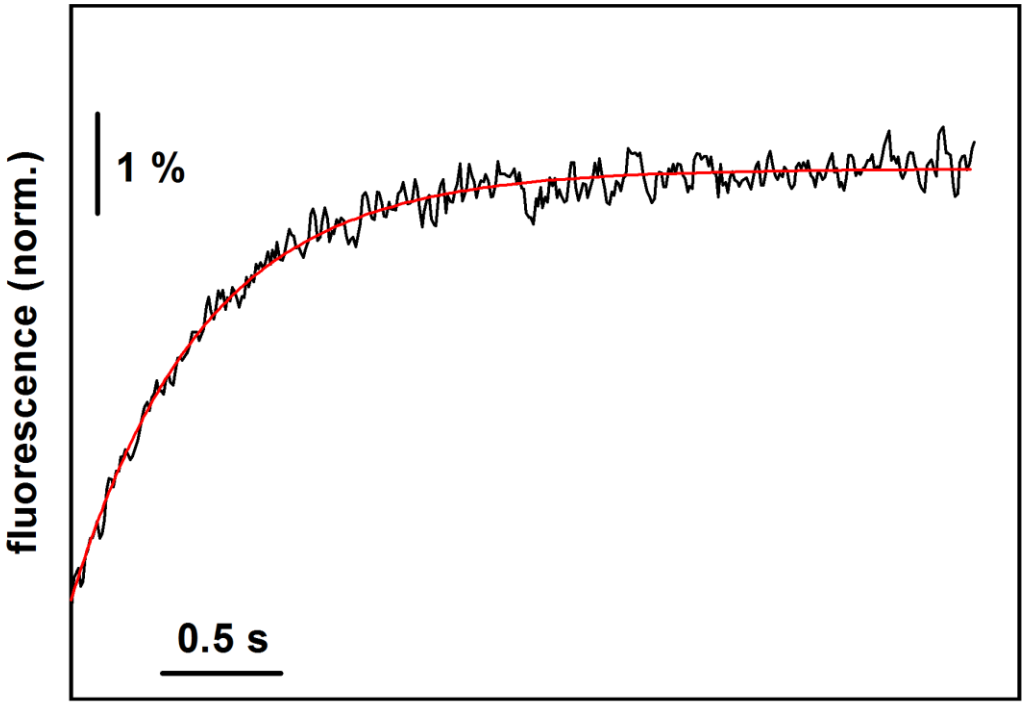

Figure 31. Transient fluorescence signal recorded after photochemical release of ATP at saturating concentrations of Na^+ ions and ATP. The signal can be fitted with a single exponential function.

At non-saturating ATP concentrations, ATP-binding becomes rate-limiting and the time constant of the fluorescence increase reflects the rate of the ATP-binding reaction. Since only part of the enzyme in the cuvette is phosphorylated and undergoes the conformational transition, the amplitude of the signal is lower than at saturating ATP concentrations. Fitting of the time constant or of the amplitude of the normalized fluorescence increase versus the ATP concentration with the Michaelis-Menten function (Eq. 4) provides the apparent ATP-binding affinity (130).

Equation 4

$$\tau = \tau_{max} + \frac{(\tau_{min} - \tau_{max})[ATP]}{K_M + [ATP]}$$

with

τ = time constant of the normalized fluorescence increase after ATP release
τ_{max} = time constant at the lowest ATP concentration
τ_{min} = time constant at the highest ATP concentration
$[ATP]$ = concentration of ATP
K_M = half-saturating ATP concentration

To obtain a reliable value of ATP-binding affinity, the concentration of free ATP released by caged ATP under the experimental conditions has been determined using the luciferin/luciferase test (149). About 10% of ATP is released from caged ATP by a single flash.

The reduction of the number of data points obtained by the program DASYLab9 and the normalization of each fluorescence trace have been performed with the program Redulite2. The signal output has been processed with the program Drifter and the fitting procedure has been performed with the data elaboration program FigP 2.98. The error is expressed as SEM.

2.4.2 The Voltage-sensitive Dye Oxonol VI

Oxonol V, VI and VII are bis(oxoisoxazolyl)polyenyl compounds. They have a pKa ~ 4.2 and are, therefore, negatively charged at physiological pH (150,151). Oxonol VI is characterized by a propyl group on the oxoisoxazolyl rings (Fig. 32).

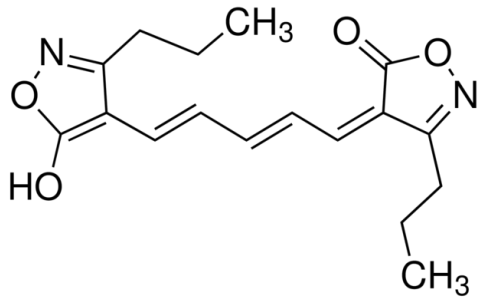

Figure 32. Structure of the voltage-sensitive dye Oxonol VI.

Oxonol dyes bind strongly to the membrane. Upon binding, the fluorescence intensity of the dyes increases significantly due to the low dielectric constant of the membrane interior (150-152). In the presence of an inside-positive electric potential across membrane vesicles, Oxonol VI has been shown to accumulate in the intravesicular aqueous space according to a Nernst equilibrium (152). This leads to an increased adsorption of the dye in the inner lipid leaflet and to a concomitant increase in fluorescence intensity. In contrast, the electric potential has only minor effects on the intrinsic fluorescence of the dye. The fluorescence intensity of Oxonol VI has been found to increase linearly in the range of inside-positive transmembrane potentials between 0 and 100 mV (152). Therefore, Oxonol VI can be exploited to measure inside-positive electric potentials across membrane vesicles. The time resolution of the method is limited by the redistribution of the dye molecules between the aqueous phase and the membrane, corresponding to ~ 300 ms (125).

Oxonol VI has been successfully applied to detect the ion transport of the Na,K-ATPase reconstituted in lipid vesicles (152-157). In the current study, the dye has been used to investigate the Na^+-binding affinity in the E_1 conformation of the native Na,K-ATPase as well as of the purified recombinant α_1/His_{10}-β_1 and α_1/His_{10}-β_1/FXYD1 reconstituted in lipid vesicles.

2.4.2a Detection of the Ion Transport of the Na,K-ATPase Reconstituted in Lipid Vesicles

As mentioned above, Oxonol VI can be applied to detect the ion transport of the Na,K-ATPase reconstituted in lipid vesicles. In proteoliposomes containing a high concentration of K^+ ions and a low concentration of Na^+ ion, the extravesicular addition of ATP in the presence of Mg^{2+} and Na^+ ions activates the enzyme molecules reconstituted with the ATP-binding site facing outward (Fig. 33). As a consequence, an inside-positive membrane potential is generated due to the electrogenic transport. In response, Oxonol VI molecules accumulate in the intravesicular aqueous space according to a Nernst equilibrium, leading to an increased adsorption of the dye in the inner lipid monolayer and to a concomitant increase in fluorescence intensity (Fig. 34).

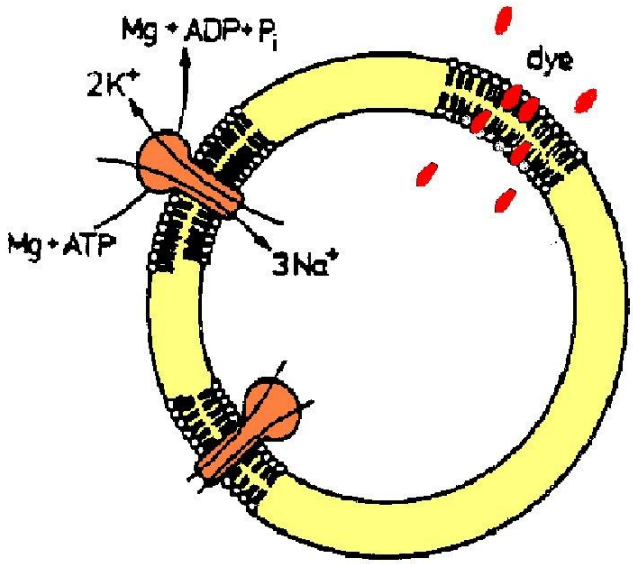

Figure 33. Upon addition of ATP in the extravesicular medium, the enzyme molecules with the ATP-binding site facing outward are activated. As a consequence, an inside-positive transmembrane potential is generated due to the electrogenic transport. In response, Oxonol VI molecules accumulate in the vesicle membrane, leading to a fluorescence increase.

The proteoliposomes prepared as described in *2.2* contain 70 mM K_2SO_4 and 5 mM Na_2SO_4. Sulfate is chosen as primary anion because it produces a significantly lower leak current than chloride (152). The experiments have been performed in a Perkin-Elmer LS 50B fluorescence spectrophotometer set at the same conditions described in *2.4.1a*.

Materials

- Tris (MP Biomedicals, UltraPure)
- Imidazole (Merck, buffer substance, ACS)
- EDTA (Merck, Titriplex® II, for analysis, ACS)
- $MgSO_4$ heptahydrated (Merck, for analysis)
- Na_2SO_4 anhydrous (Merck, for analysis, ACS)
- ATP magnesium salt (Sigma)
- Oxonol VI (Molecular Probes)
- EtOH (Merck, for spectroscopy)
- H_2SO_4 (Backer, 95-97%)
- Sodium orthovanadate (Sigma, >90%)

Solutions

- *Buffer*: 25 mM imidazole, 1 mM EDTA, pH 7.2 (H_2SO_4)
- 1 M $MgSO_4$
- 25 µM Oxonol VI in EtOH
- 2.5 M Na_2SO_4
- 1.5 M Tris/H_2SO_4, pH 7.0
- 0.5 M ATP
- 0.2 M Sodium orthovanadate, pH 7.5 (HCl)

Procedure

The experiments are performed at 20 ± 0.5 °C.

1- A cuvette made of special optical glass (Hellma, type 109.004F-OS) is filled with 1 ml of Buffer containing 2.5 mM $MgSO_4$, 25 mM Na_2SO_4, and 100 mM Tris/H_2SO_4. The addition of Tris/H_2SO_4 provides an ion strength equivalent to the one of the intravesicular solution. The cuvette is equilibrated for 10 min inside the instrument to stabilize the desired temperature.

2- At the beginning of the experiment, 25 nM Oxonol VI is added to the cuvette.

3- After 2 min, a volume of vesicles corresponding to 80 µg/ml of lipid is added. Considering an average diameter of 110 nm (113), this corresponds to about $5 \cdot 10^{11}$ vesicles. A fluorescence increase is observed due to the insertion of the dye in the vesicles membrane.

4- When a stable steady-state is reached, 2.5 mM ATP is added to the cuvette. The addition activates the enzyme molecules reconstituted with the ATP-binding site facing outwards. The enzymes pump three Na^+ ions into and two K^+ ions out of the vesicles, building up an inside-positive transmembrane potential that causes an increase of the fluorescence signal. The signal reaches another steady-state at elevated membrane potentials, when the pump current is compensated by the leak current due to the membrane conductance.

5- To evaluate the specific conductance of the membrane, 5 mM orthovanadate is added at the end of the experiment. As a result, the fluorescence signal decreases because of the transmembrane voltage decays due to the membrane conductance. The time constant, τ, of the decrease is equal to C_m/G_m, where C_m is the specific capacitance and G_m the specific conductance of the membrane. With $C_m \sim 1$ µF/cm^2, $G_m = 1/\tau$ (152).

At the end of each experiment, the cuvette is washed with 0.5 % Hellmanex II to remove any trace of lipids. The detergent is then rinsed carefully with distilled water.

To allow the comparison between different experiments, the fluorescence changes are normalized with respect to the fluorescence level after the addition of the vesicles, when the dye inserts inside the vesicles membrane. The normalized fluorescence increase can be fitted with a single exponential function (Eq. 5).

Equation 5
$$F_{norm} = F_{\min} + (F_{\max} - F_{\min}) \cdot (1 - e^{-t/\tau})$$

with

F_{norm} = normalized fluorescence
$F_{\min}$ = normalized fluorescence level before ATP addition
$F_{\max}$ = normalized fluorescence level of the steady-state after ATP addition
τ = time constant of the normalized fluorescence increase after ATP addition

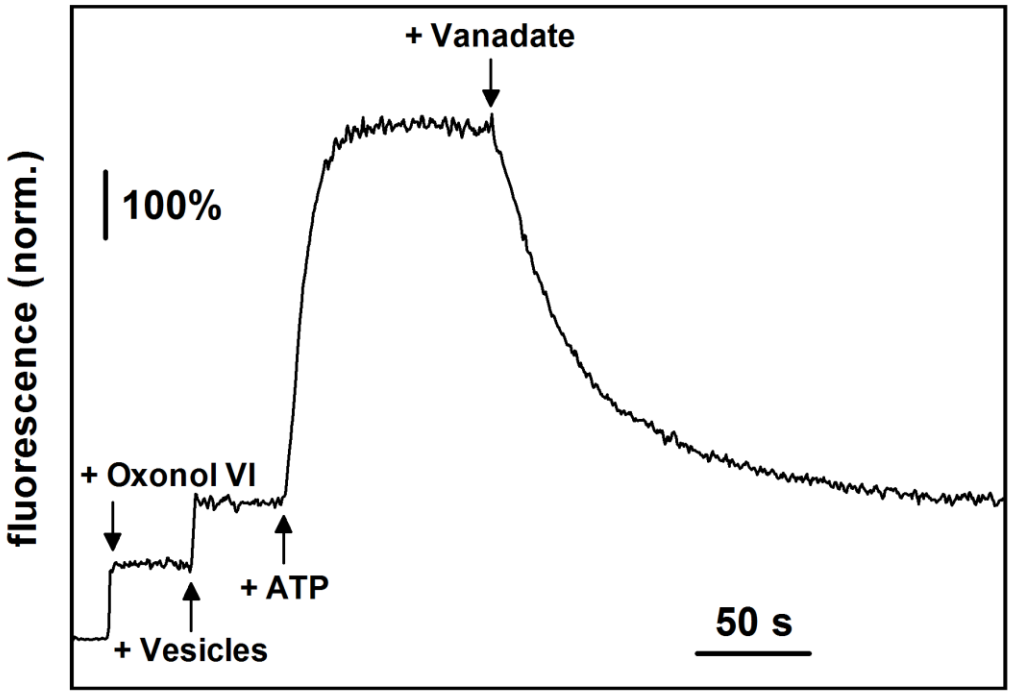

Figure 34. Detection of the enzyme-generated inside-positive transmembrane potential with Oxonol VI.

Oxonol VI can be used to investigate the Na^+-binding affinity in the E_1 conformation of the Na,K-ATPase reconstituted in lipid vesicles. In this condition, it is not possible to use the dye RH421 in equilibrium-titration experiments as described in *2.4.1a* because of the extremely low density of enzyme molecules in the vesicle membrane. To evaluate the Na^+-binding affinity of the enzyme in the E_1 conformation, the enzyme-mediated generation of the electric potential across the vesicle membrane is detected as function of the extravesicular (= cytoplasmic) sodium concentration. During the initial phase of the experiments, before a considerable membrane potential is build up and the intravesicular potassium concentration becomes limiting, the enzyme activity is controlled by the rate-limiting step of the transport cycle, which is Na^+-binding in the E_1 conformation at low extravesicular sodium concentrations. Since the initial slope of the fluorescence signal is proportional to the initial enzyme activity, the Na^+-dependence of the initial slope of the signal provides directly the Na^+-binding affinity in the E_1 conformation. In the various experiments, the ionic strength is kept constant by the addition of Tris/H_2SO_4.

The initial slope of the signal, corresponding to the derivative of the signal with respect to time at $t = 0$, is given by F_{max}/τ, as can be derived by the following considerations. The vesicle membrane can be represented by an equivalent circuit diagram with the capacitance, C_m, and the leak conductance, λ_L of the lipid bilayer and the enzyme represented as a current generator, I_P.

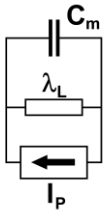

According to basic physics these elements may be linked up in the following way:

$$I = \frac{dQ}{dt} = C_m \cdot \frac{dU}{dt}$$

where Q is the electric charge on the capacitor, U the electric potential across the membrane, and I the current flowing across the membrane. The net current through the vesicle membrane is the sum of two components, the pump current, I_P, and the leak current, I_L, which flow in opposing directions,

$$I = I_P - I_L = n \cdot z \cdot e_0 \cdot v_P - \lambda_L \cdot U$$

where n is the number of enzyme molecules in the vesicle membrane, z is the number of charges transferred per pump cycle (= 1), e_0 is the elementary charge, and v_P is the pump rate. Combining the equations above leads to the inhomogeneous differential equation,

$$\frac{dU}{dt} = \frac{I_P}{C_m} - \frac{\lambda_L}{C_m} \cdot U$$

solved with the boundary condition, valid at long times, $t \rightarrow \infty$,

$$I_P = I_L = \lambda_L \cdot U_\infty$$

where U_∞ is the transmembrane voltage in the stationary phase, when the pump current is compensated by the leak current. The solution of the differential equation is

$$U(t) = U_\infty \cdot (1 - e^{-t/\tau}) \qquad \text{with} \qquad \tau = \frac{C_m}{\lambda_L}, U_\infty = \frac{I_P}{\lambda_L}$$

and its derivative with respect to time at t = 0 is the ratio between the transmembrane voltage in the steady state, U_∞, and the time constant, τ, of the voltage increase.

$$\left(\frac{dU}{dt}\right)_{t=0} = U_\infty \cdot \frac{1}{\tau} \cdot e^{-t/\tau}\Big|_{t=0} = \frac{U_\infty}{\tau}$$

In an earlier publication it has been shown that the normalized fluorescence signal of Oxonol VI in vesicles experiments is proportional to the transmembrane potential built up by the enzyme (152). Therefore, the maximum amplitude of the normalized fluorescence signal, F_{max}, is proportional to the transmembrane voltage in the stationary phase, U_∞, as well as the derivative of the fluorescence signal with respect to time at t = 0 is proportional to the derivative of the transmembrane voltage with respect to time at t = 0.

$$F_{norm} = K' \cdot U$$

$$F_{\max} = K' \cdot U_{\infty}$$

$$\left(\frac{dU}{dt}\right)_{t=0} = K^{*} \cdot \left(\frac{dF_{norm}}{dt}\right)_{t=0}$$

As a consequence, the initial slope of the normalized fluorescence signal is proportional to the ratio of the maximum amplitude, $F_{\max}$, and the time constant, τ, of the normalized fluorescence signal.

$$\left(\frac{dF_{norm}}{dt}\right)_{t=0} = K^{\#} \cdot \frac{F_{\max}}{\tau}$$

The proportionality constant, $K^{\#}$, depends on the properties of each specific vesicle preparation and is invariable within the same preparation. Therefore, the results obtained with the same preparation can be directly compared, at least within a time period in which no aging processes affect the enzyme activity. Fitting the initial slope of the normalized signal versus the extravesicular sodium concentration with the Hill function (Eq. 6) allows the evaluation of the Na^+-binding affinity in the E_1 conformation of the enzyme reconstituted in lipid vesicles.

Equation 6

$$\left(\frac{dF_{norm}}{dt}\right)_{t=0} = \frac{\left[\left(\frac{dF_{norm}}{dt}\right)_{t=0}\right]_{\max}}{1+\left(\frac{K_{1/2}}{[Na]}\right)^{n}}$$

with

$\left(\frac{dF_{norm}}{dt}\right)_{t=0}$ = initial slope of the normalized fluorescence signal

$\left[\left(\frac{dF_{norm}}{dt}\right)_{t=0}\right]_{\max}$ = initial slope at saturating Na^+ concentrations

$[Na]$ = concentration of Na^+ ions

$K_{1/2}$ = half-saturating Na^+ concentration

n = Hill coefficient

The normalization of the experiments, as well as the volume and drift corrections, has been performed with the program Drifter. The fitting procedure has been performed with the data elaboration program FigP 2.98. The error is expressed as SEM.

CHAPTER 3

RESULTS

3.1 Extension of the Methods Based on the Styryl Dye RH421 to the Purified Recombinant Na,K-ATPase

As reported in *2.4.1*, the dye RH421 has been widely and successfully used to characterize the electrogenic partial reactions in the transport cycle of the native Na,K-ATPase in open membrane fragments (32,123,127-144). The main limitation of the methods based on the application of the styryl dye RH421 is the requirement of a high density of purified active protein in the membrane (10^3-10^4 pump molecules/μm^2 (127)). In this condition, all dye molecules are close to the transmembrane domain of the enzyme and, therefore, significant fluorescence signals are detectable. The investigation of recombinant proteins expressed in heterologous systems like yeast cells would be desirable, but the expression level is too low for the successful application of such techniques directly to open membrane fragments. Recently, we have demonstrated that it is possible to overcome this limitation and extend the methods that use the dye RH421 to the detergent-solubilized Na,K-ATPase from rabbit kidney (145). The study of the transport properties has shown that the function and ion-binding properties of the detergent-solubilized and membrane-bound native Na,K-ATPase are not significantly different (145). Therefore, it is reasonable to expect significant results from the investigation with the dye RH421 of the purified, detergent-solubilized recombinant Na,K-ATPase obtained as described in *2.1*.

First of all, the steady-state fluorescence method has been applied to the α_1/His_{10}-β_1 and α_2/His_{10}-β_1 preparations. These enzymes show specific ATPase activities at 37 °C between 6 and 15 μmol of Pi/mg of protein/min, which are much lower compared to the membrane-bound Na,K-ATPase from rabbit kidney (30-35 μmol of Pi/mg of protein/min). When the two isozymes are compared, α_2/His_{10}-β_1 presents a lower specific enzyme activity (6-10 μmol of Pi/mg of protein/min) than α_1/His_{10}-β_1 (8-15 μmol of Pi/mg of protein/min).

In the RH421 standard experiments (Fig. 35), performed as described in *2.4.1a*, the detergent-solubilized recombinant proteins follow the same scheme as the membrane-bound Na,K-ATPase from rabbit kidney (145) although the fluorescence changes are smaller. In particular, the α_2/His_{10}-β_1 isozyme shows smaller fluorescence changes compared to α_1/His_{10}-β_1.

Sodium-titration experiments in the E_1 conformation have been performed as described in *2.4.1a* by adding small aliquots of NaCl up to 100 mM. The results, obtained from the average of three identical experiments carried out with one preparation for each isozyme, are compared to the membrane-bound native Na,K-ATPase (Fig. 36). No significant difference in the Na^+-binding affinity is detected between the α_1/His_{10}-β_1 and α_2/His_{10}-β_1 isozymes. The half-saturating Na^+ concentrations, $K_{1/2}$, are 5.8 ± 0.4 mM and 6.1 ± 0.9 mM, respectively, and the Hill coefficients, n, 1.6 ± 0.1 and 1.1 ± 0.2. The Na^+-binding affinity of the detergent-solubilized preparations is also similar to the one of the membrane-bound native Na,K-ATPase, 4.7 ± 0.3 mM (n = 2.1 ± 0.3). The Hill coefficient, n, of the α_1/His_{10}-β_1 isozyme is lower compared to the membrane-bound native Na,K-ATPase, but similar after reconstitution in lipid vesicles (see *3.4.2*).

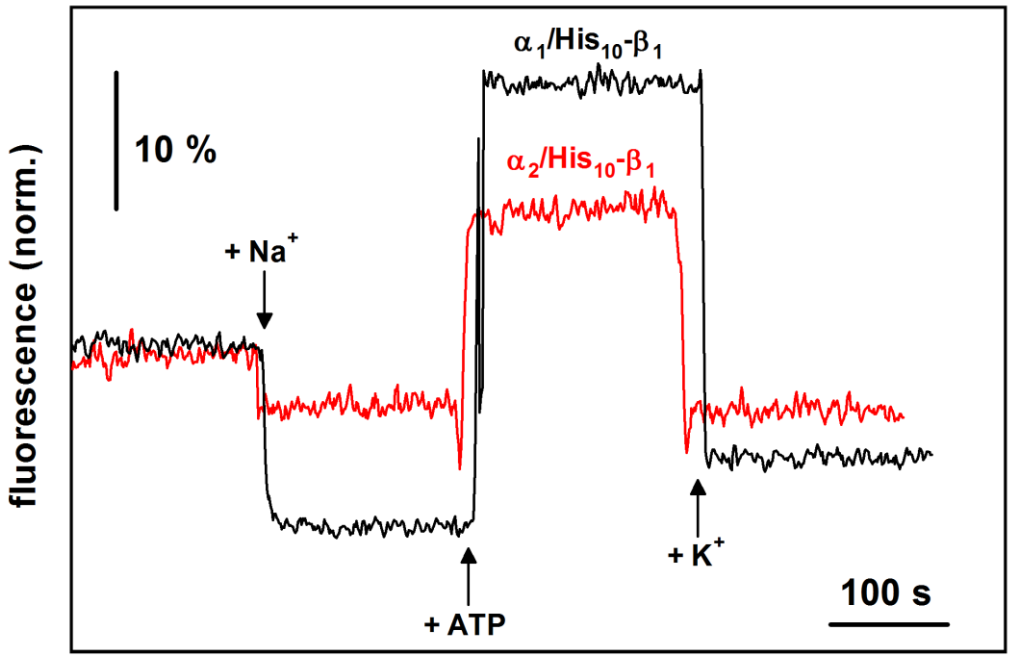

Figure 35. Standard experiments with the α_1/His_{10}-β_1 (black) and α_2/His_{10}-β_1 (red) isozymes.

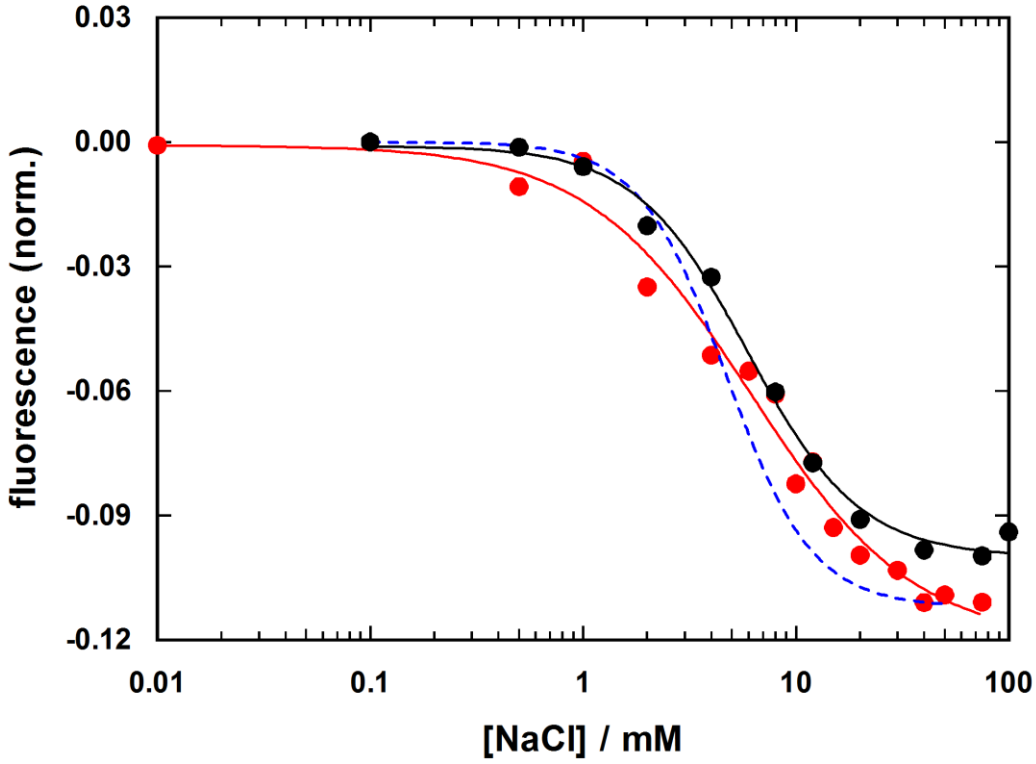

Figure 36. Sodium-titration experiments with the α_1/His_{10}-β_1 (black) and α_2/His_{10}-β_1 (red) isozymes. The results are compared to the membrane-bound native Na,K-ATPase (dashed blue line).

Potassium-titration experiments in the P-E_2 conformation have been performed as described in *2.4.1a* by adding small aliquots of KCl up to 10 mM. The results, obtained from the average of three identical experiments conducted with one preparation for each isozyme, are compared to the membrane-bound native Na,K-ATPase (Fig. 37). A 2.7-fold lower K^+-binding affinity is detected for α_2/His_{10}-β_1 relative to α_1/His_{10}-β_1. The $K_{1/2}$ is 0.31 ± 0.02 mM (n = 1.17 ± 0.07) for the α_1/β_1 and 0.83 ± 0.06 (n = 1.25 ± 0.08) for the α_2/β_1 isozyme. When these results are compared to the membrane-bound native Na,K-ATPase, $K_{1/2}$ = 0.20 ± 0.05, the detergent-solubilized recombinant α_1/His_{10}-β_1 shows a ~ 30% lower affinity.

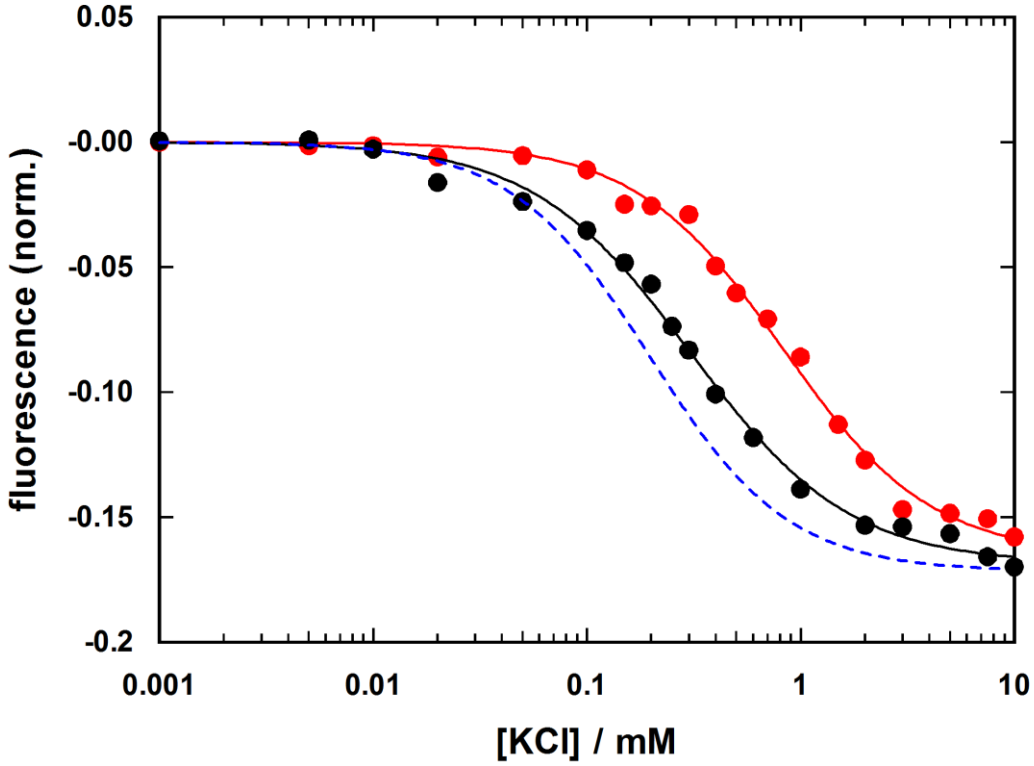

Figure 37. Potassium-titration experiments with the α_1/His_{10}-β_1 (black) and α_2/His_{10}-β_1 (red) isozymes. The results are compared to the membrane-bound native Na,K-ATPase (dashed blue line).

Sodium-titration experiments in the E_1 conformation at different Mg^{2+} concentrations have been also performed as described in *2.4.1a* (Fig. 38). The same preparations have been used to test the various Mg^{2+} concentrations. The experiments with the α_2/His_{10}-β_1 isozyme have been carried out by Michael Habeck. Both isozymes show identical half-saturating Na^+ concentrations in the range of tested Mg^{2+} concentrations. These values are very similar to those of the membrane-bound native Na,K-ATPase (dashed blue line in Fig. 38).

In summary, the presented results demonstrate that the dye RH421 is suitable to investigate the ion-binding kinetics of detergent-solubilized purified ion pumps. The experiments show that the functional properties of the purified recombinant enzymes do not differ significantly from those of the membrane-bound Na,K-ATPase from rabbit kidney and, therefore, these complexes can be successfully exploited for the investigation of the functional effects of FXYD1. This set of results is published in (145).

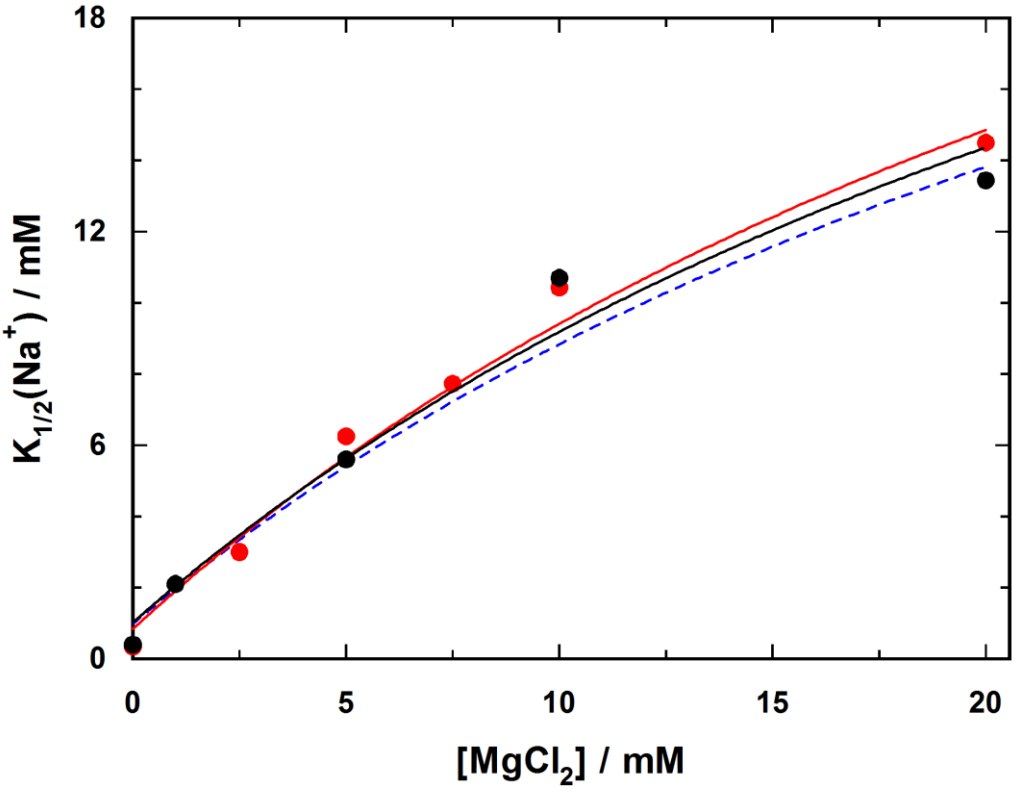

Figure 38. Sodium-titration experiments with the α_1/His_{10}-β_1 (black) and α_2/His_{10}-β_1 (red) isozymes at different Mg^{2+} concentrations. The results are compared to the membrane-bound native Na,K-ATPase (dashed blue line).

3.2 In Vitro Reconstitution of the α_1/His$_{10}$-β_1/FXYD1 Complex

Incubation of α_1/His$_{10}$-β_1 bound to the BD-Talon beads with a molar excess of FXYD1 allows spontaneous, stoichiometric reconstitution of the α_1/His$_{10}$-β_1/FXYD1 complex as previously demonstrated (38,111). The ratio between $\alpha_1\beta_1$ and FXYD1 in the purified complex has been evaluated as described in *2.1.3*. An example is reported below.

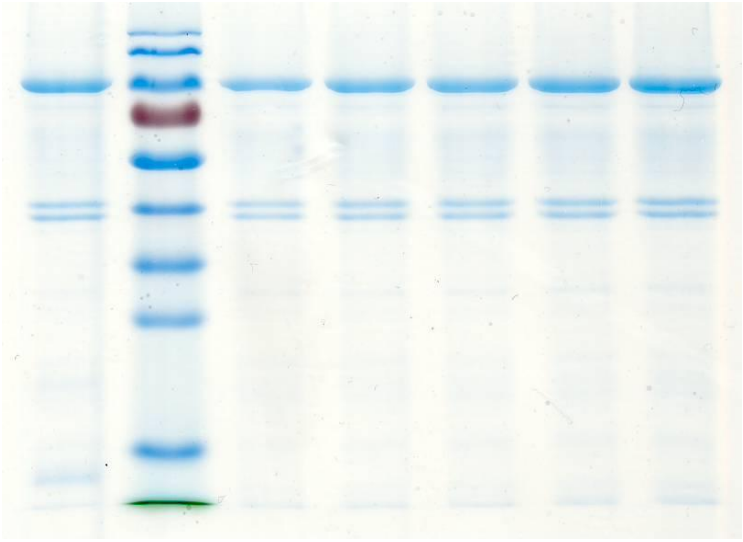

Figure 39. Gel for the evaluation of the relative amount of $\alpha_1\beta_1$ in a purified α_1/His$_{10}$-β_1/FXYD1 sample (line 1 starting from the left). The calibration curve (lines 3-7) is obtained with known amounts of purified α_1/His$_{10}$-β_1.

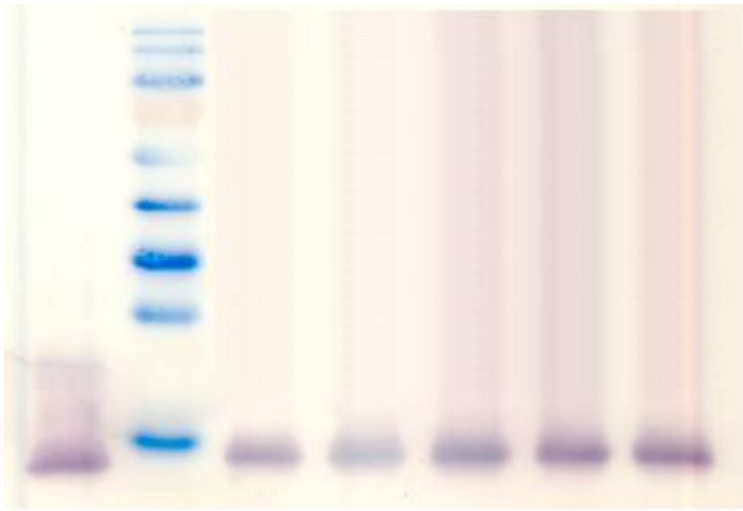

Figure 40. Western Blot for the evaluation of the relative amount of FXYD1 in a purified α_1/His$_{10}$-β_1/FXYD1 sample (line 1 starting from the left). The calibration curve (lines 3-7) is obtained with known amounts of purified FXYD1.

The β subunit runs as 2 separate bands due to a different glycosylation (27,37,74,158). Despite a lower molecular mass, FXYD1 runs at ~ 15 kDa, as can be seen in line 1 of the gel, corresponding to the α_1/His$_{10}$-β_1/FXYD1 complex, as well as in the Western Blot. This feature has been observed previously (27,37,48-50,74,158). In the example, the range of concentrations used for the calibration of $\alpha_1\beta_1$ is 3-5 µg (Fig. 39). The interpolation of the sample in the calibration curve obtained by elaboration of the gel provides an amount of

$\alpha_1\beta_1$ corresponding to 4.5 µg. The range of concentrations used for the calibration of FXYD1 is 0.1-0.3 µg (Fig. 40). The interpolation of the sample in the calibration curve obtained by elaboration of the Western Blot (excluding line 4) provides an amount of FXYD1 corresponding to 0.24 µg. The ratio of the values is ~ 1:19.

In the presence of FXYD1, the α_1/His_{10}-β_1 isozyme always shows a higher specific activity at 37 °C (9-20 µmol of Pi/mg of protein/min +FXYD1 versus 8-15 µmol of Pi/mg of protein/min -FXYD1). In the various preparations used in the current study, the difference varies between 2.5% and 40%. In previous papers, FXYD1 has been shown to stabilize the enzyme from partial detergent-mediated inactivation during the purification procedure and to protect it against thermal inactivation (38,74). To further investigate this aspect, the effects of thermal inactivation on the electrogenic partial reactions of the transport cycle have been studied with standard experiments. Experiments with α_1/His_{10}-β_1 and α_1/His_{10}-β_1/FXYD1 have been performed as described in *2.4.1a* before and after incubation at 45 °C for 10, 30 and 60 min. When the standard experiments before and after the one-hour incubation are compared (Fig. 41-42), the fluorescence jumps after incubation are smaller both in the presence and in the absence of FXYD1 because of a reduction in the number of active enzyme molecules. However, the decrease is significantly lower in the case of the α_1/His_{10}-β_1/FXYD1 complex. In the absence of FXYD1, the Na^+-binding capacity is reduced to ~ 69% of the initial value while enzyme phosphorylation to ~ 17%. In contrast, in the presence of FXYD1 the respective numbers are ~ 95 and ~ 62%. Therefore, FXYD1 protects the enzyme effectively against thermal inactivation and, in particular, it stabilizes sodium binding almost quantitatively.

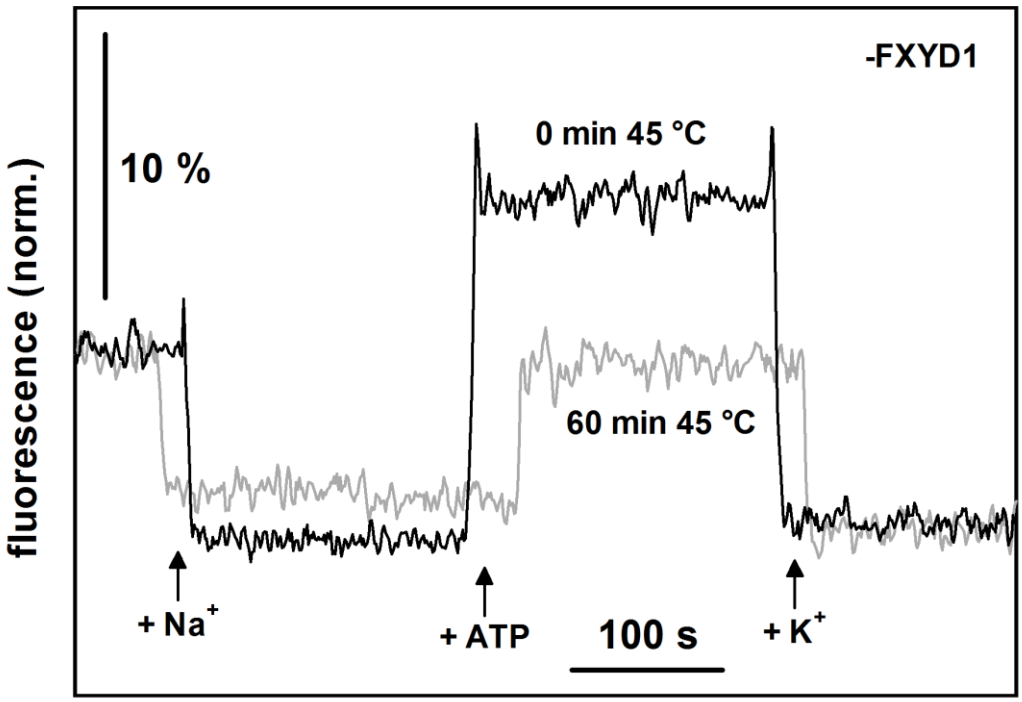

Figure 41. Standard experiments with α_1/His_{10}-β_1 before (black) and after (gray) incubation at 45 °C for 60 min.

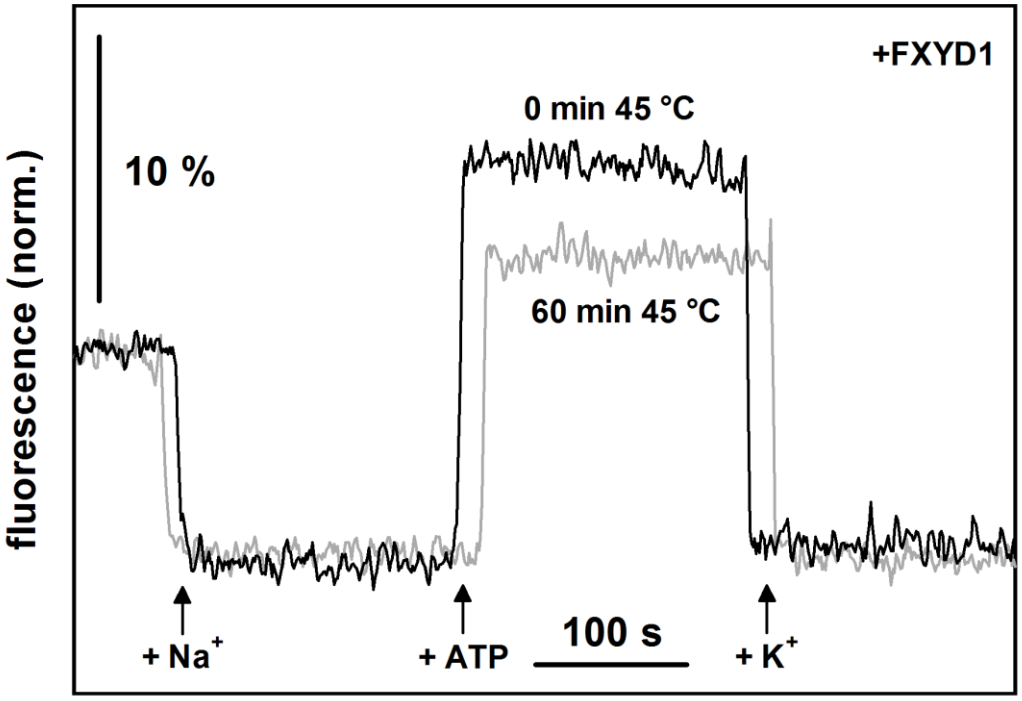

Figure 42. Standard experiments with α_1/His_{10}-β_1/FXYD1 before (black) and after (gray) incubation at 45 °C for 60 min.

In Fig. 43 and 44, the normalized fluorescence levels after addition of NaCl and ATP in the standard experiments are plotted at the various incubation times. At short incubation times, a small but significant increase in the fluorescence changes is observed, corresponding to an enhancement of both sodium binding and ATP-induced activity. This supports the previous observation that the Na,K-ATPase activity of the recombinant complexes increases after 30 min at 37 °C, probably because of a thermally induced improvement of the lipid/protein interaction (27).

This set of experiments is included in a recent detailed study about the stabilizing effects of FXYD1, FXYD2 and FXYD4 on the Na,K-ATPase (111).

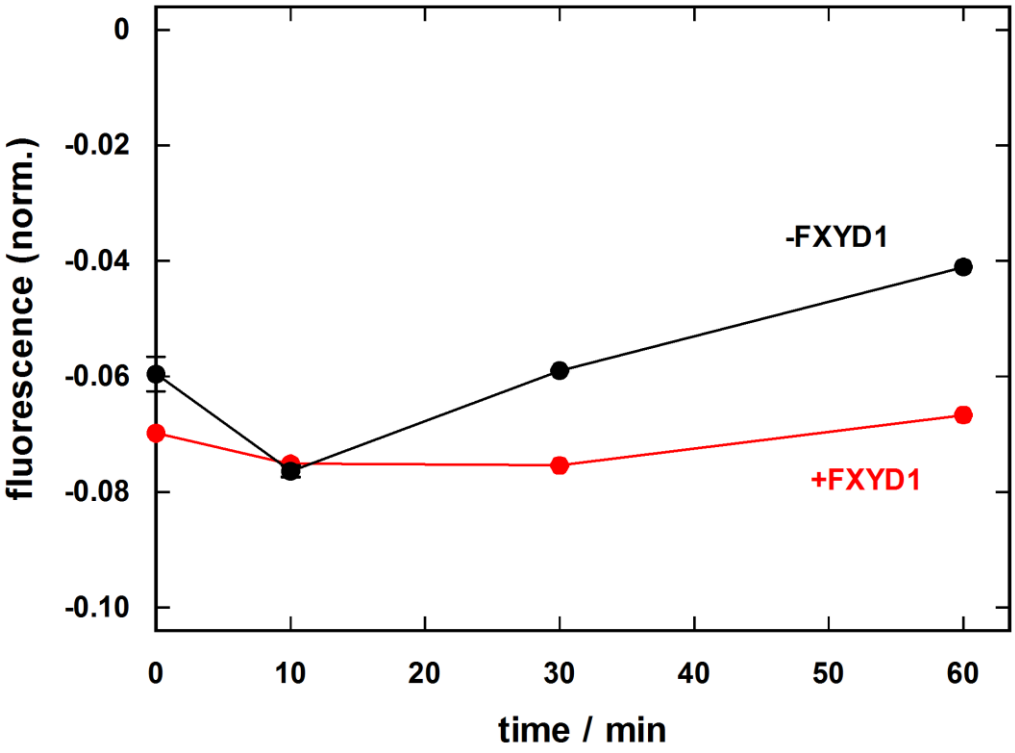

Figure 43. The normalized fluorescence levels after addition of NaCl are plotted against the incubation time for α_1/His$_{10}$-β_1 (black) and α_1/His$_{10}$-β_1/FXYD1 (red).

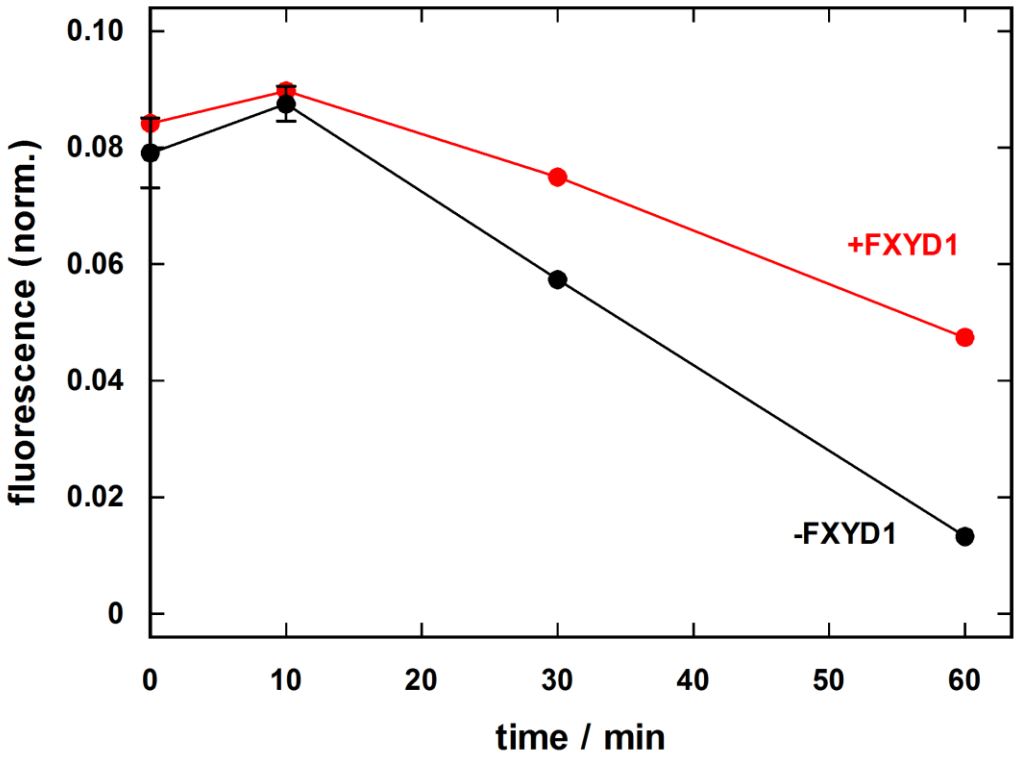

Figure 44. The normalized fluorescence levels after addition of ATP are plotted against the incubation time for α_1/His$_{10}$-β_1 (black) and α_1/His$_{10}$-β_1/FXYD1 (red).

3.3 Characterization of the Transport Properties of the Purified, Detergent-solubilized Human α_1/His$_{10}$-β_1 and α_1/His$_{10}$-β_1/FXYD1

The various reaction steps around the Post-Albers cycle of the purified α_1/His$_{10}$-β_1 and α_1/His$_{10}$-β_1/FXYD1 preparations have been investigated with the fluorescence techniques described in *2.4.1* exploiting the dye RH421. Steady-state fluorescence measurements have allowed the evaluation of the Na^+-, K^+- and Rb^+-binding affinities in the E_1 conformation as well as the Na^+- and K^+-binding affinities in the P-E_2 conformation as described in *2.4.1a*. Moreover, the backdoor phosphorylation reaction has been studied (*2.4.1a*). Time-resolved kinetic experiments after photochemical release of ATP from caged ATP have enabled us to estimate the ATP-binding affinity and the time constant of the conformational transition (Na_3)E_1-P → P-E_2Na_3 as described in *2.4.1b*.

Considering the increased specific activity of the recombinant preparations upon a short incubation at 37 °C (Fig. 43-44), the enzymes, routinely kept on ice, have been incubated for 30 min at RT before performing the biophysical experiments. This set of experiments is published in (112).

3.3.1 Standard Experiments

Standard experiments have been used to characterize the functional properties of the purified preparations (Fig. 45).

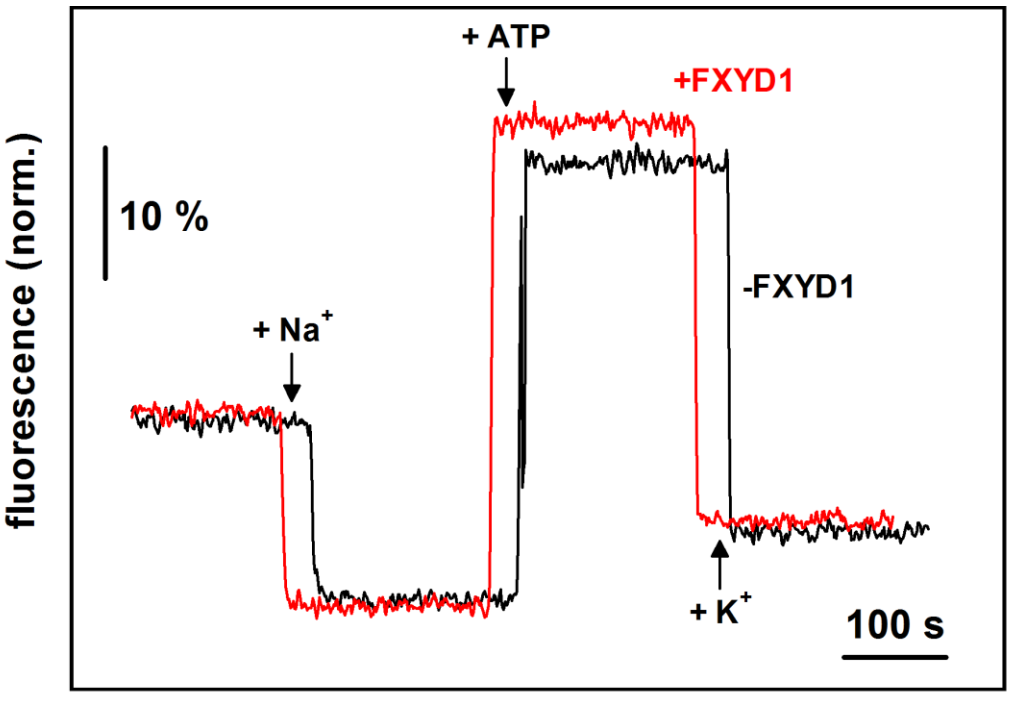

Figure 45. Standard experiments with α_1/His$_{10}$-β_1 (black) and α_1/His$_{10}$-β_1/FXYD1 (red).

When the experiments in the presence and absence of FXYD1 are compared, it can be noticed that the ATP-induced fluorescence change is larger in the presence of FXYD1. During the current study, the relative difference in the fluorescence increase, ~ 8% in the experiments in Fig. 45, has been found to be always proportional to the difference in specific ac-

tivity between α_1/His$_{10}$-β_1 and α_1/His$_{10}$-β_1/FXYD1. Indeed, a linear correlation is found between the two measures (Fig. 46).

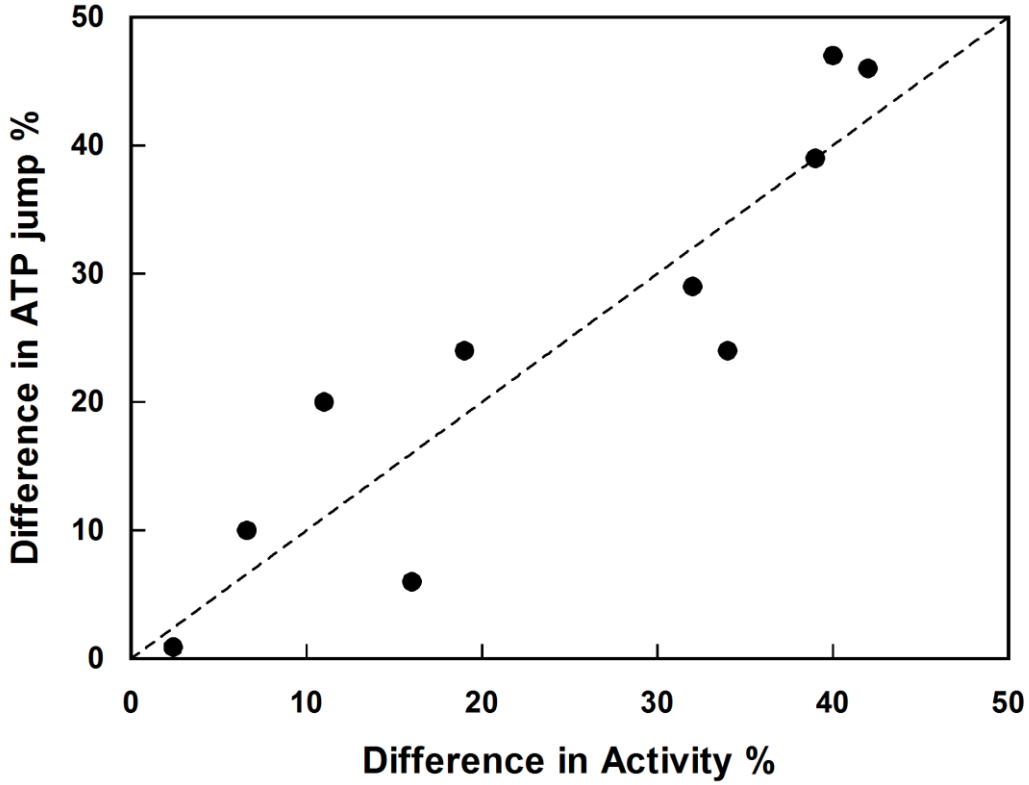

Figure 46. Plot of the relative difference in ATP-induced fluorescence increase in the standard experiment versus the relative difference in activity between the α_1/His$_{10}$-β_1 and α_1/His$_{10}$-β_1/FXYD1 preparations investigated during the current study.

Both recombinant enzymes show an ATP-induced fluorescence increase that is slightly smaller than the 3-fold fluorescence change detected with the membrane-bound Na,K-ATPase from rabbit kidney (145). As explained in *2.4.1a*, in the absence of other monovalent cations, the native Na,K-ATPase is mainly in the E_1 conformation with the ion-binding sites occupied by protons in a pH dependent manner (32). At pH 7.2, ~ 1.8 protons are bound to the protein (32). As a consequence, the sodium-induced fluorescence change represents only the binding of the last Na^+ ion, since the enzyme exchanges 3 Na^+ against ~ 2 H^+ ions. Thus, the ATP-induced fluorescence increase, which represents the quantitative release of 3 Na^+ ions on the extracellular side following the transition $Na_3E_1 \rightarrow P\text{-}E_2Na_3$, is about 3 times the sodium-induced fluorescence change. Considering this, the smaller amplitude of the ATP-induced fluorescence increase observed in the case of the recombinant enzymes can be explained by a lower number of enzyme molecules able to perform the conformational transition to P-E_2 compared to those able to bind sodium. Alternatively, it could be possible that a lower number of protons are bound initially in the E_1 conformation.

Both α_1/His$_{10}$-β_1 and α_1/His$_{10}$-β_1/FXYD1 exhibit a fluorescence decrease upon addition of 20 mM KCl that corresponds to 2.5-2.6 positive charges bound on average to the ion-binding sites. Since under turnover conditions the fluorescence level is due mainly to a mixture of the occluded states (Na_3)E_1-P and E_2(K_2), the results indicate a comparable occupation of both states. Thus, FXYD1 does not appear to affect notably the rate-limiting steps of the transport cycle.

3.3.2 Ion-binding Affinities in the E_1 Conformation

Sodium-titration experiments in the E_1 conformation have been performed by adding small aliquots of NaCl up to 100 mM (Fig. 47). In the presence of FXYD1, a ~ 20-30% higher Na^+-binding affinity has been detected in all the preparations investigated in the current study. In Fig. 47, obtained from the average of four identical experiments conducted with one preparation for both the enzyme with and without FXYD1, the half-saturating Na^+ concentration, $K_{1/2}$, is 5.8 ± 0.4 mM for α_1/His_{10}-β_1 and 4.4 ± 0.2 mM for α_1/His_{10}-β_1/FXYD1. The Hill coefficient, *n*, is the same for both preparations, 1.6 ± 0.1, demonstrating that FXYD1 does not affect the cooperativity of Na^+-binding. The maximum fluorescence change is ~ 25% larger in the presence of FXYD1.

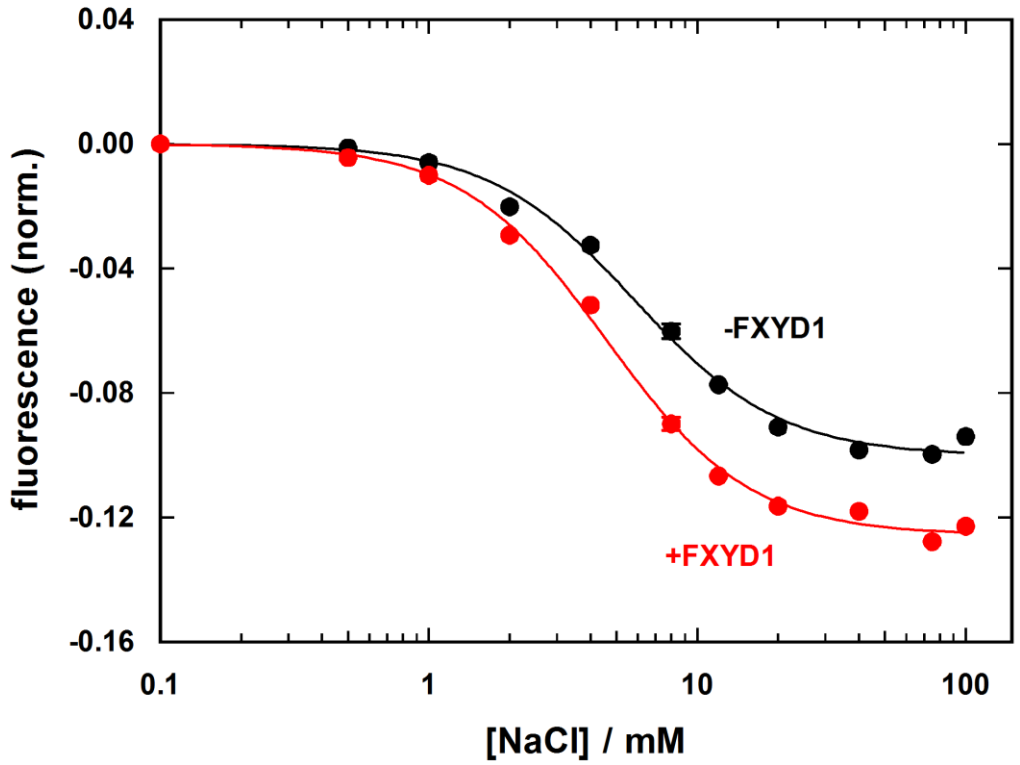

Figure 47. Sodium-titration experiments in the E_1 conformation with α_1/His_{10}-β_1 (black) and α_1/His_{10}-β_1/FXYD1 (red).

Potassium-titration experiments in the E_1 conformation are shown in Fig. 48. Small aliquots of KCl have been added up to 10 mM. The curves are obatiend from the average of six identical experiments for one α_1/His_{10}-β_1 preparation and three for one α_1/His_{10}-β_1/FXYD1. For both preparations, almost the same K^+-binding affinity is detected. $K_{1/2}$ has been determined to be 0.10 ± 0.02 mM for α_1/His_{10}-β_1 and 0.08 ± 0.01 mM for α_1/His_{10}-β_1/FXYD1. Because of the low fluorescence change in the case of α_1/His_{10}-β_1, $\Delta F_{max} < 5\%$, the error of the fitted result is large, despite the average of several identical experiments. Considering this, the small difference detected needs to be accounted as not significant. The Hill coefficients, *n*, are comparable, 0.57 ± 0.06 (-FXYD1) and 0.55 ± 0.04 (+FXYD1), respectively. The maximum fluorescence change is larger of a factor of 2 in the presence of FXYD1.

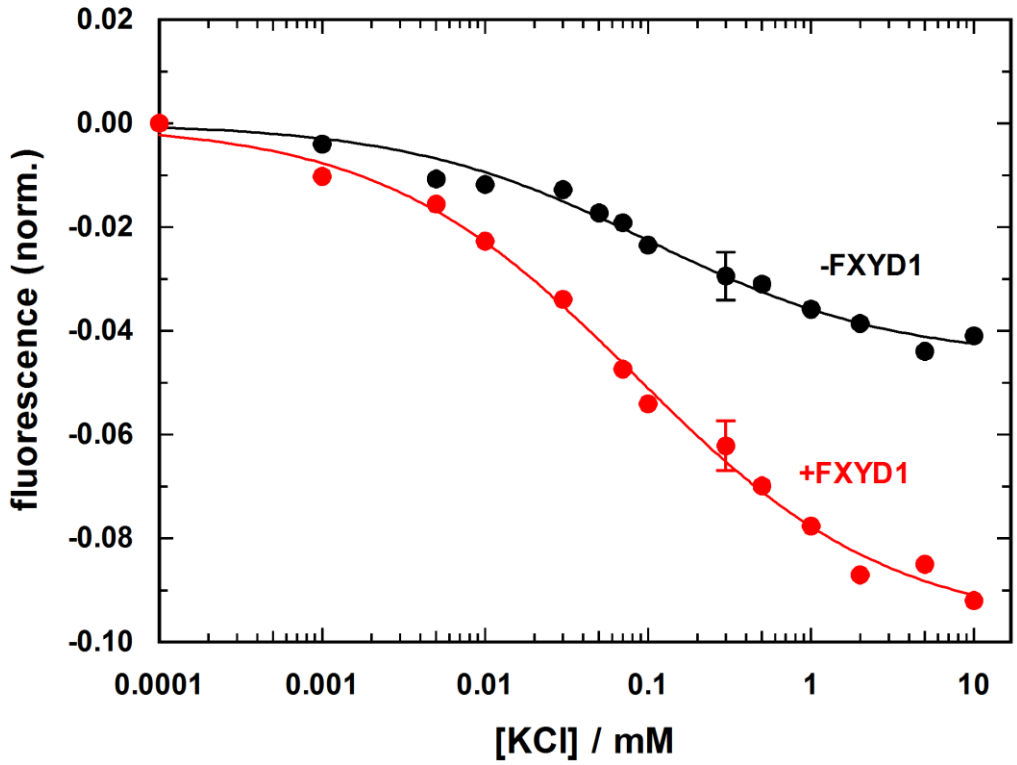

Figure 48. Potassium-titration experiments in the E_1 conformation with α_1/His_{10}-β_1 (black) and α_1/His_{10}-β_1/FXYD1 (red).

The Rb^+-binding affinity in the E_1 conformation has also been evaluated (Fig. 49). The titrations have been performed by adding RbCl up to 10 mM. The results represent the average of four identical experiments for one α_1/His_{10}-β_1 preparation and three for one α_1/His_{10}-β_1/FXYD1.

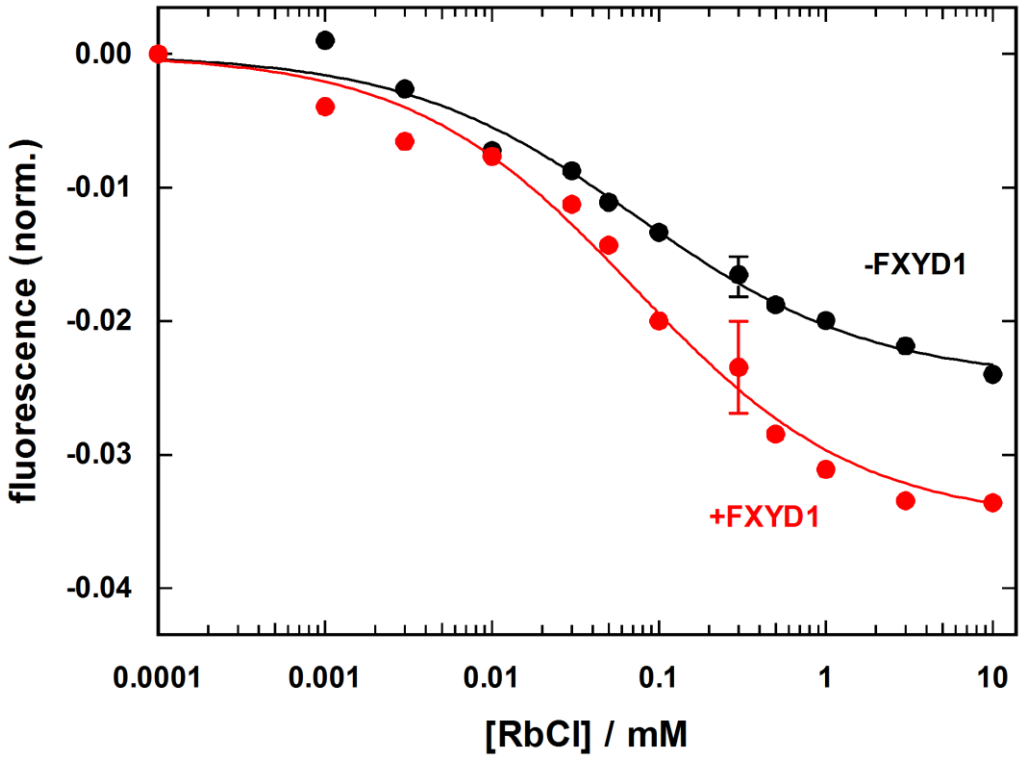

Figure 49. Rubidium-titration experiments in the E_1 conformation with α_1/His_{10}-β_1 (black) and α_1/His_{10}-β_1/FXYD1 (red).

For both α_1/His_{10}-β_1 and α_1/His_{10}-β_1/FXYD1, $K_{1/2}$ is 0.07 ± 0.02 mM, with a Hill coefficient of 0.65 ± 0.06. Again, the maximum fluorescence change is larger in the presence of FXYD1.

The difference detected in the half-saturating concentrations of Na^+ ions, but not of K^+ and Rb^+ ions, has stimulated further investigation of the effect of FXYD on the Na^+-binding affinity. To obtain experimental conditions closer to the physiological situation in cardiac myocytes, the Na^+-binding affinity in the E_1 conformation has been investigated by sodium-titration experiments in the presence of 1 mM free Mg^{2+} and 1.5 µM free Ca^{2+} ions as described in *2.4.1a* (Fig. 50). Considering the presence of EDTA in the Buffer used to perform the experiments, the amounts of $MgCl_2$ and $CaCl_2$ necessary to obtain the desired concentrations of free Mg^{2+} and Ca^{2+} ions have been calculated with the program WINMAXC32 2.51. As explained in *2.4.1a*, Mg^{2+} and Ca^{2+} ions are known to compete with Na^+ ions for a binding site on the cytoplasmic domain of the protein, in the loop between M6 and M7 (146). Occupation of this site by a Mg^{2+} or Ca^{2+} ion is assumed to impede Na^+-entrance at the cytoplasmic side (146), thus affecting the Na^+-binding affinity in the E_1 conformation. Indeed, the half-saturating Na^+ concentrations detected in the conditions of these experiments are smaller than those evaluated in Fig. 47, due to the lower total concentration of divalent cations (~ 1 mM in Fig. 50 versus 5 mM in Fig. 47). However, the effect of FXYD1 on the Na^+-binding affinity is similar, independently of the presence of calcium. With and without 1.5 µM free Ca^{2+} ions, the $K_{1/2}$ is 4.1 ± 0.3 mM and 4.0 ± 0.3 mM in the absence of FXYD1, while it is 2.8 ± 0.1 mM and 2.7 ± 0.2 mM in the presence of FXYD1. The curves are obtained from the average of three identical experiments in the different conditions conducetd with one preparation for both the enyzme with and without FXYD1.

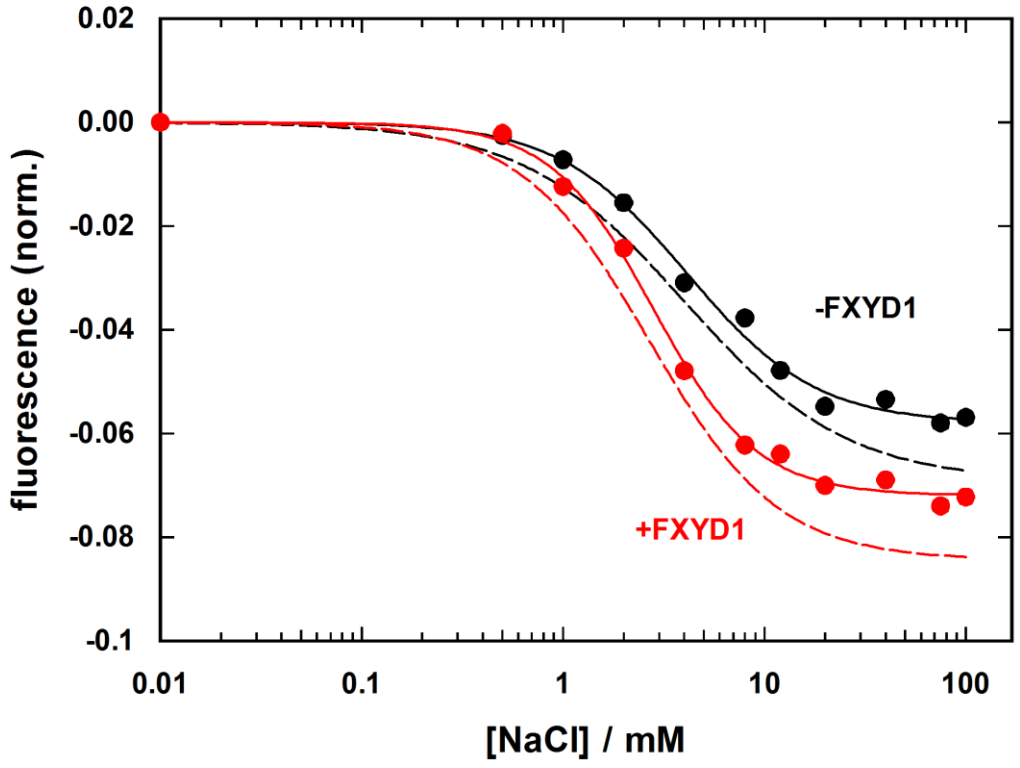

Figure 50. Sodium-titration experiments in the E_1 conformation in the presence of 1 mM free Mg^{2+} and 1.5 µM free Ca^{2+} ions with α_1/His_{10}-β_1 (black) and α_1/His_{10}-β_1/FXYD1 (red). The experiments have been repeated in the absence of calcium (dashed lines).

A further experimental parameter that has been investigated is the lipid composition of the lipid annulus surrounding the detergent-solubilized proteins. The Na^+-binding affinity in the E_1 conformation has been evaluated for a preparation obtained adding a doubled amount of SOPS (0.1 mg/ml SOPS) during the purification of α_1/His_{10}-β_1, described in *2.1.1b* (Fig. 51). Higher $K_{1/2}$ values have been detected ($K_{1/2}$ = 9.3 ± 0.9 mM for α_1/His_{10}-β_1 and $K_{1/2}$ = 6.8 ± 0.6 mM for α_1/His_{10}-β_1/FXYD1), but a similar difference, despite the increased number of negative surface charges. The results are obtained from the average of four identical experiments for α_1/His_{10}-β_1 and three for α_1/His_{10}-β_1/FXYD1.

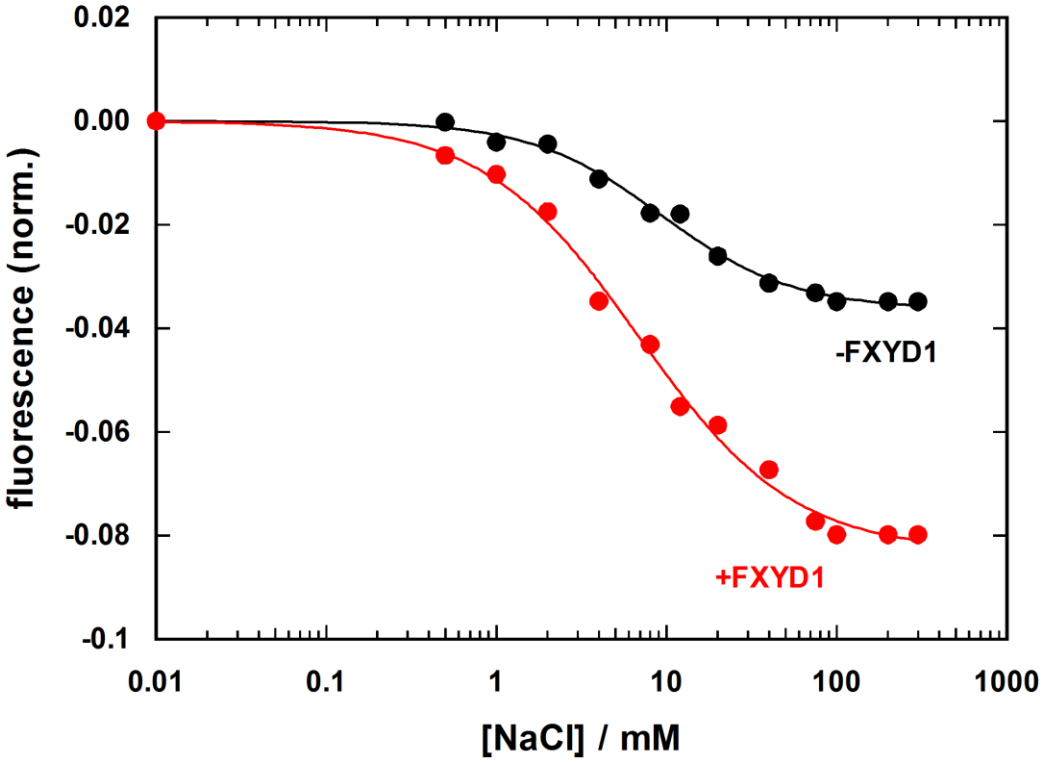

Figure 51. Sodium-titration experiments in the E_1 conformation with the α_1/His_{10}-β_1 (black) and α_1/His_{10}-β_1/FXYD1 (red) prepared with a doubled amount of SOPS.

The effect of the excess of FXYD1 during the incubation with α_1/His_{10}-β_1 bound to BD-Talon beads in the *in vitro* reconstitution procedure has been investigated to ensure that the experiments in the presence of FXYD1 are performed under saturating FXYD1 binding. The α_1/His_{10}-β_1 isozyme bound to BD-Talon beads has been incubated with molar excesses of FXYD1 up to 10-fold, and the Na^+-binding affinity has been studied as a crucial parameter that indicates the α_1/His_{10}-β_1/FXYD1 complex formation (Fig. 52). At least three experiments for each α_1/His_{10}-β_1/FXYD1 preparation have been averaged to obtain the $K_{1/2}$ values reported in Fig. 52. A maximum effect is found above a 5-fold molar excess of FXYD1. When the FXYD1-dependent half-saturating Na^+ concentration is fitted with the Hill function, it is found that about 50% of the Na,K-ATPase molecules are reconstituted with FXYD1 at a FXYD1 molar excess of 1.5 ± 0.3.

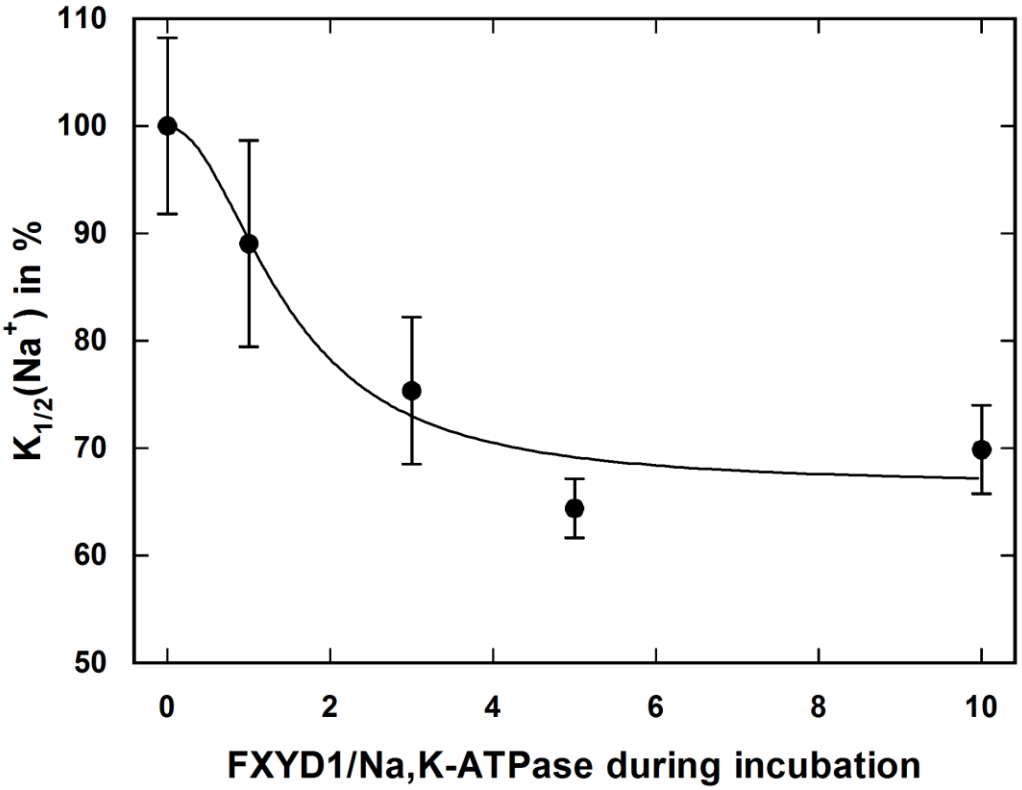

Figure 52. Half-saturating Na^+ concentrations, $K_{1/2}$, of the α_1/His_{10}-β_1/FXYD1 complex plotted against the excess of FXYD1 used during the *in vitro* reconstitution.

3.3.3 Ion-binding Affinities in the P-E_2 Conformation

Sodium-titration experiments in the P-E_2 conformation have been performed by adding NaCl up to 2.5 M (Fig. 53). However, since concentrations of 2 M and above produced unspecific artefacts on the fluorescence of the dye RH421 in the case of the α_1/His_{10}-β_1/FXYD1 complex, the data points above 1.5 M have been ignored. The half-saturating Na^+ concentration can be determined despite the fact that saturation is not completely obtained. A 20-30% higher apparent binding affinity for Na^+ ions has been detected in the presence of FXYD1 in several preparations. Fitting the data with the Hill function (Eq. 1) provides $K_{1/2}$ values of 428 ± 33 mM (-FXYD1) and 333 ± 12 mM (+FXYD1), with n = 1.7 ± 0.1 and 1.6 ± 0.2, respectively. For both α_1/His_{10}-β_1 and α_1/His_{10}-β_1/FXYD1, the curves have been obtained from the average of four identical experiments performed with two different preparations.

Potassium-titration experiments in the P-E_2 conformation have been performed by adding KCl up to 10 mM (Fig. 54). In contrast to the results obtained from the sodium- titrations, identical $K_{1/2}$ values are detected for the K^+-binding affinity, $K_{1/2}$ = 0.31 ± 0.02 mM (n = 1.17 ± 0.07) for α_1/His_{10}-β_1 and $K_{1/2}$ = 0.31 ± 0.02 mM (n = 1.18 ± 0.08) for α_1/His_{10}-β_1/FXYD1. In both the sodium- and potassium-titration experiments, a larger maximum fluorescence change is detected in the presence of FXYD1. The results represent the average of three different experiments carried out with one preparation for each enzyme.

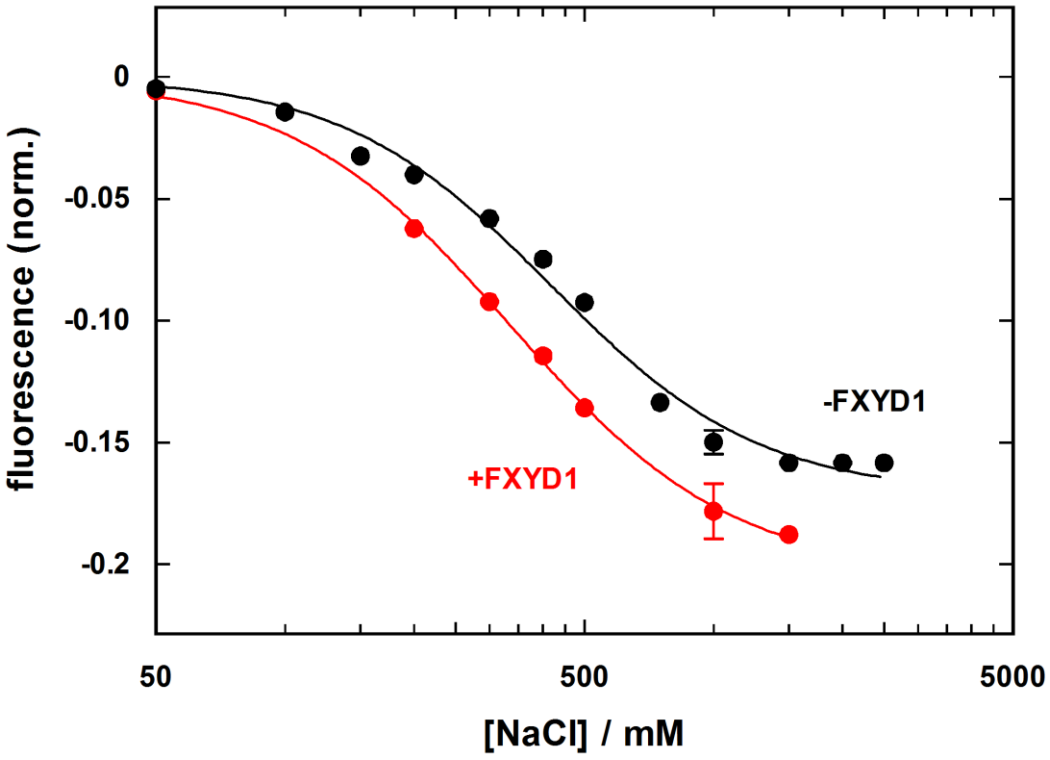

Figure 53. Sodium-titration experiments in the P-E_2 conformation with α_1/His_{10}-β_1 (black) and α_1/His_{10}-β_1/FXYD1 (red).

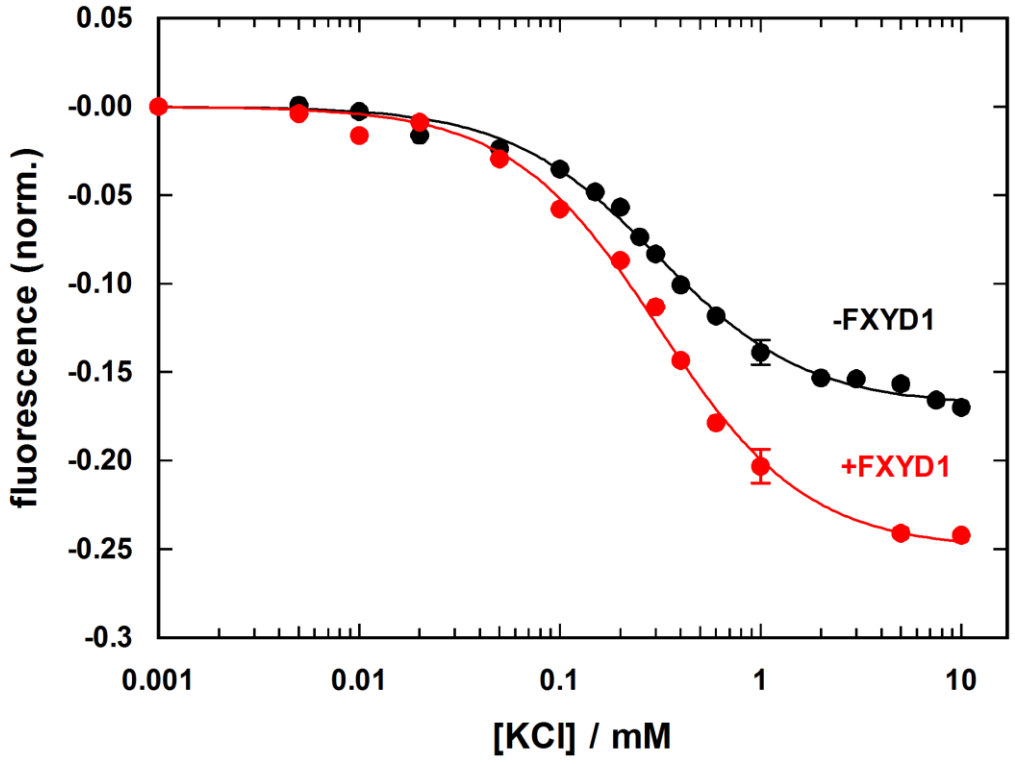

Figure 54. Potassium-titration experiments in the P-E_2 conformation with α_1/His_{10}-β_1 (black) and α_1/His_{10}-β_1/FXYD1 (red).

3.3.4 Backdoor Phosphorylation

Titration experiments with inorganic phosphate (Pi) up to 10 mM in the state H_nE_1 have enabled the evaluation of the apparent Pi-binding affinity as described in *2.4.1a* (Fig. 55). Due to the rather small fluorescence changes (<5%), the signal-to-noise ratio is quite high, despite averaging four identical experiments for each preparation. However, from the Michaelis-Menten fit (Eq. 2) of the data, similar half-saturating Pi concentrations are detected for both preparations: K_M = 100 ± 13 µM for α_1/His_{10}-β_1 and K_M = 87 ± 13 µM for α_1/His_{10}-β_1/FXYD1.

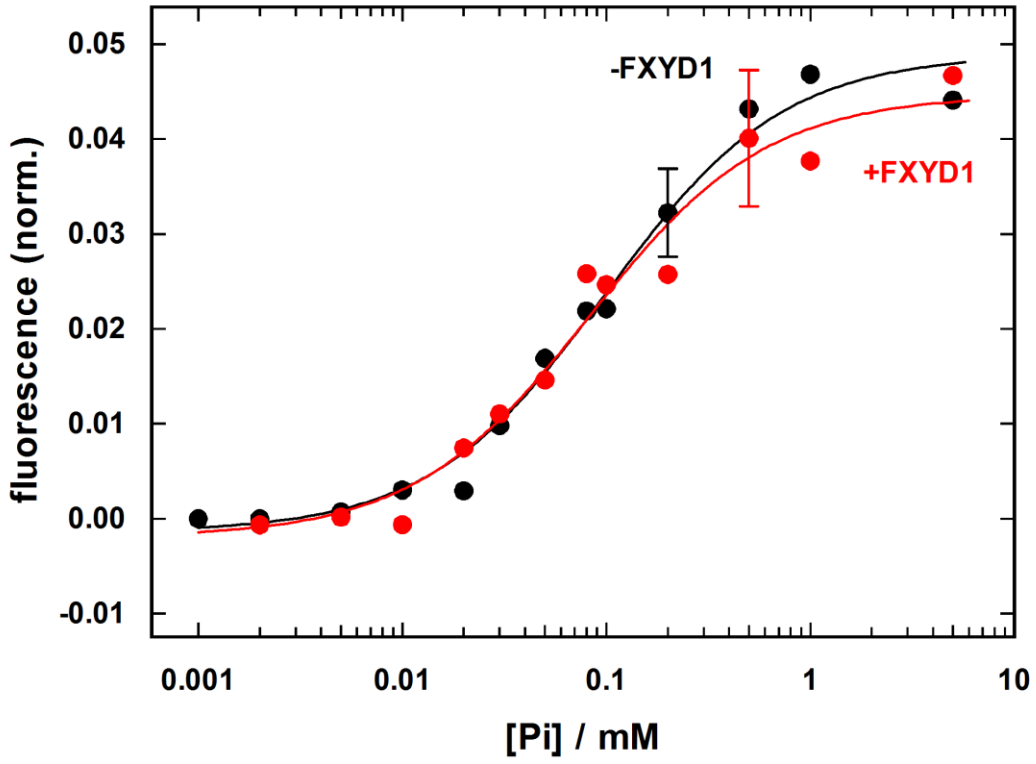

Figure 55. Evaluation of the apparent Pi-binding affinity of α_1/His_{10}-β_1 (black) and α_1/His_{10}-β_1/FXYD1 (red).

3.3.5 Time-resolved Fluorescence Signals after Photochemical Release of ATP

The rate of the conformational transition E_1-P → P-E_2 as well as the ATP-binding affinity has been studied in time-resolved experiments as described in *2.4.1b*. The fluorescence increases at saturating NaCl and ATP concentrations can be fitted by the exponential function (Eq. 3) with time constants of 276 ± 48 ms and 264 ± 30 ms in the absence and in the presence of FXYD1, respectively. Since the transition (Na_3)E_1-P → P-E_2(Na_3) is supposed to be the rate-determining step of the reaction sequence Na_3E_1 → Na_3E_1·ATP → (Na_3)E_1-P → P-E_2Na_3 → P-E_2 + 3 Na^+, these time constants represent a characteristic value of the turnover rate of the Na^+-translocating half cycle of the Na,K-ATPase. Therefore, the result shows that FXYD1 does not affect such turnover rate.

The apparent ATP-binding affinity can be evaluated by fitting the ATP-concentration dependence of the time constant or of the amplitude of the fluorescence increase. Due to the large scattering of fluorescence amplitudes in the performed experiments, it is impossible to extract sufficiently accurate values of the ATP-binding affinity from the fits. In contrast, the analysis of the time constants produced highly reliable results (Fig. 56). Fitting of the time constants plotted against the concentrations of released ATP with the Michaelis-Menten function (Eq. 4) provides similar half-saturating ATP concentrations for both preparations, K_M = 0.14 ± 0.06 µM for α_1/His_{10}-β_1 and K_M = 0.14 ± 0.02 µM for α_1/His_{10}-β_1/FXYD1. The values at different ATP concentrations in Fig. 56 are obtained from one to two experiments performed with the same α_1/His_{10}-β_1 or α_1/His_{10}-β_1/FXYD1 preparation.

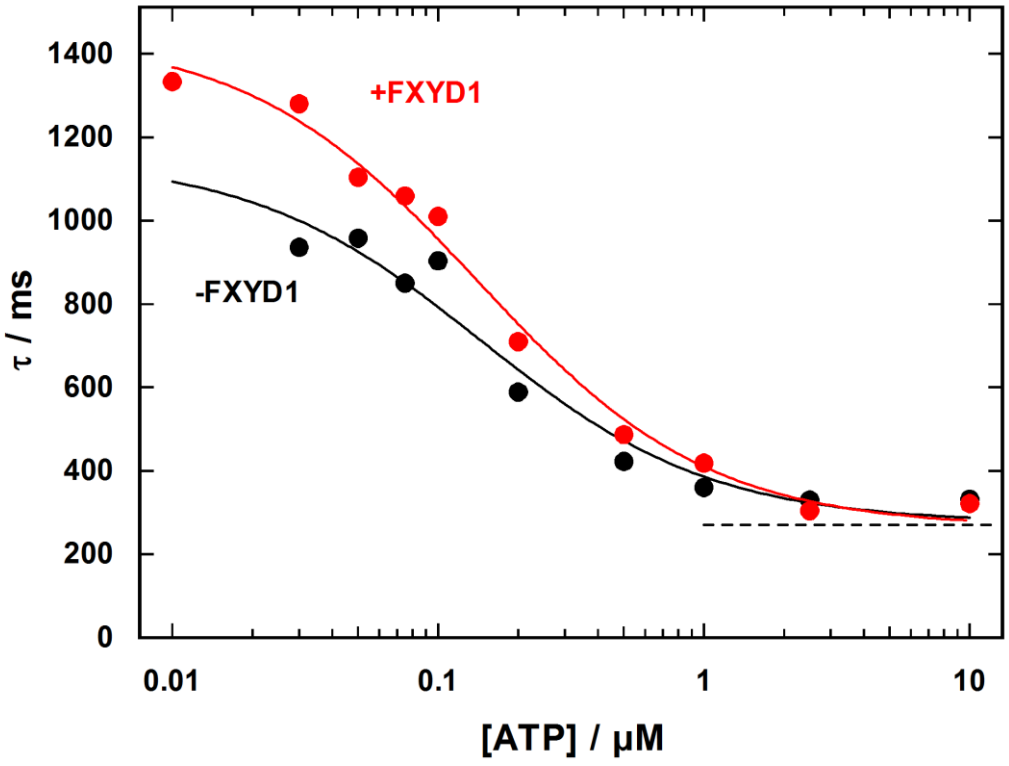

Figure 56. Evaluation of the apparent ATP-binding affinity of α_1/His_{10}-β_1 (black) and α_1/His_{10}-β_1/FXYD1 (red).

3.4 Investigation of the Na^+-binding affinity of the Na,K-ATPase in Lipid Vesicles

The presence and composition of a lipid bilayer surrounding the enzyme may be important for the correct interaction of FXYD1 with the Na,K-ATPase. In the reconstituted complexes, the proteins are surrounded by an annulus of lipid and detergent molecules that forms a hydrophobic environment and allows functional integrity of the enzyme. However, it does not form a planar membrane surface as it is present in cells, and this may potentially affect the interaction between FXYD1 and the Na,K-ATPase.

To investigate the influence of the membrane and its lipid composition on the modulation of the enzyme by FXYD1, α_1/His_{10}-β_1 with and without FXYD1 has been reconstituted in lipid vesicles as described in *2.2*. Proteoliposomes with different amounts of the anionic phospholipid DOPS have been prepared to study the effect of the surface charge density on the protein interaction. The Na^+-binding affinity of the vesicle-reconstituted enzyme has been evaluated with the dye Oxonol VI as described in *2.4.2a*.

The method has been first applied to the native Na,K-ATPase from rabbit kidney and then extended to vesicle preparations with the recombinant α_1/His_{10}-β_1 isozyme with and without FXYD1.

3.4.1 Investigation of the Native Na,K-ATPase Reconstituted in Lipid Vesicles

Proteoliposomes containing the native Na,K-ATPase from rabbit kidney have been prepared as described in *2.2*. The native Na,K-ATPase shows a significantly lower specific enzyme activity after solubilization of the protein-containing membrane fragments, 2.2 μmol of Pi/mg of protein/min at 37 °C compared to an original activity of 28.5 μmol of Pi/mg of protein/min. The specific activity of the enzyme reconstituted in vesicles with different amounts of DOPS has been investigated and compared to the one after solubilization. In Fig. 57, the ratio of the activity after reconstitution in lipid vesicles and after solubilization is plotted against the amount of DOPS in the vesicles membrane. Each value represents the average of two different vesicle preparations. Since ATP is added to the extravesicular medium, only the enzymes with the ATP-binding site facing outward are activated and contribute to the ATPase activity. On average, half of the enzyme molecules are reconstituted in the inside-out orientation. Therefore, ~ 50% of the activity of the solubilized protein could be expected. However, the lowest activity detected is 1.6-fold the activity of the detergent-solubilized protein, indicating that part of the activity lost in the solubilization process is regained once the enzyme is embedded again in a lipid bilayer. This fact demonstrates that the solubilized environment is less favorable for the enzyme activity, as it has been already observed (145). The specific activity increases linearly with the amount of DOPS in the membrane, up to almost 4-fold the activity after solubilization. This observation is not surprising, since the need of anionic phospholipids for the Na,K-ATPase activity is well documented (34-38). Even the highest pump activity detected in vesicle membranes, obtained at 50 mol % DOPS, is only 30% of the enzyme activity in native membrane fragments. Since only 50% of the ion pump molecules reconstituted in the vesicles contributes to the activity detected, the total enzyme activity is actually 60% of the one in native membrane fragments. Thus, 40% of the activity lost by solubilization could not be regained.

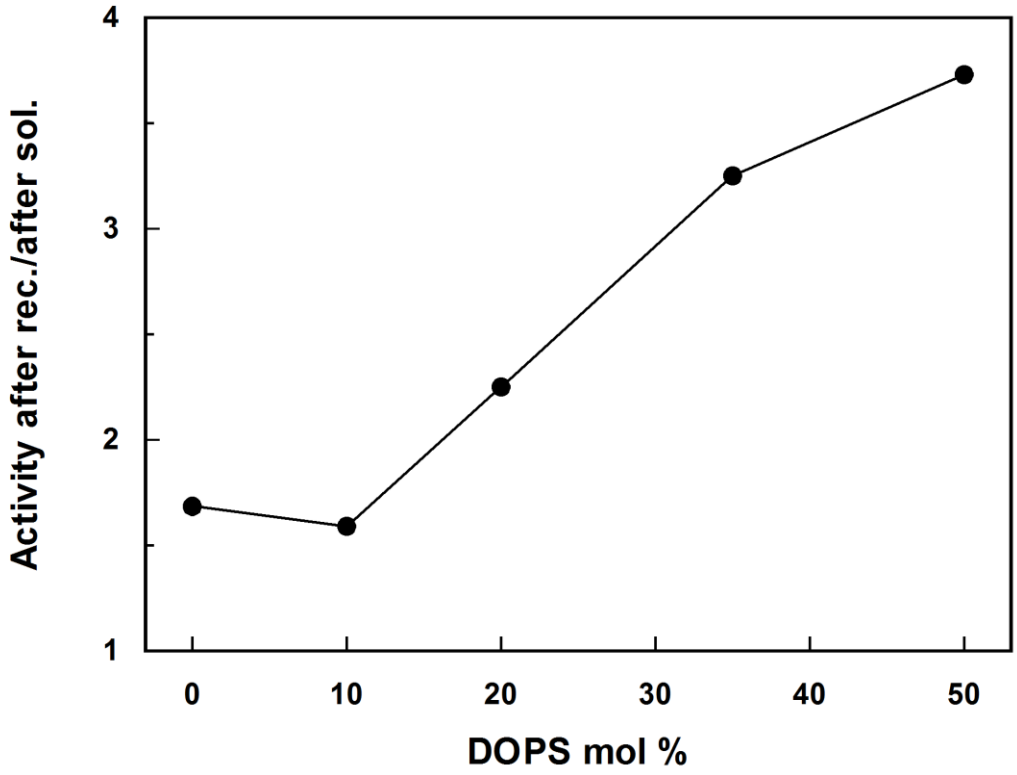

Figure 57. Ratio of specific ATPase activities obtained after reconstitution in lipid vesicles and after solubilization of the native Na,K-ATPase plotted against the amount of DOPS in the vesicles membrane.

The Na^+-binding affinity of the native Na,K-ATPase has been investigated in vesicles of different lipid composition as described in *2.4.2a*. The results, obtained from the average of three sets of experiments at various Na^+ concentrations for each vesicle preparation, are compared in Table 4.

DOPS	$K_{1/2}$ **(mM)**	***n***	$\left[\left(\frac{dF_{norm}}{dt}\right)_{t=0}\right]_{max}$ **(s^{-1})**	G_m **(nS/cm^2)**
0%	11.4 ± 0.2	2.01 ± 0.05	707 ± 8	4.1
10%	10.7 ± 0.4	1.83 ± 0.09	815 ± 17	3
20%	10.2 ± 0.4	1.9 ± 0.1	843 ± 21	3.3
35%	11.3 ± 0.2	2.05 ± 0.07	1370 ± 18	5
50%	13.2 ± 0.5	1.90 ± 0.09	1618 ± 39	10

Table 4. Comparison of the half-saturating Na^+ concentration, $K_{1/2}$, Hill coefficient, *n*, maximum initial slope, $[(dF_{norm}/dt)_{t=0}]_{max}$, and membrane conductance, G_m, of the native Na,K-ATPase reconstituted in lipid vesicles with different amounts of DOPS.

As shown in Fig. 58, the Na^+-binding affinity of the enzyme is strongly dependent on the amount of DOPS in the vesicles membrane. The half-saturating Na^+ concentration, $K_{1/2}$, decreases between 0 and 20 mol % DOPS to a minimum of 10.2 ± 0.4 mM, and then increases to a maximum of 13.2 ± 0.5 mM at 50 mol % DOPS.

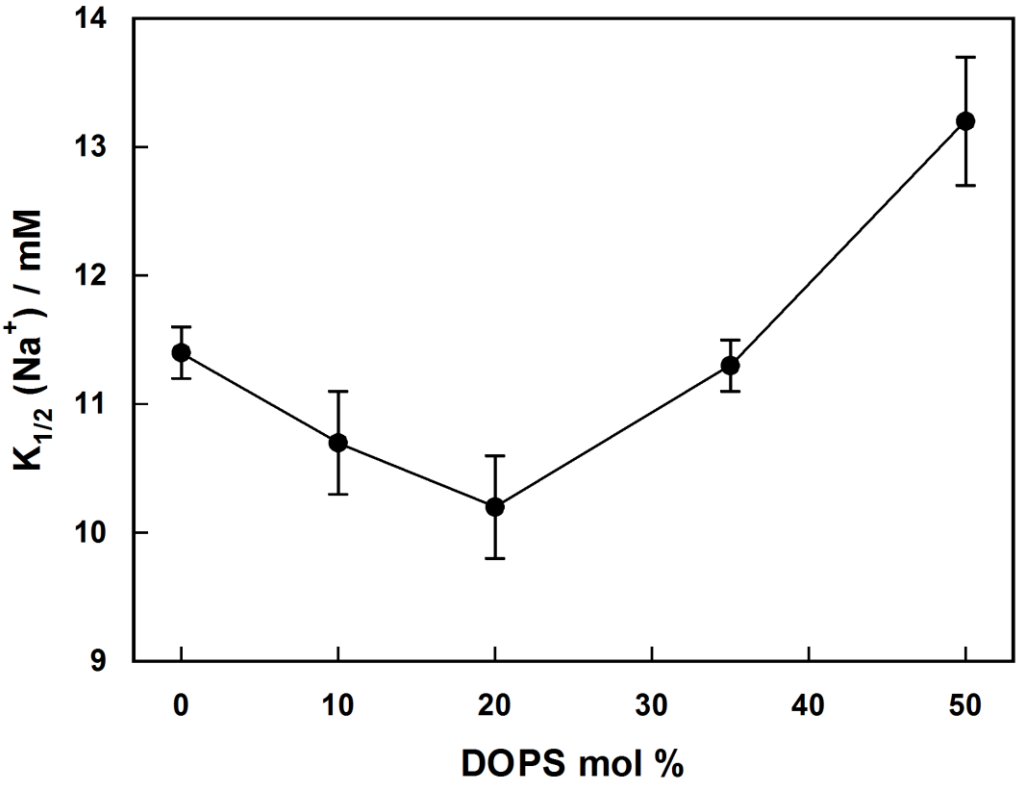

Figure 58. Half-saturating Na^+ concentration, $K_{1/2}$, of the native Na,K-ATPase reconstituted in lipid vesicles plotted against the amount of DOPS in the vesicles membrane.

Since the vesicles membrane without DOPS is formed mainly by uncharged lipid molecules (DEPC, SBPC, and cholesterol, *2.2*), the Na^+ concentration at the membrane surface corresponds to the one in the bulk of the solution. In contrast, in the presence of the anionic phospholipid DOPS, the membrane contains negative surface charges and the Na^+ concentration at the membrane surface is increased compared to the bulk of the solution according to the Gouy-Chapman theory. Indeed, the concentration at the membrane surface, c_0, is a function of the electric potential at the membrane surface, Ψ_0,

$$c_0 = c_\infty \cdot e^{\frac{F\Psi_0}{RT}}$$

with c_∞ corresponding to the concentration in the bulk phase. The electric potential, Ψ_0, is given by the surface charge density, σ, and the Debye length, ℓ_D, which is a function of the ionic strength, *J*, of the solution:

$$\Psi_0 = \frac{\sigma \cdot \ell_D}{\varepsilon \cdot \varepsilon_0}$$

$$\ell_D = \frac{1}{F}\sqrt{\frac{RT \cdot \varepsilon \cdot \varepsilon_0}{2J}}$$

with the dielectric constant in water, ε, and the dielectric constant in the vacuum, ε_0. The surface occupied by a phospholipid head, assuming a square surface, corresponds to 0.64 nm^2 (159). Therefore, for the vesicle preparation containing 50 mol % DOPS, the surface charge density is given by one elementary charge, *e*, per 1.28 nm^2.

$$\sigma = \frac{\mathrm{e}}{1.28\,\mathrm{nm}^2} = 0.78\mathrm{e}\,\frac{1}{\mathrm{nm}^2}$$

For a solution containing 25 mM Imidazole, 1 mM EDTA, 2.5 mM Mg^{2+}, 150 mM Na^+ + $Tris^+$, and 77.5 mM SO_4^{2-}, the ionic strength is 241.25 mM, giving a Debye length of 0.62 nm. The electric potential at the membrane surface becomes 0.11 V, and the factor $\frac{F\Psi_0}{RT}$ is equal to 4.25. Therefore, for the vesicle preparation containing 50 mol % DOPS, the Na^+ concentration at the membrane surface, and therefore at the entrance of the cytoplasmic access channel to the ion-binding sites, is 70 times higher than in the bulk phase. Considering this, smaller $K_{1/2}$ should be detected in the presence of DOPS compared to the one in the absence of DOPS, since saturation is obtained at lower bulk sodium concentrations. In contrast, an increase in $K_{1/2}$ is observed with more than 20 mol % DOPS. Therefore, this trend cannot be explained by a pure Gouy-Chapman effect. One possible explanation is that the amount of DOPS in the membrane affects the Na^+-binding affinity of the enzyme by altering its interaction with FXYD2, the regulatory protein associated with the $\alpha_1\beta_1$ isozyme in rabbit kidney.

It is noteworthy that even the lowest $K_{1/2}$ observed for the native Na,K-ATPase in lipid vesicles is significantly higher than the $K_{1/2}$ obtained for the enzyme in membrane fragments with the dye RH421, corresponding to 4.2 ± 0.1 mM (123). Since it can be assumed that the ion-binding sites are not affected by the solubilization/reconstitution procedure, the discrepancy can be assigned in part to the different lipid environment, but primarily to the detection method. The dye RH421 detects the actual binding of Na^+ ions to the ion-binding sites of the enzyme and provides therefore a "direct" measurement of the Na^+-binding affinity. In contrast, in vesicles experiments the evaluation of this kinetic parameter is based on the measurement of the enzyme-generated transmembrane potential and, therefore, provides an apparent Na^+-binding affinity only.

The comparison of the other parameters reported in Table 4 shows that similar Hill coefficients, *n*, are detected in all conditions, indicating no change in the cooperativity of Na^+-binding. On the other hand, the maximal initial slope, $[(dF_{norm}/dt)_{t=0}]_{max}$, differed in the various vesicle preparations. As explained in *2.3.2a*, the initial slope of the fluorescence signal can be calculated as F_{max}/τ. F_{max} is the normalized fluorescence level corresponding to the steady-state obtained after addition of ATP and τ is the time constant of the exponential fluorescence increase. F_{max} is a function of the membrane-water partition coefficient of Oxonol VI (152). The partition coefficient depends on the transmembrane voltage, which is related to the pump activity and to the membrane conductance. Moreover, since Oxonol VI is negatively charged at pH 7.2, it depends also on the lipid composition of the vesicles and in particular on the amount of negatively charged phospholipids. Therefore, F_{max} depends on parameters specific for each vesicle preparation (enzyme activity, membrane conductance and lipid composition) and, as a consequence, no information can be obtained by the direct comparison of the maximal initial slope of preparations with different lipid composition.

3.4.2 Investigation of α_1/His$_{10}$-β_1 and α_1/His$_{10}$-β_1/FXYD1 Reconstituted in Lipid Vesicles

Proteoliposomes containing the recombinant α_1/His$_{10}$-β_1 or α_1/His$_{10}$-β_1/FXYD1 enzyme have been prepared as described in *2.2*. The Na^+-binding affinity of the enzymes in lipid vesicles has been investigated as described in *2.4.2a*. The results are reported in Table 5 (-FXYD1) and 6 (+FXYD1). The values are obtained from the average of three sets of experiments at various Na^+ concentrations for each vesicle preparation. For the lipid compositions containing 0, 20, and 50 mol % DOPS, the results have been averaged with those obtained with a second vesicle preparation.

DOPS	$K_{1/2}$ **(mM)**	***n***	$\left[\left(\frac{dF_{norm}}{dt}\right)_{t=0}\right]_{max}$ **(s^{-1})**	G_m **(nS/cm^2)**
0%	15.7 ± 0.9	1.9 ± 0.1	110 ± 4	3.3
10%	12.3 ± 0.3	2.4 ± 0.1	265 ± 4	3.2
20%	14.3 ± 0.5	2.21 ± 0.08	322 ± 5	1.4
35%	14.8 ± 0.4	2.14 ± 0.09	343 ± 7	3.5
50%	13.2 ± 0.7	2.18 ± 0.06	312 ± 4	9.8

Table 5. Comparison of the half-saturating Na^+ concentration, $K_{1/2}$, Hill coefficient, *n*, maximum initial slope, $[(dF_{norm}/dt)_{t=0}]_{max}$, and membrane conductance, G_m, of α_1/His$_{10}$-β_1 reconstituted in lipid vesicles with different amounts of DOPS.

DOPS	$K_{1/2}$ **(mM)**	***n***	$\left[\left(\frac{dF_{norm}}{dt}\right)_{t=0}\right]_{max}$ **(s^{-1})**	G_m **(nS/cm^2)**
0%	19.6 ± 0.9	1.78 ± 0.08	448 ± 14	1.7
10%	15.5 ± 0.6	2.1 ± 0.1	397 ± 11	1.1
20%	15.2 ± 0.5	2.0 ± 0.1	487 ± 15	4.4
35%	15.0 ± 0.4	2.02 ± 0.08	492 ± 10	3
50%	15.8 ± 0.5	2.25 ± 0.08	416 ± 8	18.5

Table 6. Comparison of the half-saturating Na^+ concentration, $K_{1/2}$, Hill coefficient, *n*, maximum initial slope, $[(dF_{norm}/dt)_{t=0}]_{max}$, and membrane conductance, G_m, of α_1/His$_{10}$-β_1/FXYD1 reconstituted in lipid vesicles with different amounts of DOPS.

The half-saturating Na^+ concentration of α_1/His$_{10}$-β_1 shows no clear tendency with DOPS. The $K_{1/2}$ values are similar at 0, 20 and 35 mol % DOPS, but about 20% higher at 10

and 50 mol % DOPS. Therefore, DOPS does not seem to affect the Na^+-binding affinity of the $\alpha_1\beta_1$ complex with a specific mechanism. This observation supports the hypothesis that the DOPS-dependence detected with the native Na,K-ATPase is related to an interaction with FXYD2. For α_1/His_{10}-β_1/FXYD1, the Na^+-binding affinity in the absence of DOPS is about 25% lower than the affinity detected in vesicles containing DOPS, independently on the DOPS amount.

When the $K_{1/2}$ detected for α_1/His_{10}-β_1 and α_1/His_{10}-β_1/FXYD1 are plotted against the amount of DOPS in the vesicles membrane (Fig. 59), it can be noticed that, upon reconstitution in lipid vesicles, FXYD1 induces a decrease in Na^+-binding affinity, in contrast to what has been observed with the purified detergent-solubilized preparations.

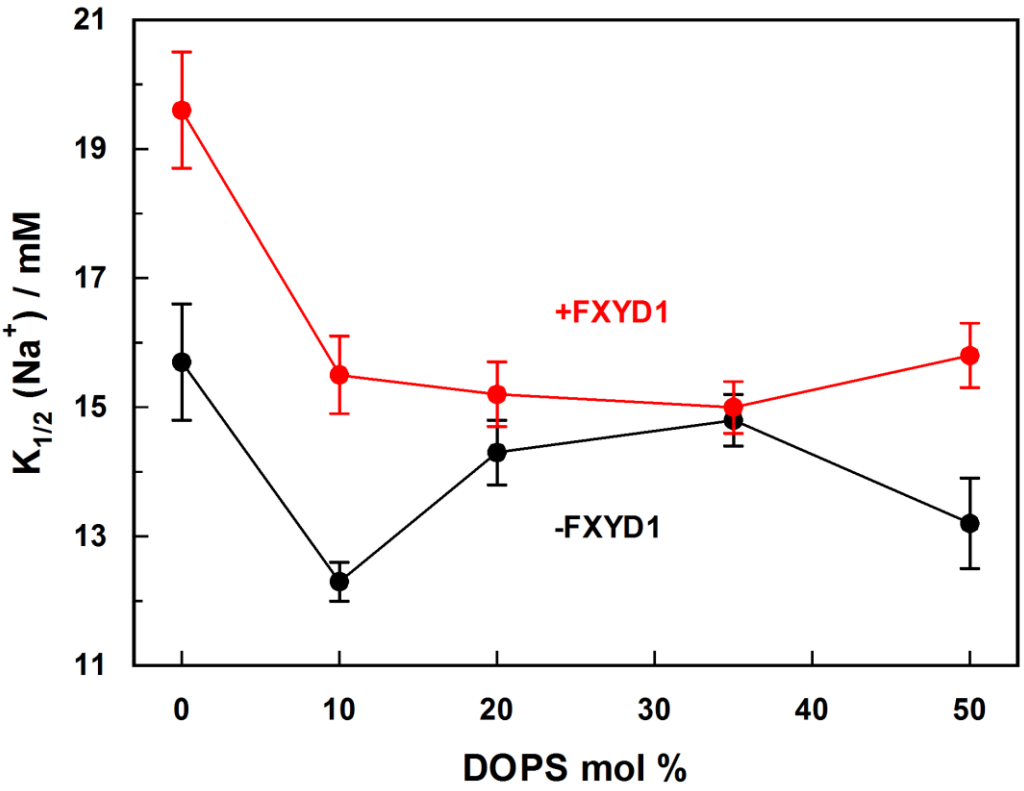

Figure 59. Half-saturating Na^+ concentration, $K_{1/2}$, of α_1/His_{10}-β_1 (black) and α_1/His_{10}-β_1/FXYD1 (red) reconstituted in lipid vesicles plotted against the amount of DOPS in the vesicles membrane.

Interestingly, the effect of FXYD1 on the Na^+-binding affinity of the enzyme depends on the fraction of DOPS in the membrane. The plot of the ratio between the $K_{1/2}$ of the complex with and without FXYD1 versus the amount of DOPS in the vesicles membrane (Fig. 60) shows clearly that the decrease in Na^+-binding affinity induced by FXYD1 in the absence of DOPS diminishes with higher amounts of DOPS. In particular, at both 0 and 10 mol % DOPS FXYD1 causes a 25% decrease in the Na^+-binding affinity, but the difference drops to 6% and 1% at 20 and 35 mol % DOPS, respectively. The only exception observed is with 50 mol % DOPS and could be related to the extremely non-physiological environment provided by this lipid composition.

The comparison of the other parameters reported in Tables 5 and 6 shows that the Hill coefficients, *n*, are similar, indicating that neither FXYD1 nor DOPS influence the cooperativity of Na^+-binding. Independently of the amount of DOPS, the maximal initial slope, $[(d(\Delta F/F_0)/dt)_{t=0}]_{max}$, and therefore the initial enzyme activity at saturating Na^+ concentrations, is always higher in the presence of FXYD1. This observation is in

agreement with the results obtained with the purified detergent-solubilized preparations, where the enzyme activity has been found always higher in the presence of FXYD1. Again, this probably needs to be assign to the stabilizing effect of FXYD1 on the enzyme, which is protected against detergent-mediated inactivation during the reconstitution in lipid vesicles.

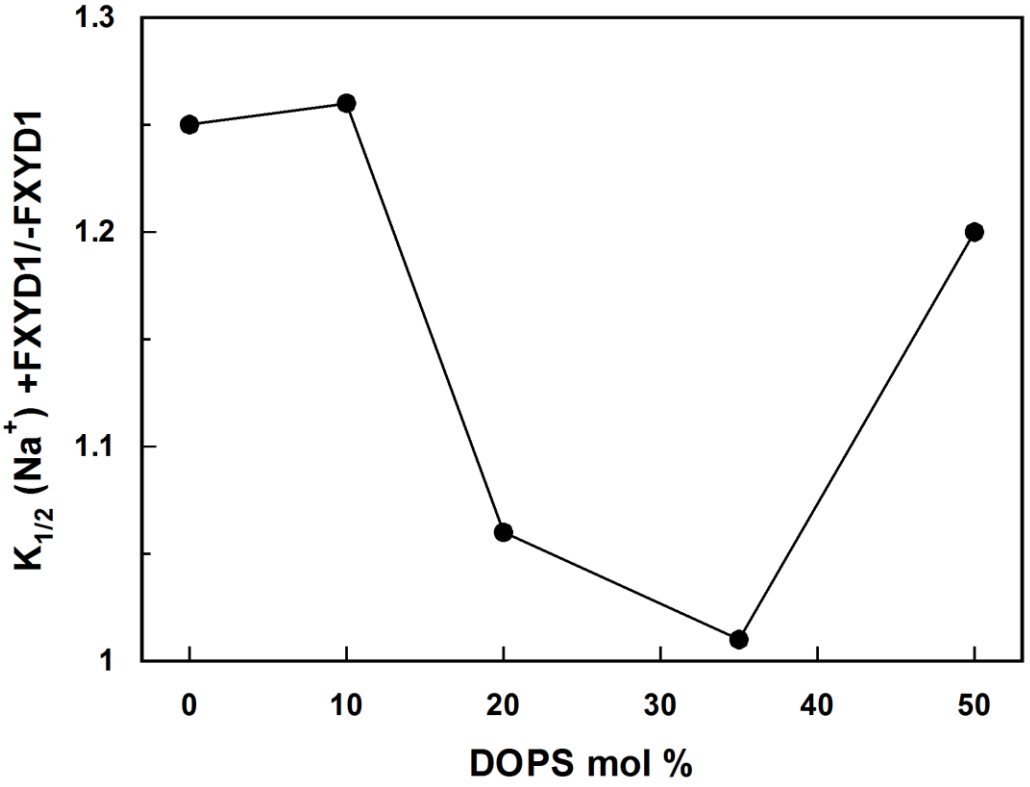

Figure 60. Ratio between the half-saturating Na^+ concentrations of α_1/His_{10}-β_1 (black) and α_1/His_{10}-β_1/FXYD1 (red) reconstituted in lipid vesicles plotted against the amount of DOPS in the vesicles membrane.

The electric potential at the membrane surface as well as in the adjacent solution created by the surface charges of the membrane depends on the ionic strength of the aqueous medium. The predominant ions in the cytoplasm under physiological conditions are Na^+, K^+ and Cl^-, in the concentration of 10, 155, and 10-20 mM, respectively (2). Other ions like Mg^{2+}, Ca^{2+}, and ATP^{2-} as well as charged proteins contribute only slightly to the ionic strength of the cytosol that, therefore, should be ~ 90-100 mM. Since the kinetic property of interest is the Na^+-binding affinity in the E_1 conformation, when the ion-binding sites are facing the cytoplasm, the experiments in lipid vesicles have been repeated at an ionic strength similar to the one of the cytoplasm to check whether a DOPS-dependence of the FXYD1 effect on Na^+-binding can be detected also in this condition. To maintain an ionic strength of ~ 110 mM, Tris/H_2SO_4 has been added to obtain a concentration of Na^+ plus $Tris^+$ ions of 50 mM. The intravesicular ionic strength could not be reduced, since that would imply a significantly lower inner potassium concentration. When the number of K^+ ions inside the vesicles is too low, after a few transport cycles the enzyme shifts from the Na/K to the Na/Na-transport mode because of intravesicular potassium depletion. In the Na/Na-transport mode, the enzyme has a lower turnover rate and, after a steep increase, the fluorescence signal decreases without reaching the steady-state which is required for the calculation of the initial slope. The Na^+-binding affinity of the enzymes has been investigated in lipid vesicles containing 0, 20, or 50 mol % DOPS. The results The values, obtained from

the average of three sets of experiments at various Na^+ concentrations for each vesicle preparation, are reported in Table 7 (-FXYD1) and 8 (+FXYD1).

DOPS	$K_{1/2}$ **(mM)**	***n***	$\left[\left(\frac{dF_{norm}}{dt}\right)_{t=0}\right]_{max}$ **(s^{-1})**	G_m **(nS/cm^2)**
0%	11.8 ± 0.3	2.2 ± 0.1	334 ± 6	1.1
20%	10.9 ± 0.4	2.0 ± 0.1	479 ± 11	1.8
50%	11.1 ± 0.3	2.4 ± 0.1	416 ± 7	16.6

Table 7. Comparison of the half-saturating Na^+ concentration, $K_{1/2}$, Hill coefficient, *n*, maximum initial slope, $[(dF_{norm}/dt)_{t=0}]_{max}$, and membrane conductance, G_m, of α_1/His_{10}-β_1 reconstituted in lipid vesicles with different amounts of DOPS. Extravesicular ionic strength ~ 110 mM.

DOPS	$K_{1/2}$ **(mM)**	***n***	$\left[\left(\frac{dF_{norm}}{dt}\right)_{t=0}\right]_{max}$ **(s^{-1})**	G_m **(nS/cm^2)**
0%	14.1 ± 0.8	1.7 ± 0.1	352 ± 13	1.1
10%	10.3 ± 0.3	2.3 ± 0.1	487 ± 11	1.5
20%	12.3 ± 0.5	2.1 ± 0.1	672 ± 19	13.2

Table 8. Comparison of the half-saturating Na^+ concentration, $K_{1/2}$, Hill coefficient, *n*, maximum initial slope, $[(dF_{norm}/dt)_{t=0}]_{max}$, and membrane conductance, G_m, of α_1/His_{10}-β_1/FXYD1 reconstituted in lipid vesicles with different amounts of DOPS. Extravesicular ionic strength ~ 110 mM.

When the $K_{1/2}$ detected for α_1/His_{10}-β_1 and α_1/His_{10}-β_1/FXYD1 are plotted against the amount of DOPS in the vesicles membrane (Fig. 61), it can be noticed that FXYD1 induces a decrease in Na^+-binding affinity in the absence of DOPS, but no change at 20 mol % DOPS, similarly to what is detected at a higher ionic strength.

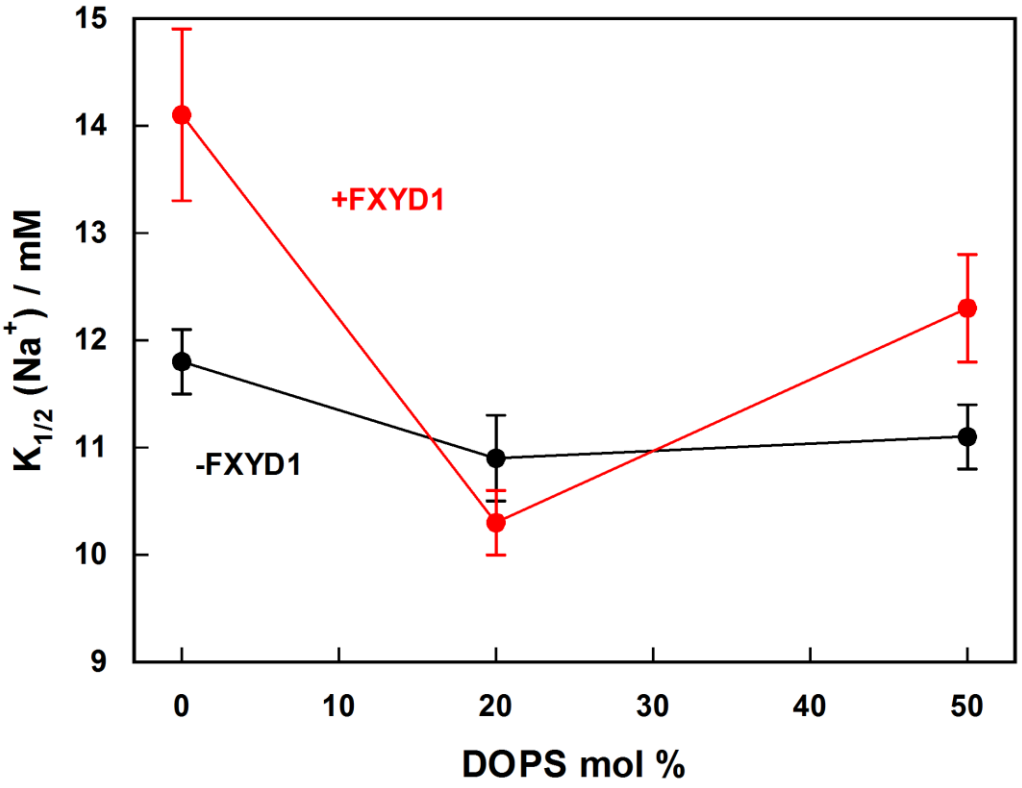

Figure 61. Half-saturating Na^+ concentration, $K_{1/2}$, of α_1/His_{10}-β_1 (black) and α_1/His_{10}-β_1/FXYD1 (red) reconstituted in lipid vesicles plotted against the amount of DOPS in the vesicles membrane. Extravesicular ionic strength ~ 110 mM.

CHAPTER 4

DISCUSSION

So far, the effects of FXYD1 on the Na,K-ATPase have been investigated mainly in intact cells, both heterologous systems and native cells. These systems allow a better characterization of the physiological effects of FXYD1, but are of limited use for the investigation of the functional and structural interactions between FXYD1 and the enzyme. In contrast, the purified, detergent-solubilized recombinant preparations provide a system that enables us to work under well defined conditions and without interference by other cellular components. Unlike in native cells, the effects of FXYD1 on the different isozymes of the Na,K-ATPase can be investigated separately. Moreover, since the phosphorylation state of FXYD1 in the purified preparations is easily controllable, the functional role of the protein kinases-mediated phosphorylation of FXYD1 can be investigated. Therefore, these systems allow the performance of a detailed functional analysis of the effects of FXYD1 on the Na,K-ATPase.

The electrochromic styryl dye RH421 has been applied in steady-state and time-resolved kinetic measurements to characterize the effects of FXYD1 on the different partial reactions of the transport cycle of the α_1/β_1 isozyme of the Na,K-ATPase. These experiments have shown a single kinetic property affected by the presence of FXYD1: in both the E_1 and $P\text{-}E_2$ conformations, the Na^+-binding affinity is increased by ~ 20-30%. The influence of the membrane and its lipid composition on the effect of FXYD1 on the Na^+-binding affinity of the enzyme has been investigated with the voltage-sensitive dye Oxonol VI in proteoliposomes containing either $\alpha_1/His_{10}\text{-}\beta_1$ or $\alpha_1/His_{10}\text{-}\beta_1$/FXYD1. These experiments have revealed an unexpected role of the lipid environment surrounding the complex in the interaction of FXYD1 with the enzyme, probably related to the cytoplasmic segment of the regulatory protein.

4.1 Extension of the Methods Based on the Styryl Dye RH421 to the Purified Recombinant Na,K-ATPase

Various biophysical techniques can be applied to investigate the transport properties of the Na,K-ATPase. In tracer flux studies, the enzyme-mediated movement of radioactive isotopes across the membrane is followed in compartmentalized preparations, such as cells or artificial proteoliposomes. The ion movements across the membrane can also be detected with electrophysiological techniques, where the current generated by the Na,K-ATPase is measured with electrodes in contact with the aqueous media on each side of the enzyme-containing membrane. The basic requirement of both techniques is the separation of the extracellular and cytoplasmic media to allow the detection of the transmembrane current. Therefore, such techniques cannot be applied to detergent-solubilized systems, since both sides of the membrane are short-circuited by the electrolyte they are suspended in.

A third approach is based on optical methods exploiting the fluorescence of external labels. Among them, the electrochromic styryl dye RH421 has been widely and successfully used to investigate the electrogenic partial reactions of the native Na,K-ATPase in open membrane fragments (32,123,127-144). This dye allows us to monitor the ion movements inside the membrane domain of the enzyme, enabling the detection of ion binding and ion

release during the transport cycle. Moreover, the time course of the signals provides information about the kinetics of the processes involved. In contrast to the above-mentioned techniques, the methods exploiting the dye RH421 do not require the separation between the two sides of the membrane and, thus, in principle they can be applied to detergent-solubilized preparations.

To obtain significant fluorescence changes upon ion binding and ion release, the dye molecules have to be close to the transmembrane domain of the enzyme. Thanks to the purification of the detergent-solubilized recombinant proteins by the His tag on the β subunit of the enzyme, the final preparations do not contain contaminant proteins or protein-free lipid/detergent micelles. Therefore, all dye molecules are inserted in the annulus of lipid and detergent molecules surrounding the Na,K-ATPase, close to the transmembrane domain.

In experiments with membrane fragments enriched in Na,K-ATPase molecules, the RH421 molecules are oriented perpendicularly to the plane of the membrane, parallel to the hydrocarbon chains of the lipids and to the transmembrane domain of the pump (Fig. 62, left panel) (127,128). This arrangement is favorable for the occurrence of large electrochromic spectral shifts in response to a change of the electric field strength in the membrane dielectric (128). In the detergent-solubilized systems, the dye molecules insert in the annulus of lipid and detergent molecules surrounding the protein, assuming many different orientations with respect to the transmembrane domain of the pump (Fig. 62, right panel). Due to the lower lipid (and detergent) packing, the dye molecules are more exposed to the aqueous medium. As a consequence, the electrochromic mechanism and/or the fluorescence response of the dye RH421 to the different occupational states of the enzyme might be affected.

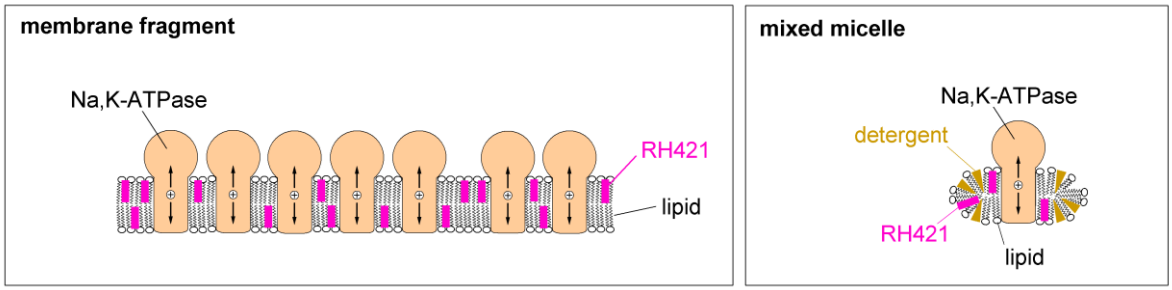

Figure 62. Disposition of the RH421 molecules in membrane fragments enriched in Na,K-ATPase molecules and in mixed lipid/detergent/Na,K-ATPase complexes.

Recently, the dye response in the detergent-solubilized environment has been shown to be comparable to the one in lipid bilayers (145). Qualitatively similar responses in the standard experiment and analogous ion-binding properties have been found for the detergent-solubilized and membrane-bound Na,K-ATPase from rabbit kidney (Table 9), demonstrating that, despite the modified environment, the styryl dye mechanism as well as the kinetic properties of the native Na,K-ATPase are not significantly altered by solubilization.

With the evidence that the method can reproduce the kinetic data obtained in membrane fragments also in detergent-solubilized preparations, the transport properties of the purified, detergent-solubilized recombinant α_1/His_{10}-β_1 and α_2/His_{10}-β_1 isozymes of the Na,K-ATPase have been investigated (*3.1*). The recombinant proteins show a specific ATPase activity that is, on average, only ~ 30% of the membrane-bound Na,K-ATPase from rabbit kidney. This difference can be assigned partly to the modified lipid environment, characterized by a different lipid content, by the partial substitution of lipid molecules with detergent molecules, and by a lower lipid packing. Indeed, the specific activity of the native Na,K-ATPase is also significantly reduced after solubilization (145). When the two isozymes are compared, α_2/His_{10}-β_1 has a specific enzyme activity ~ 30% lower than α_1/His_{10}-β_1. This observation is

in agreement with recently published data on the properties of the purified, detergent-solubilized α_2/His_{10}-β_1 isozyme (38). Such a difference can be due either to a lower turnover rate of this isozyme or to a reduced fraction of active α_2/His_{10}-β_1 enzyme molecules in a corresponding protein concentration, or both. Recently, α_2/β_1 has been found to have a significantly lower turnover rate compared to α_1/β_1 in *P. pastoris* membranes, almost 50% on average (38). Moreover, it has been shown to be less stable than α_1/β_1 against thermal inactivation in detergent-solubilized preparations as well as in intact *P. pastoris* cells and isolated membranes, suggesting an intrinsic lower stability of this isozyme (38). This aspect has been investigated in detail with site-specific mutagenesis experiments in a recently published paper (160). The instability of the α_2/β_1 isozyme has been attributed mainly to three residues unique to α_2: Ala 920, Leu 955, and Val 981. These residues, located in the transmembrane domain of the enzyme near the α/β interface, are responsible for suboptimal phosphatidylserine/protein interactions.

In the standard experiments (Fig. 35), the detergent-solubilized recombinant proteins follow the same scheme as the membrane-bound Na,K-ATPase from rabbit kidney, although the fluorescence changes are smaller (145). This may be partly due to a reduced response of the dye RH421 in the environment of the detergent-solubilized preparations. However, α_2/His_{10}-β_1 shows significantly smaller fluorescence changes compared to α_1/His_{10}-β_1, fact that cannot be attributed to an altered response of the dye. In all experiments, the same protein concentration has been used, independently of the specific ATPase activity. However, only active enzyme molecules contribute to the substrate-induced fluorescence changes in the standard experiment, that are indeed proportional to the concentration of active ion pumps (127). In contrast, they are independent of the enzyme turnover rate: for example, upon addition of ATP in the absence of K^+ ions, virtually all active enzyme molecules are trapped in the phosphorylated P-E_2 state, irrespective of their actual turnover rate. Therefore, this observation clearly indicates that the fraction of active enzyme molecules in the detergent-solubilized preparations, in particular in those of the α_2/β_1 isozyme, is lower than the one in native membrane fragments for an equal protein concentration. This also explains the differences detected in enzyme activity.

	Native α_1/β_1/FXYD2 membrane (rabbit kidney)	**Native α_1/β_1/FXYD2 solubilized (rabbit kidney)**	**Recombinant α_1/His_{10}-β_1 solubilized (human)**	**Recombinant α_2/His_{10}-β_1 solubilized (human)**
Na^+- binding affinity in E_1 (mM)	4.7 ± 0.3 (21)	5.0 ± 0.3 (21)	5.8 ± 0.4	6.1 ± 0.9
K^+-binding affinity in P-E_2 (mM)	0.20 ± 0.05 (21)	0.20 ± 0.01 (21)	0.31 ± 0.02	0.83 ± 0.06

Table 9. Comparison of the ion-binding properties of the native membrane-bound and detergent-solubilized Na,K-ATPase from rabbit kidney and of the recombinant, purified, detergent-solubilized human α_1/His_{10}-β_1 and α_2/His_{10}-β_1 isozymes investigated with the dye RH421.

When the kinetic properties are compared (Table 9), both recombinant enzymes show a similar Na^+-binding affinity, comparable to the one of the native Na,K-ATPase (Fig. 36). In a recent study on the enzymatic properties of the purified, detergent-solubilized human

α_1/His$_{10}$-β_1 and α_2/His$_{10}$-β_1 isozymes, the Na^+-dependence of the Na,K-ATPase activity has been investigated (38). A half-saturating Na^+ concentration of ~ 16 mM has been detected for both proteins, a value higher by a factor of almost 3 compared to that observed here. The discrepancy can be explained by the following considerations. First of all, the values obtained in (38) have been measured in the presence of 100 mM K^+ ions, which compete with Na^+ ions for the ion-binding sites increasing the half-saturating Na^+ concentration. In contrast, in the current study the sodium-titrations in the E_1 conformation have been performed in the absence of K^+ ions. In addition, part of the difference has to be assign to the detection method. As explained in *3.4.1*, the dye RH421 detects the actual binding of Na^+ ions to the binding sites of the protein and provides, therefore, a "direct" measurement of the Na^+-binding affinity. In contrast, the evaluation of this kinetic parameter with ATPase activity assays in (38) is based on the measurement of the enzyme-generated inorganic phosphate from the hydrolysis of ATP and, therefore, provides only an apparent Na^+-binding affinity.

In contrast to the Na^+-binding affinity, the K^+-binding affinity of α_2/His$_{10}$-β_1 is 2.7-fold lower than that of α_1/His$_{10}$-β_1 (Fig. 37). A lower K^+-binding affinity (1.8-fold) for the human α_2/β_1 compared to the human α_1/β_1 has been observed previously in detergent-solubilized preparations (38). Again, the half-saturating K^+ concentrations detected in (38) are 3 to 4 times higher than those observed here, due to reasons analogous to the ones discussed for the Na^+-binding affinity. In particular, the experiments in (38) have been performed in the presence of 130 mM sodium, while in the current study the potassium-titrations in the P-E_2 conformation have been performed in the presence of 50 mM sodium.

The α_1/His$_{10}$-β_1 isozyme shows an ~ 30% lower K^+-binding affinity compared to the native Na,K-ATPase (Fig. 37), which corresponds to the α_1/β_1/FXYD2 isozyme. FXYD2 is known to decrease the Na^+-binding affinity with no influence on the K^+-binding affinity (24-30); therefore, the difference detected cannot be due to the interaction with this regulatory protein. Since it may be assumed that the residues in the ion-binding sites are the same, the different binding properties may be caused by modifications in the extracellular access channel, or on the protein surface close to the entrance of the extracellular access channel, due to the different enzyme source (human vs rabbit).

At present, only one study has been published on the transport properties of the various human isozymes of the Na,K-ATPase (28). In this study, the isozymes have been expressed in *X. oocytes* in the absence of FXYD proteins. A lower turnover rate and K^+-binding affinity for the α_2/β_1 isozyme compared to the α_1/β_1 isozyme have been detected also in (28), in agreement with the results obtained with the detergent-solubilized preparations. In contrast, a slightly higher Na^+-binding affinity has been observed for α_1/β_1 compared to α_2/β_1. However, in the current study both α_1/His$_{10}$-β_1 and α_2/His$_{10}$-β_1 show identical Na^+-binding affinity at several Mg^{2+} concentrations (Fig. 38), indicating that the ion-binding sites as well as the entrance of the cytoplasmic access channel to the ion-binding sites are not significantly different.

In conclusion, the results demonstrate that the dye RH421 is suitable to investigate the transport properties of purified, detergent-solubilized ion pumps. Moreover, since the solubilization procedure does not seem to alter significantly the kinetic properties of the enzyme, these preparations may be exploited successfully to investigate the functional effects of FXYD1 on the Na,K-ATPase.

4.2 FXYD1 Stabilizes the Na,K-ATPase

The α_1/His_{10}-β_1 isozyme always shows a higher specific enzyme activity in the presence of FXYD1 (*3.2*). The reason for the broad range of this increase (2.5-40%) detected in the numerous preparations used in the current study is unclear and could be related to minor differences of each preparation (e.g., slightly varying lipid/detergent composition). It is, however, not due to a different α_1/β_1/FXYD1 ratio. In principle, the higher specific activity of the α_1/His_{10}-β_1/FXYD1 complex may result from either a specific effect of FXYD1 on the turnover rate of the enzyme or a stabilizing effect of FXYD1 on the ion pump, or both. The rate-limiting reaction steps of the pump cycle are the conformational transitions $(Na_3)E_1$-P $\rightarrow$ P-E_2Na_3 and $E_2(K_2) \rightarrow K_2E_1$. The time-resolved experiments with the dye RH421 have demonstrated that the transition $(Na_3)E_1$-P $\rightarrow$ P-E_2Na_3 is not affected by FXYD1 (Fig. 56). The analogous result has been obtained for the transition $E_2(Rb_2) \rightarrow Rb_2E_1$, investigated in time-resolved experiments with FITC using Rb^+ ions as congeners of K^+ ions (112). These findings clearly demonstrate that the turnover rate of the α_1/His_{10}-β_1 isozyme is not affected by the presence of FXYD1.

When the standard experiments in the presence and absence of FXYD1 are compared (Fig. 45), the ATP-induced fluorescence changes are larger in the presence of FXYD1. The relative difference in the fluorescence increase is proportional to the difference in specific activity (Fig. 46). Moreover, larger substrate-induced fluorescence changes are detected in the presence of FXYD1 throughout all the experiments with the dye RH421 (*3.3*). As already mentioned in paragraph *4.1*, the substrate-induced fluorescence changes are proportional to the concentration of active enzyme molecules (127). Therefore, these observations indicate that the preparations with FXYD1 are characterized by a higher fraction of active enzymes for an equal protein concentration. This supports the hypothesis, proposed previously (38,74), of a stabilizing effect of FXYD1 on the Na,K-ATPase, which is protected from partial detergent-induced inactivation during the purification procedure.

The comparison of the standard experiments performed in the absence and presence of FXYD1 after incubation at 45 °C clearly shows that FXYD1 protects the enzyme against thermal inactivation (Fig. 41-42). After 1 h incubation at 45 °C, all fluorescence jumps are smaller because of a reduction in the number of active enzymes, but significantly less for the α_1/His_{10}-β_1/FXYD1 complex. In particular, it can be noticed that the ATP-induced fluorescence jump is more sensitive compared to the Na^+-induced jump. In the absence of FXYD1, Na^+-binding is inactivated by about 30% after incubation at 45 °C for 1 h, while the ATP-induced jump is inactivated by over 80%. This observation indicates that the stabilizing effect occurs primarily at the transmembrane level. The ATP-induced jump reflects the reaction sequence $Na_3E_1 + ATP \rightarrow Na_3E_1{\cdot}ATP \rightarrow (Na_3)E_1$-P $\rightarrow$ P-$E_2Na_3 \rightarrow E_2$-P + 3 Na^+. From the standard experiments it is not possible to determine whether it is phosphorylation and Na^+ occlusion or the following conformational transition to be preferentially inactivated, since the dye monitors the subsequent release of Na^+ ions.

Two recent papers have shed light on the FXYD1 mechanism of stabilization. In a first study (111), three FXYD proteins (FXYD1, FXYD2, and FXYD4) have been shown to protect the $\alpha_1\beta_1$ isozyme of the Na,K-ATPase against thermal and detergent-induced inactivation in detergent-solubilized preparations and against thermal inactivation in intact HeLa cell membranes. A detailed investigation of the detergent-solubilized preparations has shown that FXYD proteins increase the enzyme affinity for phosphatidylserine-binding. Therefore, the authors assigned the protective effect of FXYD proteins to a stabilization of specific protein/phosphatidylserine interactions, which are required to preserve enzyme activity. This aspect has been suggested as a general feature of FXYD proteins *in vivo* (111). In a second paper (160), the phosphatidylserine-binding pocket has been identified between helices M8, M9, and M10 of the α subunit and the transmembrane segment of the FXYD

protein. The head group of the phospholipid is localized at the α/β/FXYD interface on the extracellular side (Fig. 63).

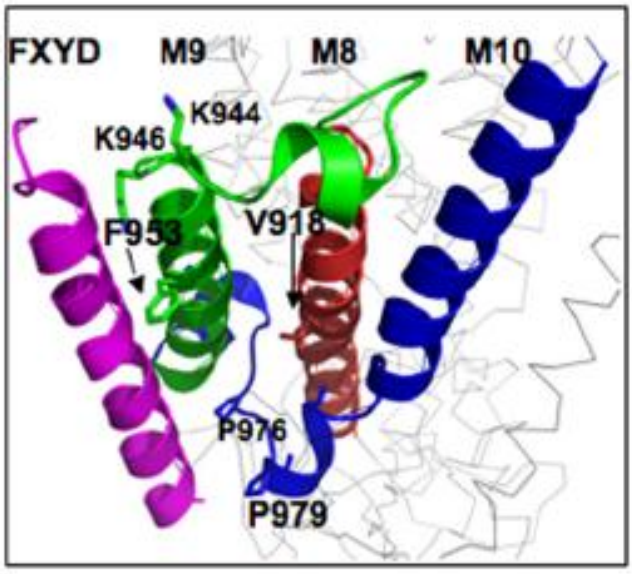

Figure 63. The phosphatidylserine-binding pocket is localized between helices M8, M9, and M10 of the α subunit and the FXYD protein (111).

The authors have proposed that thermally- or detergent-mediated displacement of the specifically bound phosphatidylserine from the binding pocket is followed by irreversible disruption of the subunit interactions and protein inactivation. Thus, by stabilizing the protein/phosphatidylserine interactions, FXYD proteins are crucial to maintain the subunit interactions and, therefore, functional structure and folding.

4.3 FXYD1 Increases the Na^+-binding Affinity in the E_1 and P-E_2 Conformations of the Na,K-ATPase

The kinetic properties of α_1/His_{10}-β_1 and α_1/His_{10}-β_1/FXYD1 determined with the methods exploiting the dye RH421 are summarized in Table 10. Since comparable investigations have been performed only with membrane-bound Na,K-ATPase from rabbit kidney, the parameters of the recombinant, purified, detergent-solubilized human preparations are compared with the respective values of the native Na,K-ATPase in membrane fragments. The equilibrium dissociation constants of the recombinant proteins are very similar to those of the native enzyme, especially in the case of the α_1/His_{10}-β_1/FXYD1 complex. The rabbit enzyme consists of the heterotrimer α_1/β_1/FXYD2. FXYD2 is a regulatory subunit closely related to FXYD1, but reported to decrease the Na^+-binding affinity (52-58).

	Native α_1/β_1/FXYD2 membrane (rabbit kidney)	**Recombinant α_1/His_{10}-β_1 solubilized (human)**	**Recombinant α_1/His_{10}-β_1/FXYD1 solubilized (human)**
Na^+- binding affinity in E_1 (mM)	4.7 ± 0.3 (145)	5.8 ± 0.4	4.4 ± 0.2
K^+- binding affinity in E_1 (mM)	0.100 ± 0.003 (132)	0.10 ± 0.02	0.08 ± 0.01
Rb^+- binding affinity in E_1 (mM)	0.08 ± 0.03 (140)	0.07 ± 0.02	0.07 ± 0.02
Na^+-binding affinity in P-E_2 (mM)	387 ± 22 (133)	428 ± 33	333 ± 12
K^+-binding affinity in P-E_2 (mM)	0.190 ± 0.009 (131)	0.31 ± 0.0.2	0.31 ± 0.02
ATP-binding affinity (µM)	0.05-0.2 (130)	0.14 ± 0.06	0.14 ± 0.02
Pi-binding affinity (µM)	24 ± 1 (134)	87 ± 13	100 ± 13
Time constant $(Na_3)E_1$-P → P-E_2Na_3 (ms)	170 ± 1 (22)	276 ± 48	264 ± 30

Table 10. Comparison of the kinetic properties of the native membrane-bound Na,K-ATPase from rabbit kidney and of the recombinant, purified, detergent-solubilized human α_1/His_{10}-β_1 and α_1/His_{10}-β_1/FXYD1 investigated with the dye RH421. The references for the data of the rabbit enzyme are given in parenthesis.

As discussed in *4.1*, the detergent-solubilized α_1/His_{10}-β_1 enzyme has a lower specific activity compared to the membrane-bound native Na,K-ATPase. The reason has been assigned both to the modified lipid environment and to a lower number of active enzyme molecules due to partial detergent-induced inactivation during the purification procedure. The

complex with FXYD1 also shows an ~ 50% lower specific ATPase activity compared to that of the membrane-bound native Na,K-ATPase, (*3.2*). Since FXYD1 has a strong stabilizing effect against detergent-mediated inactivation, as discussed in *4.2*, such a difference is likely to arise mainly from a lower turnover rate of the recombinant enzymes in the solubilized environment. Indeed, the time constant of the conformational transition $(Na_3)E_1\text{-}P \rightarrow P\text{-}E_2Na_3$ is ~ 40% larger for the recombinant preparations compared to the membrane-bound native enzyme under similar conditions. In principle, this difference could also be due to the presence of FXYD2 in the native enzyme; since the conformational transitions of the detergent-solubilized rabbit enzyme have not been investigated, it is not possible to assign this effect more precisely.

The comparison of the reaction steps of the Post-Albers cycle of the enzyme with and without FXYD1 reveals a single kinetic modification induced by FXYD1, an ~ 20-30% increase in Na^+-binding affinity in both the E_1 and $P\text{-}E_2$ conformations. In contrast, the binding affinities for K^+ and Rb^+ ions are independent of the presence of FXYD1. All three ion species are able to bind to the two bifunctional ion-binding sites, but only sodium is able to occupy the third ion-binding site. Therefore, the result that sodium binding, but not potassium and rubidium binding, is affected by the presence of FXYD1 indicates a specific effect of FXYD1 on the third, Na^+-selective ion-binding site. The result fits with the proximity of FXYD proteins to helix M9 of the α subunit that is supposed to be involved in the binding of the third Na^+ ion (29) (Fig. 64).

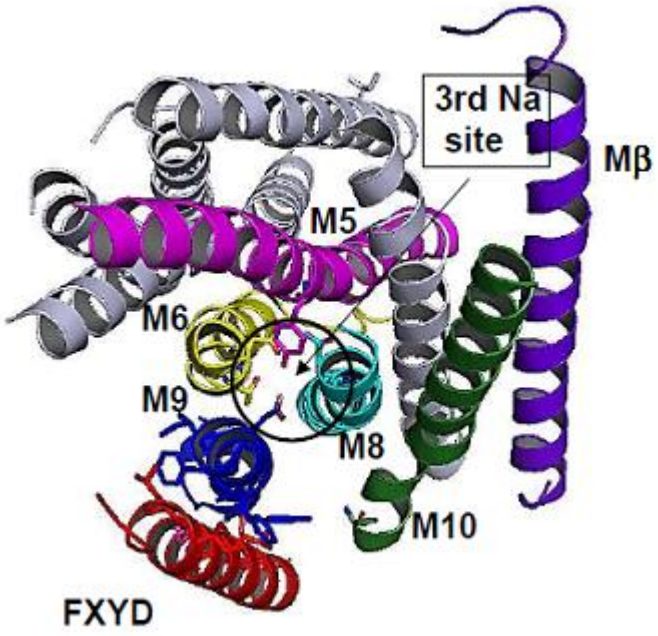

Figure 64. View from cytoplasmic surface of the transmembrane segments of the shark Na,K-ATPase, showing the interaction of FXYD10 with helix M9 of the α subunit (111).

As reported in *1.4.4*, the current hypothesis about the mechanism of interaction of FXYD1 with the Na,K-ATPase is the following: the unphosphorylated FXYD1 may inhibit the enzyme by reducing the Na^+- and, possibly, the K^+-binding affinity, while FXYD1 phosphorylated by PKA may stimulate the ion pump by abolishing the effect on the Na^+-binding affinity. Since phosphorylation by PKA occurs at Ser 68, localized in the cytoplasmic segment of FXYD1, the effect on the Na^+-binding affinity seems to be due to the interaction of the enzyme with this segment. However, experiments with a FXYD1/FXYD4 chimera containing the transmembrane segment of FXYD1 have shown

that this segment is responsible for an increase of about 20% in the intracellular Na^+-binding affinity of the enzyme (74). Considering this, it is possible that the different segments of FXYD1 affect the Na^+-binding affinity of the Na,K-ATPase in a distinct way: on the one hand, the unphosphorylated cytoplasmic segment could decrease the apparent Na^+-binding affinity; on the other hand the transmembrane segment may increase the intrinsic Na^+-binding affinity. This second effect could be masked by the decrease induced by the unphosphorylated cytoplasmic segment and be revealed only upon phosphorylation of it, depending on the degree of phosphorylation. Therefore, the effect of FXYD1 on the Na^+-binding affinity detected in the current study could be explained by the interaction of the enzyme with only the transmembrane segment of FXYD1. The interaction with the cytoplasmic segment of FXYD1 may be somehow missing.

A higher apparent Na^+-binding affinity of the detergent-solubilized recombinant α_1/His_{10}-β_1/FXYD1 compared to α_1/His_{10}-β_1 has been already detected in Na,K-ATPase activity assays (74). In this paper, it has been observed that the purified, detergent-solubilized recombinant α_1/His_{10}-β_1/FXYD1 complex obtained by *in vitro* reconstitution after separate expression in *P. pastoris* has the same functional properties of the purified, detergent-solubilized recombinant complex obtained after co-expression in the yeast membrane. As a consequence, it can be excluded that the α_1/β_1/FXYD1 association during the *in vitro* reconstitution is improper in some way. In (74), FXYD1 expressed in *P. pastoris* has been found to be partially phosphorylated at Ser 68. Thus, the higher Na^+-binding affinity in the presence of FXYD1 observed with the detergent-solubilized preparations in such study has been related to the phosphorylated state of FXYD1. However, in the current study FXYD1 has been expressed in *E. coli*, where it is not phosphorylated (112). Therefore, phosphorylation cannot be made responsible for the observed increase in Na^+-binding affinity. The fact that the detergent-solubilized recombinant α_1/His_{10}-β_1/FXYD1 preparations show an increase in Na^+-binding affinity independently of the phosphorylation state of FXYD1 (unphosphorylated in the current study, partially phosphorylated at Ser 68 in (74)) supports the hypothesis that the cytoplasmic segment of FXYD1 does not interact properly with the enzyme in the detergent-solubilized system.

4.4 The Lipid Environment Surrounding the Complex Affects the Interaction of FXYD1 with the Na,K-ATPase

The presence and composition of a lipid bilayer surrounding the enzyme has been investigated as the possible origin of the missing interaction between the cytoplasmic segment of FXYD1 and the enzyme. In the detergent-solubilized preparations, the proteins are surrounded by an annulus of lipid and detergent molecules that forms a hydrophobic environment and allows functional integrity of the Na,K-ATPase. However, it does not form a planar membrane surface as present in a cell, and this may potentially affect the interaction between FXYD1 and the enzyme.

Upon reconstitution in lipid vesicles without DOPS or with 10 mol % of DOPS, FXYD1 induces a decrease in Na^+-binding affinity of about 25% (Fig. 59), similarly to what has been detected in intact cells in the presence of unphosphorylated FXYD1 (51,74,77,106,107). This demonstrates that FXYD1 associates correctly with the enzyme during the *in vitro* reconstitution.

The dependence of the effect of FXYD1 on the Na^+-binding affinity upon the amount of DOPS in the membrane (Fig. 59-61) reveals an unexpected role of the lipids in the interaction of the two proteins. The DOPS-dependence can be explained by an alteration in the interaction of the enzyme either with the cytoplasmic segment or with the transmembrane segment of FXYD1, or both. Alternatively, it is possible that the affinity of FXYD1 for the Na,K-ATPase is reduced in the presence of high amounts of DOPS and that the α_1/His_{10}-β_1/FXYD1 complex dissociates. When vesicles of different lipid composition have been tested, the zwitterionic phospholipid DEPC (20:1) has been replaced by the anionic DOPS (18:1). Since the difference in their fatty acid chains is of 2 carbon atoms only, the hydrophobic portion of the vesicle membrane is less affected than the surface charge density. Therefore, the DOPS-dependence of the effect of FXYD1 on the Na^+-binding affinity is more likely to arise from a modification of the interaction of the enzyme with the cytoplasmic segment of FXYD1 rather than with the transmembrane segment. The cytoplasmic segment of FXYD1 contains several basic residues (Fig. 65). These residues may be attracted by the negative surface charge density on the DOPS-containing vesicles membrane, altering the interaction of the cytoplasmic segment of FXYD1 with the cytoplasmic domains of the enzyme.

ESPKEHDPFTYDYQSLQIGGLVIAGILFILGILIVLSRRCRCKFNQQQRTG
1 10 20 30 40 50

EPDEEEGTFRSSIRRLSTRRR
60 70

Figure 65. Primary sequence of the human FXYD1. The extracellular, transmembrane, and cytoplasmic sequences are shown in blue, red, and green, respectively.

The NMR structure of the free FXYD1 monomer in SDS micelles (60) as well as solid-state NMR data of FXYD1 in lipid bilayers (DOPC/DOPG 4:1) (61) indicate that parts of the cytoplasmic segment of FXYD1, corresponding to helices H3 and H4 (Fig. 18), associate to the micelle/bilayer surface. Moreover, isothermal titration calorimetric experiments have shown that a 35-amino acid peptide representing the cytoplasmic sequence $FXYD1_{38–72}$ associates with the membrane depending on the amount of negatively charged phospholipids (62). These observations prove that the cytoplasmic segment of FXYD1 is attracted by negative charges and is able to interact with anionic phospholipids. However, so far there are no data indicating a similar propensity when FXYD1 interacts

with the enzyme. The results presented in the current study are the first ones to suggest this hypothesis.

Among the basic residues in the cytoplasmic sequence of FXYD1, four of them are located close to the cytoplasm-membrane interface (Arg 38, Arg 39, Arg 41, and Lys 43). These residues are likely to be the ones that mainly experience the surface charge density of the membrane. Thus, they could be the primary residues involved in the DOPS-dependence of the effect of FXYD1 on the Na^+-binding affinity observed in the current study. In a similar manner, the respective basic residues in FXYD10 have been supposed to be responsible for the dependence on the presence of anionic phospholipids in the membrane of the functional effects of FXYD10 on the enzyme (161). It is interesting to notice that a sequence of basic residues located close to the cytoplasm-membrane interface is highly conserved in all FXYD proteins (Fig. 66). This fact suggests a specific common function.

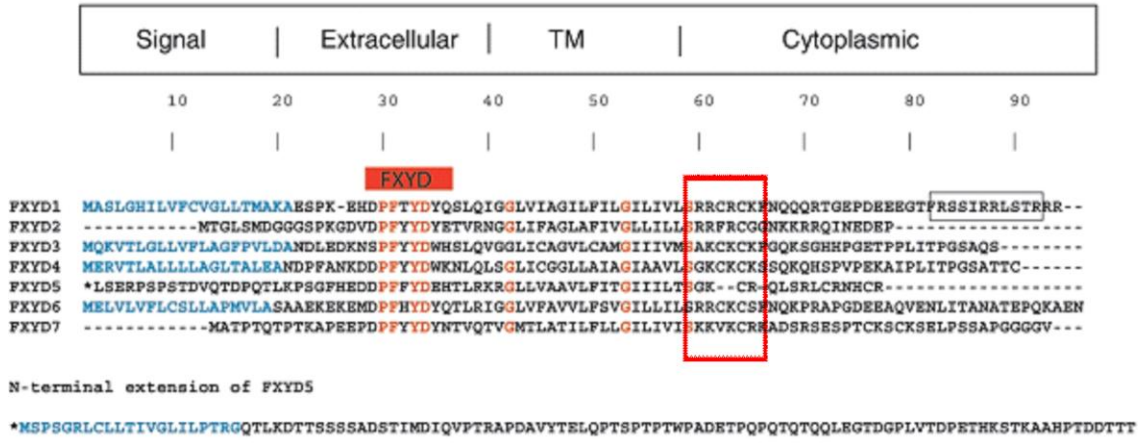

Figure 66. Alignment of the primary sequences of the currently known 7 human FXYD proteins. The sequence containing the basic residues located close to the cytoplasmic membrane surface is framed in red (53).

4.5 Conclusions and Outlook

The experimental findings in the current study support the concept of a stabilizing effect of FXYD1 on the Na,K-ATPase, in agreement with other studies (38,74,111,160). The investigation of the functional effects of FXYD1 on the different partial reactions of the transport cycle of the human α_1/β_1 isozyme of the Na,K-ATPase in purified detergent-solubilized preparations has revealed that FXYD1 induces an increase in Na^+-binding affinity, as already observed before (74). However, upon reconstitution in lipid vesicles FXYD1 induces the opposite effect, similarly to what detected in intact cells (51,74,77,106,107). Moreover, the experiments in proteoliposomes have revealed an unexpected role of the surface charge density of the environment surrounding the α_1/β_1/FXYD1 complex in the interaction of FXYD1 with the Na,K-ATPase, probably related to the cytoplasmic segment of FXYD1.

The apparently contradicting results obtained in the current study can be explained by the hypothesis that multiple structural and functional interactions between FXYD1 and the Na,K-ATPase are responsible for the effect of FXYD1 on the Na^+-binding affinity. On the one hand, the interaction of the unphosphorylated cytoplasmic segment of FXYD1 may decrease the apparent Na^+-binding affinity, as indicated by the present experiments with proteoliposomes and by those in intact cells (51,74,77,106,107). On the other hand, the interaction of the transmembrane segment of FXYD1 may increase the intrinsic Na^+-binding affinity, as suggested by the results obtained with the detergent-solubilized preparations and with a FXYD1/FXYD4 chimera (74). The interaction of the cytoplasmic segment of FXYD1 with the Na,K-ATPase depends not only on the degree of phosphorylation, but also on the amount of DOPS or, more generally, anionic phospholipids in the membrane. However, when the complete FXYD1 interacts with the enzyme, the effect of the transmembrane segment is probably always masked by the decrease induced by the cytoplasmic segment.

In the detergent-solubilized preparations, the exogenous SOPS added to preserve enzyme activity (*2.1.1*) might create a highly negatively charged environment surrounding the protein. This could attract the cytoplasmic segment of FXYD1 and relieve its interaction with the cytoplasmic domains of the pump, while maintaining an intact interaction at the transmembrane level. In detergent-solubilized preparations obtained with both exogenous SOPS and SOPC, FXYD1 induces a decrease in Na^+-binding affinity (unpublished results by Mishra et al.), supporting this hypothesis. However, it has to be noticed that in the experiments with proteoliposomes performed in the current study an increase in Na^+-binding affinity has never been detected, not even with high amounts of DOPS.

The effect of a peptide representing the transmembrane segment of FXYD1 on the Na^+-binding affinity of the enzyme reconstituted in proteoliposomes may provide a conclusive picture of the multiple structural and functional interactions between FXYD1 and the Na,K-ATPase involved in the effect of FXYD1 on this kinetic property. Moreover, the investigation of the dependence of such effect on the amount of DOPS in the membrane may enable us to assign the DOPS-dependence of the effect of FXYD1 on the Na^+-binding affinity observed in the current study to the interaction of the enzyme with either the cytoplasmic or the transmembrane segment of FXYD1, or both. Experiments with mutants representing the phosphorylated FXYD1 and mutants in which the basic residues close to the membrane-cytoplasm interface (Arg 38, Arg 39, Arg 41, and Lys 43) are replaced by neutral residues can be exploited to further investigate the interaction of the cytoplasmic segment of FXYD1 with the Na,K-ATPase.

References:

1. Stein, W.D. Transport and diffusion across cell membranes (1986) *ACADEMIC PRESS*
2. Alberts, B., Bray, D., Hopkin, K., Johnson, A., Lewis, J., Raff, M., Roberts, K., and Walter, P. L'essenziale di biologia molecolare della cellula (2005) *Zanichelli*
3. www.en.wikipedia.org/wiki/Cell_membrane
4. www.freewebs.com/mascibiology
5. Purves, W., Sadava, D., Orian, G., and Heller, C. Life: The Science of Biology (1995) *Sinauer Associates*
6. Läuger, P. Electrogenic Ion Pumps (1991) *Sinauer Associates*
7. Nelson, D., and Cox, M. I principi di biochimica di Lehninger (2002) *Zanichelli*
8. Boyer, P.D. (1997) *Annu. Rev. Biochem.* 66: 717-749
9. Stock, D., Gibbons, C., Arechaga, I., Leslie, A.G., and Walker, J.E. (2000) *Curr. Opin. Struct. Biol.* 10: 672-679
10. Futai, M., Wada, Y., and Kaplan J.H. Handbook of ATPases: Biochemistry, Cell Biology, Pathophysiology (2004) *WILEY-VCH*
11. Pedersen P.L. (2007) *J. Bioenerg. Biomembr.* 39: 349-355
12. Jones, P.M., O'Mara, M.L., and George, A.M. (2009) *Trends Biochem. Sci.* 34: 520-531
13. www.biodiscover.com
14. Kühlbrandt, W. (2004) *Nature Reviews* 5: 282-295
15. Palmgren, M.G., and Nissen, P. (2011) *Annu. Rev. Biophys.* 40: 243-266
16. www.people.eku.edu
17. Therien A.G., and Blostein R. (2000) *Am. J. Physiol. Cell Physiol.* 279: C541-C566
18. Albers, R.W. (1967) *Ann. Rev. Biochem.* 36: 727-756
19. Post, R.L., Hegyvary, C., and Kume, S. (1972) *J. Biol. Chem.* 247: 6530-6540
20. Apell, H.J., and Karlish, S.J. (2001) *J. Memb. Biol.* 180: 1-9
21. Apell H.J. (2003) *Rev. Physiol. Biochem. Pharmacol.* 150: 1-35
22. Apell, H.J., Benz, G., and Sauerbrunn, D. (2011) *Biochemistry* 50: 409-418
23. Blanco, G., and Mercer, R.W. (1998) *Am. J. Physiol.* 275: F633-F650
24. Geering, K.J. (2001) *Bioenerg. Biomembr.* 33: 425-438
25. Geering, K. (2008) *Curr. Opin. Nephrol. Hypertens.* 17: 526-532
26. Lutsenko, S., and Kaplan, J.H. (1993) *Biochemistry* 32: 6737-6743
27. Haviv, H., Cohen, E., Lifshitz, Y., Tal, D.M., Goldshleger, R., and Karlish, S.J. (2007) *Biochemistry* 46: 12855-12867
28. Crambert, G., Hasler, U., Beggah, A.T., Yu, C., Modyanov, N.N., Horisberger, J.D., Lelièvre, L., and Geering, K. (2000) J. Biol. Chem. 275: 1976-1986
29. Morth, J.P., Pedersen, B.P., Toustrup-Jensen, M.S., Sørensen, T.L., Petersen, J., Andersen, J.P., Vilsen, B., and Nissen, P. (2007) *Nature* 450: 1043-1049
30. Shinoda, T., Ogawa, H., Cornelius, F., and Toyoshima, C. (2009) *Nature* 459: 446-450
31. Jorgensen, P., Håkanssson, K., and Karlish, S. (2003) *Annu. Rev. Physiol.* 65: 817-849
32. Apell, H.J., and Diller, A. (2002) *FEBS Letters* 198-202
33. Therien, A.G., and Blostein, R. (2000) *Am. J. Physiol. Cell. Physiol.* 279: C541-C566
34. De Pont, J.J., Van Prooijen-Van Eeden, A., and Bonting, S.L. (1978) *Biochim. Biophys. Acta.* 1978 508: 464-477
35. Wheeler, K.P., and De Caldentey, M.I. (1980) Biochem. Soc. Trans. 8: 46-48
36. Perttilä, U. (1984) *Biochemistry International* 8: 77-82
37. Cohen, E., Goldshleger, R., Shainskaya, A., Tal, D.M., Ebel, C., le Maire, M., and Karlish, S.J. (2005) *J. Biol. Chem.* 280: 16610-16618

38. Lifshitz, Y., Petrovich, E., Haviv, H., Goldshleger, R., Tal, D.M., Garty, H., and Karlish, S.J. (2007) *Biochemistry* 46: 14937-14950
39. Cornelius, F. (1995) *Biochim. Biophys. Acta* 1235: 205-212
40. Oishi, K., Zheng, B., and Kuo, J.F. (1990) *J. Biol. Chem.* 265: 70-75
41. Katz, A., Lifshitz, Y., Bab-Dinitz, E., Kapri-Pardes, E., Goldshleger, R., Tal, D.M., and Karlish, S.J. (2010) *J. Biol. Chem.* 285:19582-19592
42. Cantley, L.C. Jr, Josephson, L., Warner, R., Yanagisawa, M., Lechene, C., and Guidotti, G. (1977) *J. Biol. Chem.* 252: 7421-7423
43. Sweadner, K.J., and Rael, E.(2000) *Genomics* 68: 41-56
44. Mahmmoud, Y.A., Vorum, H., and Cornelius, F. (2000) *J. Biol. Chem.* 275: 35969-35977
45. Tipsmark, C.K. (2008) *Am. J. Physiol. Regul. Integr. Comp. Physiol.* 294: R1367-R1378
46. Forbush, B. 3rd, Kaplan, J.H., and Hoffman, J.F. (1978) *Biochemistry* 17: 3667-3676
47. Beguin, P., Wang, X., Firsov, D., Puoti, A., Claeys, D., Horisberger, J.D., and Geering, K. (1997) *EMBO J.* 16: 4250-4260
48. Presti, C.F., Jones, L.R., and Lindemann, J.P. (1985) *J. Biol. Chem.* 260: 3860-3867
49. Presti, C.F., Scott, B.T., and Jones, L.R. (1985) *J. Biol. Chem.* 260: 13879-13889
50. Palmer, C.J., Scott, B.T., and Jones, L.R. (1991) *J. Biol. Chem.* 266: 11126-11130
51. Crambert, G., Fuzesi, M., Garty, H., Karlish, S., and Geering, K. (2002) *Proc. Natl. Acad. Sci. USA* 99: 11476-11481
52. Crambert, G., and Geering, K. (2003) *Sci STKE* 166: RE1
53. Cornelius, F., and Mahmmoud, Y.A. (2003) *News Physiol. Sci.* 18: 119-124
54. Geering, K., Beguin, P., Garty, H., Karlish, S., Füzesi, M., Horisberger, J.D., and Crambert, G. (2003) *Ann. NY Acad. Sci.* 986: 388-394
55. Geering, K. (2005) *J. Bioenerg. Biomembr.* 37: 387-392
56. Geering, K. (2006) *Am. J. Physiol. Renal. Physiol.* 290: F241-F250
57. Garty, H., and Karlish, S.J. (2006) *Annu. Rev. Physiol.* 68: 431-459
58. Geering, K. (2008) *Curr. Opin. Nephrol. Hypertens.* 17: 526-532
59. Franzin, C.M., Gong, X.M., Teriete, P., and Marassi, F.M. (2007) *J. Bioenerg. Biomembr.* 39: 379-383
60. Teriete, P., Franzin, C.M., Choi, J., and Marassi, F.M. (2007) *Biochemistry* 46: 6774-6783
61. Franzin, C.M., Gong, X.M., Thai, K., Yu, J., and Marassi, F.M. (2007) *Methods* 41: 398-408
62. Hughes, E., Whittaker, C.A., Barsukov, I.L., Esmann, M., and Middleton, D.A. (2011) *Biochim. Biophys. Acta.* 1808: 1021-1031
63. Franzin, C.M., Yu, J., Thai, K., Choi, J., and Marassi, F.M. (2005) *J. Mol. Biol.* 354: 743-750
64. Walaas, S.I., Czernik, A.J., Olstad, O.K., Sletten, K., and Walaas, O. (1994) *Biochem. J.* 304: 635-640
65. Fuller, W., Howie, J., McLatchie, L.M., Weber, R.J., Hastie, C.J., Burness, K., Pavlovic, D., and Shattock, M.J. (2009) *Am. J. Physiol. Cell. Physiol.* 296: C1346-C1355
66. Teriete, P., Thai, K., Choi, J., and Marassi, F.M. (2009) *Biochim. Biophys. Acta.* 1788: 2462-2470
67. Bossuyt, J., Despa, S., Martin, J.L., and Bers, D.M. (2006) J. Biol. Chem. 281: 32765-32773
68. Bossuyt, J., Despa, S., Han, F., Hou, Z., Robia, S.L., Lingrel, J.B., and Bers, D.M. (2009) *J. Biol. Chem.* 284: 26749-26757
69. Song, Q., Pallikkuth, S., Bossuyt, J., Bers, D.M., and Robia, S.L. (2011) J. Biol. Chem. 286: 9120-9126

70. Cortes, V.F., Ribeiro, I.M., Barrabin, H., Alves-Ferreira, M., and Fontes, C.F. (2011) *Arch. Biochem. Biophys.* 505: 75-82
71. Tulloch, L.B., Howie, J., Wypijewski, K.J., Wilson, C.R., Bernard, W.G., Shattock, M.J., and Fuller, W. (2011) *J. Biol. Chem.* 286: 36020-36031
72. Beguin, P., Crambert, G., Monnet-Tschudi, F., Uldry, M., Horisberger, J.D., Garty, H., and Geering, K. (2002) *EMBO J.* 21: 3264-3273
73. Cheung, J.Y., Zhang, X.Q., Song, J., Gao, E., Rabinowitz, J.E., Chan, T.O., and Wang, J. (2010) *Clin. Transl. Sci.* 3: 189-196
74. Lifshitz, Y., Lindzen, M., Garty, H., and Karlish, S.J. (2006) *J. Biol. Chem.* 281: 15790-15799
75. Fuller, W., Eaton, P., Bell, J.R., and Shattock, M.J. (2004) *FASEB J.* 18: 197-199
76. Bossuyt, J., Ai, X., Moorman, J.R., Pogwizd, S.M., and Bers, D.M. (2005) *Circ. Res.* 97: 558-565
77. Bibert, S., Roy, S., Schaer, D., Horisberger, J.D., and Geering, K. (2008) *J. Biol. Chem.* 283: 476-486
78. Chen, L.S., Lo, C.F., Numann, R., and Cuddy, M. (1997) *Genomics* 41: 435-443
79. Silverman, B.Z., Fuller, W., Eaton, P., Deng, J., Moorman, J.R., Cheung, J.Y., James, A.F., and Shattock, M.J. (2005) *Cardiovasc. Res.* 65: 93-103
80. Zhang, X.Q., Qureshi, A., Song, J., Carl, L.L., Tian, Q., Stahl, R.C., Carey, D.J., Rothblum, L.I., and Cheung, J.Y. (2003) *Am. J. Physiol. Heart. Circ. Physiol.* 284: H225-H233
81. Feschenko, M.S., Donnet, C., Wetzel, R.K., Asinovski, N.K., Jones, L.R., and Sweadner, K.J. (2003) *J. Neurosci.* 23: 2161-2169
82. Wetzel, R.K., and Sweadner, K.J. (2003) *Am. J. Physiol. Renal. Physiol.* 285: F121-F129
83. Wang, J., Gao, E., Song, J., Zhang, X.Q., Li, J., Koch, W.J., Tucker, A.L., Philipson, K.D., Chan, T.O., Feldman, A.M., and Cheung, J.Y. (2010) *Am. J. Physiol. Heart. Circ. Physiol.* 298: H807-H815
84. Zahler, R., Gilmore-Hebert, M., Baldwin, J.C., Franco, K., and Benz, E.J. (1993) *Biochim. Biophys. Acta.* 1149: 189-194
85. Gao, J., Wymore, R., Wymore, R.T., Wang, Y., McKinnon, D., Dixon, J.E., Mathias, R.T., Cohen, I.S., and Baldo, G.J. (1999) *J. Physiol.* 516: 377-383
86. Floyd, R.V., Wray, S., Martin-Vasallo, P., and Mobasheri, A. (2010) *Ann. Anat.* 192: 7-16
87. Ahlers, B.A., Zhang, X.Q., Moorman, J.R., Rothblum, L.I., Carl, L.L., Song, J., Wang, J., Geddis, L.M., Tucker, A.L., Mounsey, J.P., and Cheung, J.Y. (2005) *J. Biol. Chem.* 280: 19875-19882
88. Wang, X., Gao, G., Guo, K., Yarotskyy, V., Huang, C., Elmslie, K.S., and Peterson, B.Z. (2010) *Biophys. J.* 98: 1149-1159
89. Moorman, J.R., Palmer, C.J., John, J.E. 3rd, Durieux, M.E., and Jones, L.R. (1992) *J. Biol. Chem.* 267: 14551-14554
90. Moorman, J.R., Ackerman, S.J., Kowdley, G.C., Griffin, M.P., Mounsey, J.P., Chen, Z., Cala, S.E., O'Brian, J.J., Szabo, G., and Jones, L.R. (1995) *Nature* 377: 737-740
91. Kowdley, G.C., Ackerman, S.J., Chen, Z., Szabo, G., Jones, L.R., and Moorman, J.R. (1997) *Biophys. J.* 72: 141-145
92. Li, C., Grosdidier, A., Crambert, G., Horisberger, J.D., Michielin, O., and Geering, K. (2004) *J. Biol. Chem.* 279: 38895-38902
93. Lindzen, M., Aizman, R., Lifshitz, Y., Lubarski, I., Karlish, S.J., and Garty, H. (2003) *J. Biol. Chem.* 278: 18738-18743
94. Lubarski, I., Karlish, S.J., and Garty, H. (2007) *Am. J. Physiol. Renal. Physiol.* 293: F1818-F1826

95. Zouzoulas, A., Therien, A.G., Scanzano, R., Deber, C.M., and Blostein, R.J. (2003) *Biol. Chem.* 278: 40437-40441
96. Crambert, G., Li, C., Swee, L.K., and Geering, K. (2004) *J. Biol. Chem.* 279: 30888-30895
97. Li, C., Crambert, G., Thuillard, D., Roy, S., Schaer, D., and Geering, K. (2005) *J. Biol. Chem.* 280: 42738-42743
98. Beguin, P., Crambert, G., Guennoun, S., Garty, H., Horisberger, J.D., and Geering, K. (2001) *EMBO J.* 20: 3993-4002
99. Füzesi, M., Gottschalk, K.E., Lindzen, M., Shainskaya, A., Küster, B., Garty, H., and Karlish, S.J. (2005) *J. Biol. Chem.* 280: 18291-18301
100. Lindzen, M., Gottschalk, K.E., Füzesi, M., Garty, H., and Karlish, S.J. (2006) *J. Biol. Chem.* 281: 5947-5955
101. Therien, A.G., Karlish, S.J., and Blostein, R. (1999) *J. Biol. Chem.* 274: 12252-12256
102. Pu, H.X., Cluzeaud, F., Goldshleger, R., Karlish, S.J., Farman, N., and Blostein, R. (2001) *J. Biol. Chem.* 276: 20370-20378
103. Pu, H.X., Scanzano, R., and Blostein, R. (2002) *J. Biol. Chem.* 277: 20270-20176
104. Pavlovic, D., Fuller, W., and Shattock, M.J. (2007) *FASEB J.* 2007 21: 1539-1546
105. Bell, J.R., Kennington, E., Fuller, W., Dighe, K., Donoghue, P., Clark, J.E., Jia, L.G., Tucker, A.L., Moorman, J.R., Marber, M.S., Eaton, P., Dunn, M.J., and Shattock, M.J. (2008) *Am. J. Physiol. Heart Circ. Physiol.* 294: H613-H621
106. Despa, S., Bossuyt, J., Han, F., Ginsburg, K.S., Jia, L.G., Kutchai, H., Tucker, A.L., and Bers, D.M. (2005) *Circ. Res.* 97: 252-259
107. Han, F., Bossuyt, J., Martin, J.L., Despa, S., and Bers, D.M. (2010) *Am. J. Physiol. Cell Physiol.* 299: C1363-C1369
108. Han, F., Tucker, A.L., Lingrel, J.B., Despa, S., and Bers, D.M. (2009) *Am. J. Physiol. Cell Physiol.* 297: C699-705
109. Han, F., Bossuyt, J., Despa, S., Tucker, A.L., and Bers, D.M. (2006) *Circ. Res.* 99: 1376-1383
110. Jia, L. G., Donnet, C., Bogaev, R. C., Blatt, R. J., McKinney, C. E., Day, K. H., Berr, S. S., Jones, L. R ., Moorman, J. R., Sweadner, K. J., and Tucker , A. L . (2005) *Am. J. Physiol. Heart Circ. Physiol*. 288: H1982-H1988
111. Mishra, N. K., Peleg, Y., Cirri, E., Belogus, T., Lifshitz, Y., Voelker, D. R., Apell, H. J., Garty, H., and Karlish, S. J. (2011) *J. Biol. Chem.* 286: 9699-9712
112. Cirri, E., Katz, A., Mishra, N. K., Belogus, T., Lifshitz, Y., Garty, H., Karlish, S. J., and Apell, H. J. (2011) *Biochemistry* 50: 3736-3748
113. Lambert, O., Levy, D., Ranck, J. L., Leblanc, G., and Rigaud, J. L. (1998) *Biophys. J.* 74: 918-930
114. Jørgensen, P.L. (1974) *Methods Enzymol.* 32: 277-290
115. Lowry, O. H., Rosebrough, N. J., Farr, A. L., and Randall, R. J. (1951) *J. Biol. Chem.* 193: 265-275
116. Schwartz, A. K., Nagano, M., Nakao, M., Lindenmayer, G. E., and Allen, J. C. (1971) *Meth. Pharmacol.* 1: 361-388
117. Lämmli, U.K. (1970) *Nature* 227: 680-685
118. Lakowicz, J.R. Principles of Fluorescence Spectroscopy (2006) *Springer*
119. Karlish, S.J. (1980) *J. Bioenerg. Biomembr.* 12: 111-136
120. Karlish, S.J. (1988) *Methods Enzymol.* 156: 271-277
121. Rephaeli, A., Richards, D., and Karlish, S.J. (1986) *J. Biol. Chem.* 261: 6248-6254
122. Farley, R.A., and Faller, L.D. (1985) *J. Biol. Chem.* 260: 3899-3901
123. Schneeberger, A. and Apell, H. J. (1999) *J. Membr. Biol.* 168: 221-228
124. Müller, W., Windisch, H., and Tritthart, H.A. (1986) *Eur. Biophys. J.* 14: 103-111
125. Clarke, R.J., and Apell, H.J. (1989) *Biophys. Chem.* 34: 225-237

126. Grinvald, A., Hildesheim, R., Farber, I. C., and Anglister, L., (1982) *Biophys. J.* 39:301-308
127. Bühler, R., Stürmer, W., Apell, H. J., and Läuger, P. (1991) *J. Memb. Biol.* 121: 141-161
128. Pedersen, M., Roudna, M., Beutner, S., Birmes, M., Reifers, B., Martin, H.D., and Apell, H.J. (2002) *J. Memb. Biol.* 185: 221-236
129. Stürmer, W., Bühler, R., Apell, H. J., and Läuger, P. (1991) *J. Membr. Biol.* 121: 163-176
130. Heyse, S., Wuddel, I., Apell, H. J., and Stürmer, W. (1994) *J. Gen. Physiol.* 104: 197-240
131. Bühler, R., and Apell, H.J. (1995) *J. Membr. Biol.* 145: 165-173
132. Schulz, S., and Apell, H.J. (1995) *Eur. Biophys. J.* 23: 413-421
133. Wuddel, I., and Apell, H.J. (1995) Biophys. J. 69: 909-921
134. Apell, H. J., Roudna, M., Corrie, J. E., and Trentham, D. R. (1996) *Biochemistry* 35: 10922-10930
135. Kane, D.J., Fendler, K., Grell, E., Bamberg, E., Taniguchi, K., Froehlich, J.P., and Clarke, R.J. (1997) *Biochemistry* 36: 13406-13420
136. Kane, D.J., Grell, E., Bamberg, E., and Clarke, R.J. (1998) *Biochemistry* 37: 4581-4591
137. Clarke, R.J., Kane, D.J., Apell, H.J., Roudna, M., and Bamberg, E. (1998) *Biophys. J.* 75: 1340-1353
138. Apell, H.J., Schneeberger, A., and Sokolov, V.S. (1998) *Acta Physiol. Scand. Suppl.* 643: 235-245
139. Domaszewicz, W., and Apell, H. (1999) *FEBS Lett.* 458: 241-246
140. Schneeberger, A. and Apell, H. J. (2001) *J. Membr. Biol.* 179: 263-273
141. Lüpfert, C., Grell, E., Pintschovius, V., Apell, H.J., Cornelius, F., and Clarke, R.J. (2001) *Biophys. J.* 81: 2069-2081
142. Humphrey, P.A., Lüpfert, C., Apell, H.J., Cornelius, F., and Clarke, R.J. (2002) *Biochemistry* 41: 9496-9507
143. Clarke, R.J., Humphrey, P.A., Lüpfert, C., Apell, H.J., and Cornelius, F. (2003) *Ann. NY Acad. Sci.* 986: 159-162
144. Clarke, R.J., Apell, H.J., and Kong, B.Y. (2007) *Biochemistry* 46: 7034-7044
145. Habeck, M., Cirri, E., Katz, A., Karlish, S. J., and Apell, H. J. (2009) *Biochemistry* 48: 9147-9155
146. Shainskaya, A., Schneeberger, A., Apell, H.J., and Karlish, S.J. (2000) *J. Biol. Chem.* 275: 2019-2028
147. McCray, J.A., Herbette, L., Kihara, T., and Trentham, D.R. (1980) *Proc. Natl. Acad. Sci. USA* 77: 7237-7241
148. Borlinghaus, R., Apell, H.J., and Läuger, P. (1987) *J. Membr. Biol.* 97: 161-178
149. Deluca, M., and McElroy, M.D. (1978) *Methods Enzymol.* 57: 3-15
150. Smith, J.C., Russ, P., Cooperman, B.S., and Chance, B. (1976) *Biochemistry* 15: 5094-5105
151. Bashford, C.L., Chance, B., Smith, J.C., and Yoshida, T. (1979) *Biophys. J.* 25: 63-85
152. Apell, H. J., and Bersch, B. (1987) *Biophys. Biochim. Acta* 903:480-494
153. Cornelius, F. (1989) *Biochem. Biophys. Res. Commun.* 160: 801-807
154. Clarke, R.J., Apell, H.J., and Läuger, P. (1989) *Biochim. Biophys. Acta* 981: 326-336
155. Goldshleger, R., Shahak, Y., and Karlish, S.J. (1990) *J. Membr. Biol.* 113: 139-154
156. Apell, H.J., Häring, V., and Roudna, M. (1990) *Biochim. Biophys. Acta* 1023: 81-90
157. Alpes, H., Apell, H.J., Knoll, G., Plattner, H., and Riek, R. (1998) *Biochim. Biophys. Acta* 946: 379-388

158. Strugatsky, D., Gottschalk, K.E., Goldshleger, R., Bibi, E., and Karlish, S.J. (2003) *J. Biol. Chem.* 278: 46064-46073
159. Adam, G., Läuger, P., and Stark, G Physikalische Chemie und Biophysik (2007) Springer Berlin
160. Kapri-Pardes, E., Katz, A., Haviv, H., Mahmmoud, Y., Ilan, M., Khalfin-Penigel, I., Carmeli, S., Yarden, O., and Karlish, S. J. (2011) *J. Biol. Chem.* 286: 42888-42899
161. Cornelius, F., and Mahmmoud, Y. A. (2007) *Biochemistry* 46: 2371-2379